

Nordic Master's Programme in Innovative Sustainable Energy Engineering

# **Seawater heat recovery by the utilisation of phase change heat of freezing**

Technical feasibility study of a system for District Heating in the city of Helsinki

---

**Rakesh Ramesh**

**Master's Thesis  
2021**

**Author** Rakesh Ramesh

---

**Title of thesis** Seawater heat recovery by the utilisation of phase change heat of freezing

---

**Programme** Nordic Master's Programme in Innovative Sustainable Energy Engineering

---

**Thesis supervisor** Dr. Annukka Santasalo-Aarnio

---

**Thesis advisors** Dr. Ari Seppälä, M.Sc. Aleksi Barsk and Jaakko Nummelin

---

**Collaborative partner** Helen Oy

---

**Date** 27.10.2021

**Number of pages** 78+10

**Language** English

---

## Abstract

With the Paris agreement calling to limit global warming to 2°C below pre-industrial levels, with further efforts to ensure it stays below 1.5°C, the Finnish government passed the Laki hiilen energiakäytön kieltämisestä (416/2019), i.e., Act of Prohibition of Coal Energy, which stipulates that the use of coal as a fuel for heat/electricity production to be banned from 1 May 2029. This affects Helsinki's energy industry and a key concern to this work is the Salmisaari Combined Heat and Power plant, which is set to be decommissioned. This plant currently generates heat and electricity by using wood pellets and coal to cater to around 25-45% of the District Heating consumption of the city of Helsinki.

To compensate for this decommissioning, there arises a need for more heat production, around 300-500MW of capacity. One alternative is the heat recovery of seawater by utilising the phase change heat of freezing. The present project investigates a technical feasibility study of a system to generate ice slurry, which is then used to extract heat from seawater at ~0°C via a heat pump. The competitiveness of an ice-slurry based system to state-of-the-art water or ice-based storage is analysed as well. The proposed system is then modelled in Aspen Plus, and the pressure drop characteristics of the generated ice slurry are studied. Finally, a sensitivity analysis of the pressure ratio of the compressor on the performance of the system is studied.

Based on prior works, level of commercialisation and technical feasibility, it was found that a vacuum ice generation method, in combination with heat pumps, is a viable solution to cater to the district heating demand of the city. Further, it is concluded that the pressure drop occurring during transport of the ice slurry is quite minimal – less than 0.5% of the total power consumed whilst producing 300MW of district heat. The COP of the system varies between 2.6-2.8 depending on the pressure ratio of the compressor and thus is energy efficient. Overall, the proposed solution seems to be promising and with further socio-techno-economic analysis, this could be the potential alternative to bridge the deficit.

---

**Keywords** District heating, Seawater, Ice slurry, Aspen Plus, Pressure drop

---

**Työn nimi** Meriveden lämmön talteenotto jäätyamisen faasimuutoslämpöä hyödyntämällä

**Koulutusohjelma** Nordic Master's Programme in Innovative Sustainable Energy Engineering

**Vastuupettaja/valvoja** Dr. Annukka Santasalo-Aarnio

**Työn ohjaajat** Dr. Ari Seppälä, M.Sc. Aleksi Barsk and Jaakko Nummelin

**Yhteistyötaho** Helen Oy

**Päivämäärä** 27.10.2021

**Sivumäärä** 78 / 10

**Kieli** Suomi

## Tiivistelmä

Pariisin sopimuksessa kehoitettiin rajoittamaan ilmaston lämpeneminen 2° C: een esiteollista tasoa alhaisemmalle tasolle ja jatkamaan pyrkimyksiä sen varmistamiseksi, että lämpeneminen pysyy alle 1,5° C: ssa. Kivihiilen käyttö lämmön- ja sähköntuotannon polttoaineena on tarkoitus lopettaa 1. toukokuuta 2029. Tämä vaikuttaa Helsingin energia-alaan ja tämän työn kannalta keskeinen huolenaihe on Salmisaaren yhdistetty lämpö- ja voimalaitos, joka on määrä poistaa käytöstä. Tämä laitos tuottaa tällä hetkellä lämpöä ja sähköä käyttämällä puupellettejä ja hiiltä noin 25–45 prosenttia Helsingin kaupungin kaukolämmön kulutuksesta. Laitoksen käytöstä poistamisen kompensoimiseksi tarvitaan lisää lämmöntuotantoa noin 300–500 MW.

Yksi vaihtoehto on meriveden lämmön talteenotto hyödyntämällä jäätyamisen faasimuutoslämpöä. Tässä hankkeessa tutkitaan jääsohjon tuottamisjärjestelmän teknistä toteutettavuutta sekä analysoidaan myös jääsohjon perustuvan lämmön talteenottojärjestelmän kilpailukykyä. Ehdotettu järjestelmä mallinnettiin Aspen Plus -ohjelmalla. Lisäksi työssä tutkittiin syntyneen jääsohjon painehäviöominaisuuksia sekä tehtiin herkkyysanalyysi kompressorin painesuhteesta järjestelmän suorituskykyyn.

Aiempien töiden, kaupallistamisen tason ja teknisen toteutettavuuden perusteella havaittiin, että jään valmistaminen tyhjiömenetelmällä yhdessä lämpöpumppujen kanssa on toteuttamiskelpoinen ratkaisu kaupungin kaukolämmön kysynnän tyydyttämiseksi. Jääsohjon kuljetuksen aikana tapahtuva painehäviö havaittiin varsin vähäiseksi - alle 0,5 % kokonaistehosta, joka kulutetaan tuotettaessa 300 MW kaukolämpöä. Järjestelmän COP vaihtelee välillä 2,6–2,8 kompressorin painesuhteesta riippuen ja on siten energiatehokas. Kaiken kaikkiaan ehdotettu ratkaisu näyttää lupaavalta, ja sosio- teknis- taloudellisen analyysin myötä se voisi olla mahdollinen vaihtoehto poistuvien voimaloiden lämmöntuotannon kompensoimiseksi.

**Avainsanat** Kaukolämpö, Merivesi, Jääsohjo, Aspen Plus, Painehäviö.

# Table of Contents

Abstract.....	2
Preface .....	6
Abbreviations and Symbols .....	7
<b>1. Introduction</b> .....	<b>8</b>
1.1 Carbon Neutrality goals of Helsinki .....	8
1.2 Problem Definition .....	12
1.3 Research Question .....	12
1.4 Methodology .....	13
1.5 Thesis Outline.....	13
<b>2. Theoretical Background</b> .....	<b>15</b>
2.1 Water vs ice slurry .....	15
2.2 Theory of Crystallisation, Ice slurry formation and Melting .....	16
2.2.1 Supersaturation .....	17
2.2.2 Nucleation .....	17
2.2.3 Growth .....	18
2.2.4 Attrition.....	18
2.2.5 Agglomeration .....	18
2.2.6 Ostwald ripening.....	19
2.2.7 Spheroidization .....	19
2.2.8 Heat transfer rate and Crystal morphology .....	19
2.2.9 Melting .....	20
2.3 Baltic Seawater properties .....	20
2.3.1 Salinity .....	21
2.3.2 Oxygen Content .....	23
<b>3. Methods of Ice Slurry Generation</b> .....	<b>26</b>
3.1 Scraped-Surface Ice Slurry Generator .....	26
3.2 Direct Contact Ice Slurry Generators with Immiscible Primary Refrigerant ..	30
3.3 Direct Contact Generators with Immiscible Secondary Refrigerant.....	32
3.4 Supercooled Method .....	33
3.5 Hydro-Scraped Ice Slurry Generator .....	35
3.6 Fluidised Bed Crystalliser .....	36
3.7 High-Pressure Ice Slurry Generator .....	38
3.8 Recuperative Ice Making .....	40

3.9 Vacuum Ice Generation .....	41
<b>4. Modelling in Aspen Plus .....</b>	<b>47</b>
4.1 Introduction to Aspen Plus .....	47
4.2 Choice of Refrigerant - R1234ze.....	47
4.3 The Aspen Plus Model.....	48
4.3.1 Overview .....	48
4.3.2 Components and Setup parameters.....	49
4.3.3 Model Validation.....	52
<b>5. Pressure drop analysis of ice slurry during transport .....</b>	<b>53</b>
5.1 Pressure loss evaluation based on laboratory-scale experimental data .....	53
5.2 Viscosity based pressure drop calculation .....	55
<b>6. Results and Discussions .....</b>	<b>57</b>
6.1 Selection of Ice Slurry Generation method.....	57
6.2 Pressure Drop Analysis .....	59
6.3 Performance of the system .....	65
6.4 Contribution to SDG.....	66
6.5 Future Work.....	67
<b>7. Conclusion.....</b>	<b>69</b>
<b>8. Bibliography .....</b>	<b>70</b>
<b>Appendix.....</b>	<b>81</b>
A1 – Augustenborg District Heating Plant .....	81
A2 – Refrigerant R-1234ze .....	83
A3 – Experimental values used in Pressure drop studies .....	84
A4 – Extension of Pressure Drop studies.....	85

## Preface

Throughout the writing of this thesis, I have received a great deal of support and assistance.

Firstly, I would first like to thank my supervisor, Dr. Annukka Santasalo-Aarnio and advisor Dr. Ari Seppälä for helping in setting up an interview for this position and whose expertise was invaluable in formulating the research questions. I am extremely grateful to Ari and Aleksi Barsk, without whom this work would not have been possible. Their insightful feedback pushed me to sharpen my thinking and helped me improve the quality of my work. I would like to thank Judit Nyári and Shouzhuang Li for their guidance in developing the Aspen model. I would like to acknowledge my other supervisor, Dr Justin Ning-Wei Chiu, for his astute comments and help in the shaping up of my thesis.

I would particularly like to express my gratitude to Jaakko Nummelin and Laura Korhonen of Helen Oy, for offering me this position. I want to thank you for your patient support and for all the opportunities I was given to further my research.

In addition, I would like to thank my parents, and my brother for everything. Finally, I could not have completed this thesis without the support of my friends who provided happy distractions in these testing COVID times.

Otaniemi, 27<sup>th</sup> October 2021  
Rakesh Ramesh

# Abbreviations and Symbols

## Abbreviations

BAU - Business-as-usual  
CHP - Combined heat and power  
CO<sub>2e</sub> - Carbon-dioxide equivalent  
COP - Coefficient of Performance  
DC - District cooling  
DH - District Heating  
DTI - Danish Technological Institute  
EU - European Union  
F-gas - Fluorinated gas  
GHG - Greenhouse gas  
GWP - Global Warming Potential  
HCl - Hydrogen chloride  
HF - Hydrogen fluoride  
HFC - Hydrofluorocarbons  
HFO - Hydrofluoro-olefins  
HPAF - High-pressure assisted freezing  
HPSF - High-pressure shift freezing  
HSY - Helsingin seudun ympäristöpalvelut  
I/O - Input/output  
IEA - International Energy Agency

IPCC - Intergovernmental Panel on Climate Change  
ISG - Ice slurry generator  
LNG - Liquefied natural gas  
NaCl - Sodium Chloride  
NH<sub>3</sub> - Ammonia  
NO<sub>x</sub> - Nitrogen Oxides  
O&M - Operation and Maintenance  
O<sub>2</sub> - Oxygen  
ODP - Ozone Depletion Potential  
ORE - Orbital rod evaporators  
R12 - Dichlorodifluoromethane  
R1234ze - 1,3,3,3-tetrafluoropropene  
R143a - 1,1,1-Trifluoroethane  
R717 - Refrigerant grade Ammonia  
rpm - revolutions per minute  
SDG - Sustainable Development Goals  
USD - United States Dollar  
VIH - Vacuum Ice Heat Pump  
VIM - Vacuum Ice Maker

## Symbols in equations

A - cross-sectional area (m<sup>2</sup>)  
D - Diameter (m)  
f - friction factor  
g - gravitational acceleration constant (m/s<sup>2</sup>)  
L - length  
L<sub>water → ice</sub> - specific latent heat of fusion of water (kJ/kg)  
 $\dot{m}$  - mass flow rate (kg/s)  
P - Pumping power (kW)  
P<sub>t</sub> - Triple point pressure (bar)  
Q - Flow rate (m<sup>3</sup>/s)

Re - Reynolds number  
S - salinity of water (‰, per mille)  
v - flow velocity (m/s)  
v<sub>min</sub> - Minimum velocity (m/s)  
x - ice fraction  
ΔG - Gibbs free energy state  
ΔP - Pressure Drop (Pa)  
η<sub>pump</sub> - efficiency of pump  
μ - Dynamic viscosity (kg/ms)  
ρ - density (kg/m<sup>3</sup>)  
ρ<sub>cf</sub> - Carrier fluid density (kg/m<sup>3</sup>)  
ρ<sub>i</sub> - Density of ice (kg/m<sup>3</sup>)

## 1. Introduction

Ever since the Industrial revolution 350 years ago, anthropogenic greenhouse gas (GHG) emissions have put our planet on the pathway to a climate catastrophe. Human activities are estimated to have triggered approximately 1.0°C of global warming above pre-industrial levels, with the figure expected to reach 1.5°C between 2030 and 2050 if it continues to increase at the current pace [1].

Immediate and collective action by all of mankind towards lowering the levels of it in the atmosphere is the only way to avoid such a disaster. Decades of global co-operation amongst the 196 countries bore fruit in 2015 in the form of the Paris agreement, which aims at significantly cutting down on the emissions of the greenhouse gases and thereby limiting the global temperature rise to 2°C, with further efforts to keep the temperature rise to below 1.5° [2, 3].

The member states of the European Union (EU) are legally bound to the policy decisions agreed upon on climate issues. This includes the EU's commitment to achieving zero net anthropogenic greenhouse gas emissions by the year 2050, in addition to individual targets for each sector. The objective is to cut greenhouse gas emissions by at least 40% to 2030 from the 1990 levels. Other means of mitigating the emissions are by improving the energy efficiency and the share of renewables in electricity generation; this has been an important cornerstone in the EU's quest for a greener world. In numbers, a target of improved energy efficiency by at least 32.5% by 2030, with an improvement of 0.8% per year in the current decade. and share of renewable energy to 32% by the end of this decade. [4, 5, 6].

In addition to the above-mentioned, every country has their national targets that they strive to achieve for a cleaner future. Of particular interest to this work, is the city of Helsinki in Finland, which is discussed in detail subsequently.

### 1.1 Carbon Neutrality goals of Helsinki

Carbon neutrality is defined as a state of having net-zero CO<sub>2</sub> emissions. This could be achieved by either carbon offsetting or balancing the emitted and removed emissions. For the City of Helsinki to become carbon-neutral by 2035, it requires that GHG emissions are reduced by at least 80% from the levels 30 years back, with further increase of carbon sinks. The remaining 20 percent will be compensated for by Helsinki taking care of implementing



emission reductions outside the city or, for example, increasing the number of carbon sinks. [7, 8]

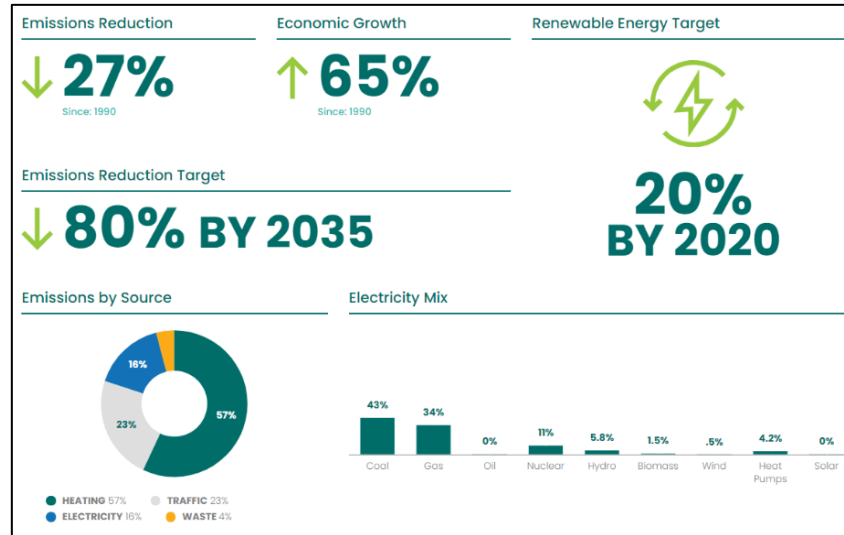


Figure 1: An infographic depicting the energy, emission levels and targets for Helsinki [9]

In 2002, Helsinki's Sustainability Action Plan, comprising its objectives for GHG emissions, was approved, and the city became the first European capital with an all-inclusive sustainable development pathway. This plan, which turned out to be successful, called for emissions in 2010 to be at the same level as it was in 1990 [10].

So far, there has been steady progress, with some significant milestones. In 2018, Helsinki's total GHG emissions were about 27% lower than in 1990. Per capita emissions are 45% lower than in 1990. Despite population growth by 150,000, the total energy consumption in urban areas remains unchanged, which speaks volumes about the development of energy efficiency. As of 2018, renewable energy accounts for 12% of the city's total output [9].

Helen Oy, owned 100% by the city of Helsinki, is one of Finland's largest energy companies and caters to the district heating (DH), cooling (DC) and electricity demand in Helsinki. Helen Oy was the first energy company in Finland that was dedicated to setting an emissions reduction target, not just for CO<sub>2</sub>, but for the other GHG gases as well based on their entire life cycle [11]. In accordance with the 2035 plan to achieving carbon neutrality, Helen Oy fulfils its obligation through measures that would reduce the DH emissions of the population of Helsinki by ~75% by 2035. The measures include phasing out of fossil fuel-based generation, uptake of renewable

energy sources, especially in electricity production, introducing Demand side response measures, storage measures to name a few [12].

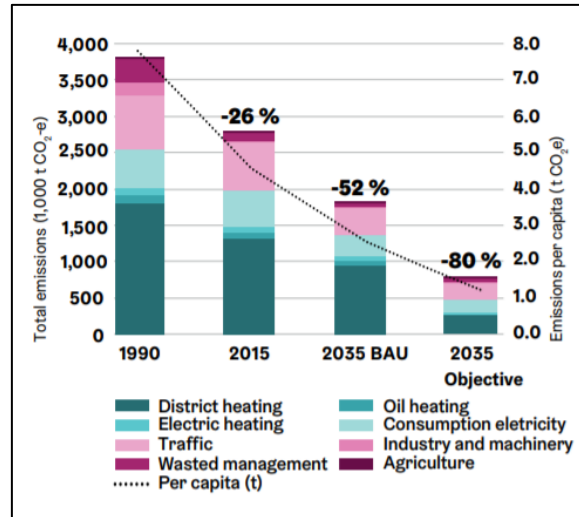


Figure 2: The development of Helsinki's emissions from 1990 to 2015, the BAU scenario for 2035 and the target scenario for 2035 [8].

Helen Oy is analysing several scenarios to provide sustainable fossil-free power. As compared to the BAU scenario, the target scenario for 2035 includes an assumption that clean energy sources would make up around 70% of heat produced (Figure 2). Further, usage of natural gas produces emissions that must be balanced by development of carbon sinks. In 2017, in Salmisaari and Hanasaari alone, burning a mixture of wooden pellets and coal instead of only coal diminished the GHG emissions by almost 80kt of CO<sub>2</sub>e [8]. The city of Helsinki and Helen Oy have developed a strategy to decommission the coal-based powerplants during this decade [8, 13].

The Salmisaari CHP plant is completely owned by Helen Oy. Salmisaari A commenced producing electricity in 1953, and four years later became the first plant to produce DH in Helsinki. Salmisaari B, its coal fired counterpart, produces 300MW of DH and 160 MW of electricity. The 65m x 40m silos present in the premises, 120m below the surface ground can store up to 250000 tons of coal [14]. The A plant, these days, is used to generate heat when DH from cogeneration is not adequate. Heavy fuel oil, stored in a rock storage in the site, acts as the backup fuel for A and B power. In summer, in addition to DH and electricity, the B-plant also generates energy for district cooling purposes. It is complemented by the Kellosaari reserve power plant, operated on light fuel oil, and ensures there is no dearth of demand [15, 16, 17, 18, 19].



Figure 3: Salmisaari B power plant, located at Porkkalankatu 9–11 in Helsinki [20]

Table 1: Technical datasheet of Salmisaari – B (coal/pellet boiler) [21]

<b>Intended use</b>	Base load boiler
<b>Year of introduction</b>	1984
<b>Main Fuel</b>	Coal, Pellet
<b>Auxiliary/Backup fuel</b>	Heavy fuel oil
<b>Burners</b>	Coal burners – 16 Oil burners - 12
<b>Rated Power</b>	
- Electricity	160MW
- District Heating	300MW
<b>Running time</b>	5000-7800h/a
<b>Chimney height</b>	153m
<b>Gross electricity production</b>	962.4 GWh/a
<b>Thermal energy production</b>	1741.5 GWh/a
<b>Fuel consumption, as of 2017</b>	
- Coal	418980 t
- Pellets	8692 t
- Heavy fuel oil	350.5 t

With demands for increased share of renewables rising, a pellet system, including the receiving, preparation, storage and feeding of the fuel, was built in 2014, ensuring greener energy [21]. Further, in 2018, Helen Oy

inaugurated a 92MW wood pellet-fired boiler in Salmisaari, with it providing enough heat for a town the size of Savonlinna, Finland [22, 23].

## 1.2 Problem Definition

To reach the 2035 carbon-neutrality target, it is required to reduce the usage of fossil fuels. In its quest to create a cleaner future for the next generation, the Ministry of the Environment and Climate Change of Finland passed the decree of Laki hiilen energiakäytön kieltämisestä (416/2019), i.e., Act of Prohibition of Coal Energy, which stipulates that the use of coal as a fuel for heat/electricity production be banned from May 1, 2029. This also has the added benefit of no further dependence on Russia for coal import. In March 2020, the Finnish Government introduced an investment fund for schemes that fast-track the phase-out of coal in power generation [24, 25, 26].

Employing wood pellets and coal as their major source of fuel, the Salmisaari CHP plant has been generating heat and power that caters to around 25-45% of District Heating consumption of the city of Helsinki. To ensure they abide by the governmental laws and by virtue of their own carbon neutrality goals, Helen Oy has decided to decommission the plant. To compensate for this phase-out, there arises a need for more heat production equivalent to around 300-500MW capacity. [27, 26, 28].

## 1.3 Research Question

The objective of this work is to propose a solution to recompense for the deficit of the district heat brought about by closure of the Salmisaari CHP plant. This research will critically examine the solution of heat recovery of seawater by utilising the phase change heat of freezing by means of a technical feasibility study. The research questions this work attempts to answer are:

- a. What is be the best-suited ice slurry generation method that, in combination with heat pumps, would enable the extraction of heat from surface seawater and compensate for the deficit of ~300 MW of District Heat at Salmisaari?
- b. What are the associated rheological characteristics involved in the transport of the generated ice slurry back into the sea?

## 1.4 Methodology

For the current work of heat recovery from seawater using the phase change heat of ice slurry, there is a critical examination of the literature to analyse the various ice slurry generation methods. A method suitable for the current application, in integration with heat pumps, and based on previous large-scale works is then selected and studied further. The system is then modelled in Aspen Plus, a process simulation software package and the mass flow rate of the ice slurry is determined. The system is designed in such a way that the DH water temperature is raised from 45°C to 90°C, to cater to the demand in the winter. This is followed by a study of the pressure drop during ice slurry flow, that is characteristic of transport of fluids. Since, the physics of ice slurry transport and its rheological characteristics is not well-defined, a sensitivity analysis for the friction factor models and viscosities are performed and the changes in pressure drop are observed.

## 1.5 Thesis Outline

The thesis is structured as follows: it progresses from initially presenting the objectives and literature review of ice slurries, with particular focus on its application in integration with the District Heating system of the city of Helsinki, followed by modelling in Aspen Plus and culminated with the conclusions based on the results and subsequent discussions.

Firstly, an overlook of the Carbon Neutrality goals of the city of Helsinki and Helen Oy is presented. The current situation of the Salmisaari CHP plant is then briefly described. Section 2 introduces a theoretical framework used in this paper that could serve as the basis of further developments. It further discusses the chemistry of latent heat storage, its advantages, and the selection of ice-water slurry for this work. The science of crystal formation is also communicated in this section. Since this work is centred around Salmisaari, the properties of seawater at Länsi-Tonttu monitoring station, 15kms from the focal area of this work, was analysed and the results conclude this section. The potential applications and previous research on ice slurry generation methods, including large-scale systems were studied deeply and the findings are put forth in Section 3. A model of a vacuum ice generation system based on the application for the current work is developed and is presented in Section 4. The definitive aim of the thesis is to identify the best suited method of ice slurry generation for this case and attempt to model it and calculate the pressure drop that occurs during its transport. The pressure drop studies are explained in Section 5. The results are presented in Section

6 along with some suggestions for future work, while the conclusions are drawn in [Section 7](#).

This work would then serve as one of the underlying support materials for the construction of a seawater-based DH system by Helen Oy in the near future. This field of study, being relatively unexplored, also helps in identifying important areas for future work.

## 2. Theoretical Background

### 2.1 Water vs ice slurry

Water, owing to its superior properties of neither having global warming potential (GWP) or ozone depletion potential (ODP) nor being flammable or toxic, is a suitable candidate for being a refrigerant from an environmental point of view. In the earlier days, due to risk of freezing, surface waters of seas, rivers etc. exhibiting near zero temperatures, were not extensively used as heat sources for heat pumps. With the advent of ice slurry systems, this could be made possible in a cascade of heat pumps [29]. Among the different states of water, the advantages of a two-phase fluid (ice slurry) over a single-phase liquid (water/ice) are plentiful. Ice slurries, double up as storage medium and a transportation fluid, both of which are explained below.

In sensible thermal energy storage, energy is stored by changing the temperature of the material, without it undergoing phase change. The total energy stored is dependent on the mass of the storage material, the specific heat capacity, and the change in temperature. The inherent disadvantages associated with sensible heat storage are low storage density per degree temperature change and large temperature range for storing the energy.

Latent heat thermal energy storage systems can store the latent heat of fusion in an isothermal process which corresponds to phase transition temperature of the phase change material. The enthalpy (334kJ/kg at 0°C) associated with the phase change of water [30] corresponds to a high energy storage density and thus, it requires lesser space, and the system becomes compact.

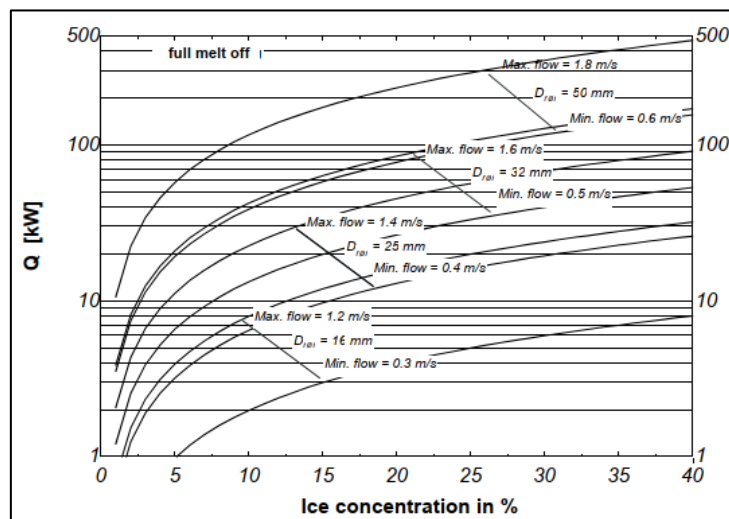


Figure 4: Transport capacity in pipe having inner diameter 16-50mm [31]

Hansen et. al., in their work [32] have discoursed the superior transport properties of ice slurry with increasing flow rate and ice fraction, that is depicted in Figure 4. Similarly, a recent study by ILK Dresden [33] contrasts ice vs water vs ice-slurry through the means of an interesting graphic (Figure 5).

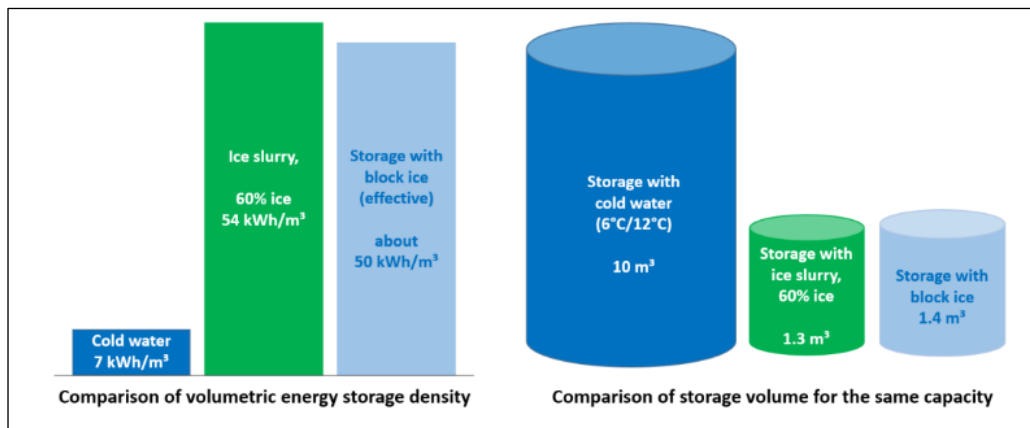


Figure 5: Comparison of volumetric energy storage density and comparison of volume for same capacity [33]

The results of the work state that, in cold water modules, for temperature difference of 6 °C to 12 °C, the stored energy was only ~7 kWh/m<sup>3</sup>. This pales in comparison with a conventional ice block, which was found to have stored effectively ~45-55 kWh/m<sup>3</sup>. On the other hand, the energy storage density of ice slurry at 60% ice content was found to be comparable to that of conventional ice with ~54 kWh/m<sup>3</sup>. Figure 5 shows that although water is a pumpable medium, it has a low energy storage density. Conventional block ice has a high energy storage density, but since it is rigid, it could not be pumped through pipes. The drawbacks of ice and water are recompensed in ice slurry, which has a comparable energy storage density as that of ice and is pumpable like water (with some limitations). In addition, on examining the thermophysical properties of ice slurry, one can conclude that higher the ice content, higher the density of cooling capacity per unit volume. Choi and Knodel [34] discuss in their work, on how 30% ice fraction in the slurry could potentially reduce the pipe diameter by 40% and economically save about 70% in piping installations.

## 2.2 Theory of Crystallisation, Ice slurry formation and Melting

In this section, we attempt to chronicle the theory of crystallisation, understand how ice slurry is formed and discuss briefly about the phenomenon of melting.



### 2.2.1 Supersaturation

The generation of ice crystals involves several steps, the first of which is need for the solution to be supersaturated. This is necessitated because crystallisation occurs only if sufficient driving force is applied. [35]. A saturated solution is in thermodynamic equilibrium with the solid phase and contains maximum amount of solute that could be dissolved at the specified temperature and pressure. A supersaturated solution contains more dissolved solid than that maximum as characterised by the equilibrium saturation [36]. In other words, the solution is said to be in a metastable state.

Supersaturation can be brought about by either changing the pressure and thus, shifting the equilibrium temperature or by supercooling the solution at the equilibrium temperature or by changing the concentration of the additive [31]. In the case of ice, when water is maintained at triple point conditions, evaporation of water (partial) creates the potential difference, making way for the formation of ice crystals. The ice crystals continue to form till the equilibrium is attained and saturation is ensured.

### 2.2.2 Nucleation

Okolieocha et. al. define nucleation in the following manner:

*“Nucleation is simply defined as the first random formation of a distinct thermodynamic new phase (daughter phase or nucleus) that have the ability to irreversibly grow into larger sized nucleus within the body of a metastable parent phase.”*  
[37].

As defined above, in a supersaturated solution, molecules congregate and form stable clusters, thus ensuing the formation of the initial nuclei. This can transpire in two ways: homogeneously or heterogeneously.

In the former mechanism, ‘statistical fluctuation’ of the aggregated molecules results in the formation of the initial nuclei. This is difficult to control owing to the low temperature levels and the high crystal formation rate. In the case of water-ice, this happens at very low temperatures and with the Baltic seawater having foreign objects that act as nucleation spots, homogeneous nucleation is not likely to occur in our application. In heterogeneous primary nucleation, which is expected to occur, the initial nuclei are formed with the aid of extraneous particles or foreign surfaces. These occur at relatively

higher temperatures as compared to homogeneous nucleation and the orientation of molecules in the crystal lattice is controlled to an extent by the surface of foreign particles. Heterogeneous nucleation can be further divided into two mechanism: primary and secondary nucleation. [31, 35].

Primary nucleation is the direct materialisation of ice crystals from the solution, while secondary nucleation is the realisation of ice crystals from already existing ice crystals in the solution [38].

### **2.2.3 Growth**

The final step is the growth phase, where the crystals get bigger till the desired size is attained. Crystal growth follows three basic steps: initially, there is a mass transfer across the boundary layer from the bulk of the solution by means diffusion of molecules. These molecules are then assimilated into the surface, and finally, phase change heat transfer occurs from the crystal to the bulk. The rate of crystal growth is influenced by either of these three stages, the driving force, the remaining supersaturation of the solution and the residence times in the crystalliser. Ice slurry removed from an ice slurry generator (ISG) do not necessarily maintain the same shape and texture as it did in the generator, owing to a few pertinent processes like attrition, agglomeration, Ostwald ripening etc [31, 39]. These processes are described in detail in the following chapters.

### **2.2.4 Attrition**

The process of a crystal breaking off on being subject to stress and forming fragments is termed attrition [35]. The shear stress of fluids while mixing, particle collisions with each other, with pumps, walls, other components are some examples of stresses the crystals are subjected to. The fragments thus formed act as secondary nuclei. The attributes of attrition happening could be due to a variety of factors. The texture of the original crystal affects the amount of fragments, with ice crystals having a rougher surface producing a larger number of fragments as compared to smooth crystals. In addition, smaller crystals tend to display less attrition. Attrition is considered either desired or detrimental depending on the application and the choice of ice slurry generator used.

### **2.2.5 Agglomeration**

The process of crystals colliding with one another, adhering to them, and coalescing together to form a crystal larger in size and more stable is termed

agglomeration [35]. The higher the level of supersaturation of the solution, the higher the rate of agglomeration. Additionally, as the slurry is disturbed with growing intensity, the degree of agglomeration decreases. Although it might mildly influence the size of crystals formed in the ISGs, agglomeration is a side effect and not a primary process.

### **2.2.6 Ostwald ripening**

The phenomenon of Ostwald ripening affects the distribution of crystal size in a solution. Owing to the solubility difference amongst the different crystals formed and, in a quest, to attain the most stable minimum Gibbs free energy state ( $\Delta G$ ), smaller crystals tend to dissolve and are assimilated on to the larger ones [35]. This effect is slow and is prominent only in systems over a long period of time (ex. ice slurry storage systems, ice creams stored in freezer etc.) and thus, are not so relevant in our application.

### **2.2.7 Spheroidization**

Spheroidization is a process germane to crystal formation. Ice crystals on exiting the ISG try to attain the thermodynamically favourable least energy state. Amongst the shapes, a sphere has the least surface area to volume ratio and is considered to be the most stable [40]. As a result, the dendritic crystals try to attain spheroidal shape to minimise its energy during the transport, just as the name suggests.

### **2.2.8 Heat transfer rate and Crystal morphology**

Continuing on the theory of crystallisation, it is important to discuss other issues related to ice slurry generation. Amongst them, two things are of high importance: high heat transfer rate and ideal crystal shape and size. When ice crystals are formed, they tend to adhere to the heat exchanging surfaces. As a result, a layer of ice is built up on the walls. Ice has a low thermal conductivity (2.22 W/mK at 0°C) and thus, this impedes the heat transfer rates. Thus, for high heat transfer rates and indirectly, lower O&M costs, one needs to remove the layers of ice either mechanically or by defrosting it at regular intervals using a recuperative heat exchanger. An ideal size and shape of ice crystals are to be generated by the ISGs for optimal functioning of the system. Typically, in several applications, round and small crystals are preferred. A larger crystal usually exhibits a dawdling melt-off rate and requires more power to pump. As a result, proper research of the morphology of the crystals must be done to find the shape and size, and subsequently the method best suited for the application [41].

## 2.2.9 Melting

The process involving phase change of an object from a solid to liquid state is defined as melting [42]. When heat is supplied to ice crystals, the thermal driving force causes the atoms to move faster and break the chemical hydrogen bonds to form water, in a liquid state [43]. Since the surface atoms have relatively fewer bonds as compared to the atoms at the centre, energy of the atoms is transferred from the surface to the bulk and thus, melting usually initiates from the surface [44]. One major difference between crystallisation and melting of ice is - in the former, there is a metastable supercooled state observed (discussed earlier in this section) [31], whereas in the latter, there is no associated metastable effect (superheating). But since this work entails the use of the heat released when water crystallises and not the heat gained while melting, we do not explore the mechanism of melting any further.

## 2.3 Baltic Seawater properties

In this work, an attempt is made to utilise the latent heat of seawater for district heating. The proposed plant is likely to be located in the Salmisaari area, in the current premises of the CHP plant [45]. The Salmisaari plant is surrounded by Lapinlahti and Lauttasaarensalmi on either side, as it can be seen from the Figure 6. The Gulf of Finland, which is a part of the Baltic Sea serves as the base for extracting heat during the winter. This will be looked into in detail in the following sections.

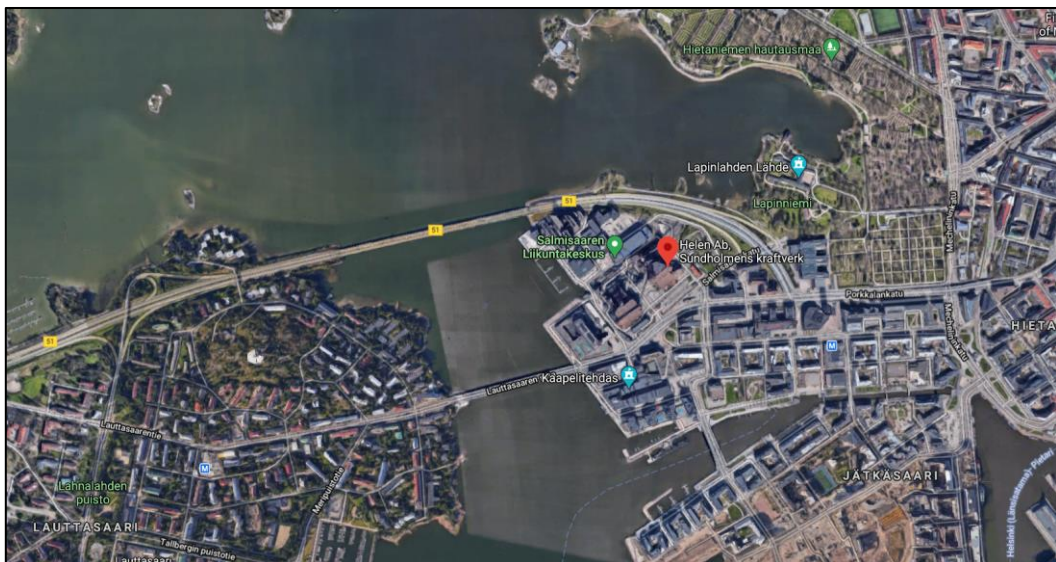


Figure 6: A map of the Salmisaari B powerplant (denoted by the red pin) [46]

Since the propositioned plant is in the same site as Salmisaari A and B, the water source would be the from the Baltic Sea. The generation of ice slurry is

inherently determined by the quality of the water, its salinity, temperature, and other properties.

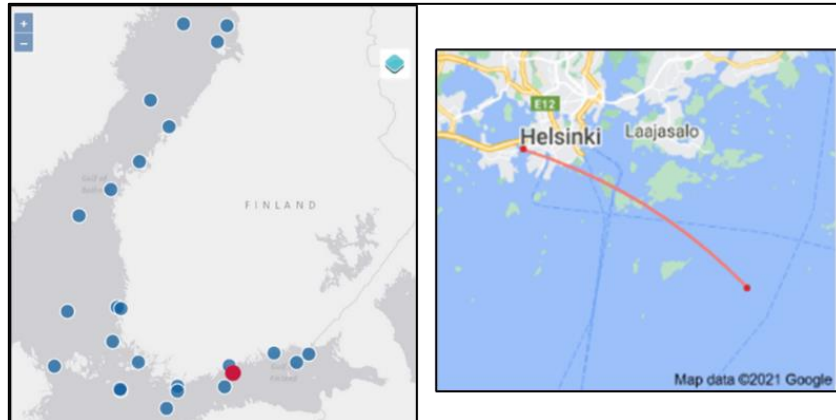


Figure 7: (left) Länsi-Tonttu monitoring station in the Baltic Sea, denoted by a red dot [47]; (right) 15km – the distance between the proposed plant at Salmisaari and Länsi-Tonttu monitoring station in West Tukan [48]

The two major properties – salinity and dissolved oxygen of the water at the target site are ascertained using relevant literature and other available sources. Amongst them, the Länsi-Tonttu station is 15kms away to the south of Salmisaari at a depth of 53m (Figure 7). Being located at the outer edge of the archipelago, beyond the islands of Vallisaari and Isosaari, it is linked to the open sea and the properties of seawater here closely resemble to what Helen Oy’s seawater-based DH plant would be operating with.

### 2.3.1 Salinity

The Baltic Sea is typified by low-salinity brackish water. The Gulf of Finland is an estuarine sea in the north-eastern part of Baltic sea, encompassing Finland to the north and Estonia to the south, to St. Petersburg in Russia to the east, lying between  $59^{\circ}11' N$ ,  $22^{\circ}50' E$  and  $60^{\circ}46' N$ ,  $30^{\circ}20' E$ . It receives briny water from the Baltic Sea Proper in the west, while it receives huge influx of fresh water from the east, majorly (~15% of total flow) from River Neva. As a result, there occurs a salinity gradient in both ways. The salinity increases from north to south and from east to west. The surface salinity varies from 5–7‰ in the western Gulf of Finland to about 0–3‰ in the east. At the bottom of the sea, the salinity varies from 8-10‰ in the western Gulf of Finland. Salinity affects the freezing point of the surface water, typified by varying the freezing point of  $-0.17^{\circ} C$  in the east to  $-0.33^{\circ} C$  in the west [49].



Figure 8: Map of the Baltic Sea and its easternmost arm - the Gulf of Finland [50]

As depicted in Figure 9, the salinity of the water around the Länsi-Tonttu station is quite steady (5-6‰) and does not fluctuate much across seasons [51]. This is well in synergy with other literature on the salinity of the Gulf of Finland, as it can be seen from Figure 10. Although the salinity is relatively low, this serves the purpose of being a freezing point depressant. The reason behind the requirement of a minimum level of salinity for this work is explained in the subsequent chapters [52].

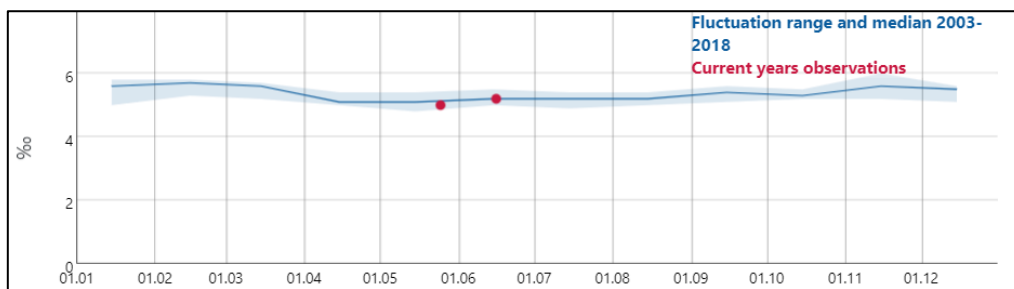


Figure 9: Seasonal variation of salinity of seawater at the Länsi-Tonttu station [53]

As salinity of water increases, the electrical conductivity of water increases while the oxygen content decreases. The presence of salt indicates the presence of chloride ions that have the potential to destroy the oxide layer on the metal surface and as a result, corrosion happens [54]. In a system like the one proposed in this thesis, a lot of components and pipes contain metal and so, there arises a need to give a protective layer of coating and prevent corrosion. This should be studied in detail.

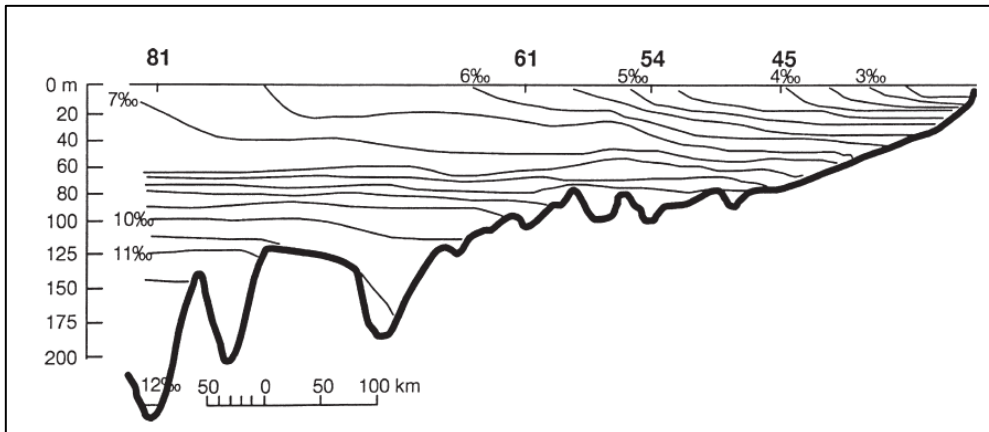


Figure 10: Vertical salinity gradient across the Gulf of Finland and Northern Baltic Sea. (the numbers indicating each location, with 54 corresponding to the region off Helsinki, 61 – Hanko, 81 – east of Gotland [49])

### 2.3.2 Oxygen Content

In any water body, oxygen is present in a dissolved form. Due to seawater pulses and ocean-warming driven deoxygenation, the oxygen levels are relatively low. Because of seawater pulses, oxygen-scant water from deep parts of the Baltic sea flow into Gulf of Finland, lowering its oxygen levels, while a warmer sea increases the oxygen demand of the organisms present, thereby depleting the oxygen content available [55].

At the bottom of the Gulf of Finland, it is almost completely anoxic; bereft of oxygen, while in the surface near Länsi-Tonttu, it fluctuates between 6.5-13 mg/L depending on the season as it can be seen from the Figure 11.

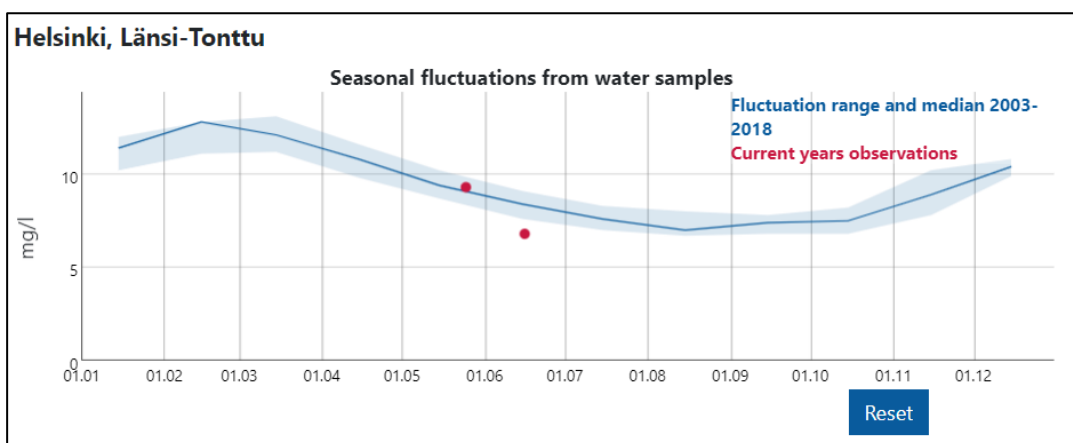


Figure 11: Seasonal variation of oxygen levels of the seawater at Länsi-Tonttu station [56]

This is corroborated with the data available in other literature as it could be observed in distribution of oxygen concentration data in Figure 12 [57].

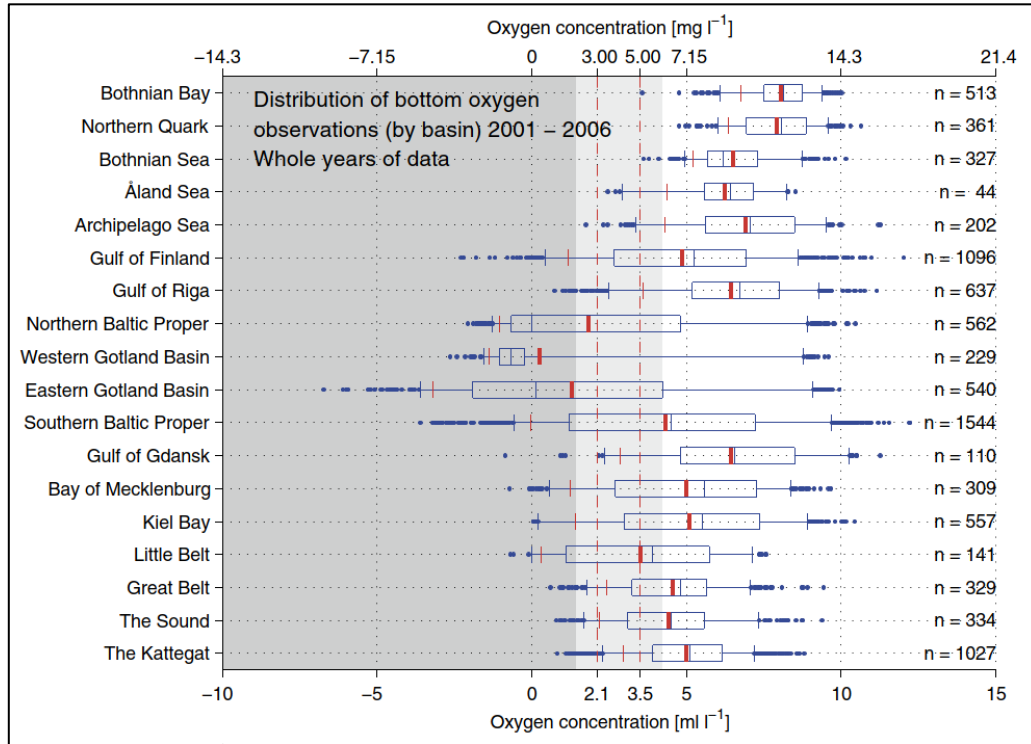


Figure 12: Oxygen concentrations, 2001–2006. The greyness indicates the lack of oxygen, with the darker the shade, the more it lacks in oxygen.

The amount of oxygen present in dissolved form in seawater determines the rate of corrosion. The higher the  $O_2$  levels of the sea, the greater the electrode potential of the metal, which in turn causes the rate of corrosion to be more rapid [54, 58]. If the piping of the system is to be placed on or near the surface, it must be ensured that the oxygen doesn't attack the metal since the proposed system would be vital to the functioning of the city and cannot fail.

The temperature levels of the seawater determine the energy required to bring it down to triple point. The closer it is to the triple point temperature, the less energy required and as it can be observed from Figure 13 (d), the temperature in the winter is close to  $0^\circ C$ . In addition, as the temperature increases, the solubility of oxygen decreases, and corrosion slows down. Other properties like the amount of turbidity, chlorophyll- $\alpha$  [59, 60], phosphorous content [61, 62]) also affect the crystallisation of water particles and the corrosion rate and these are exhibited in Figure 13 (a), (b), (c). These are outside the scope of this work.



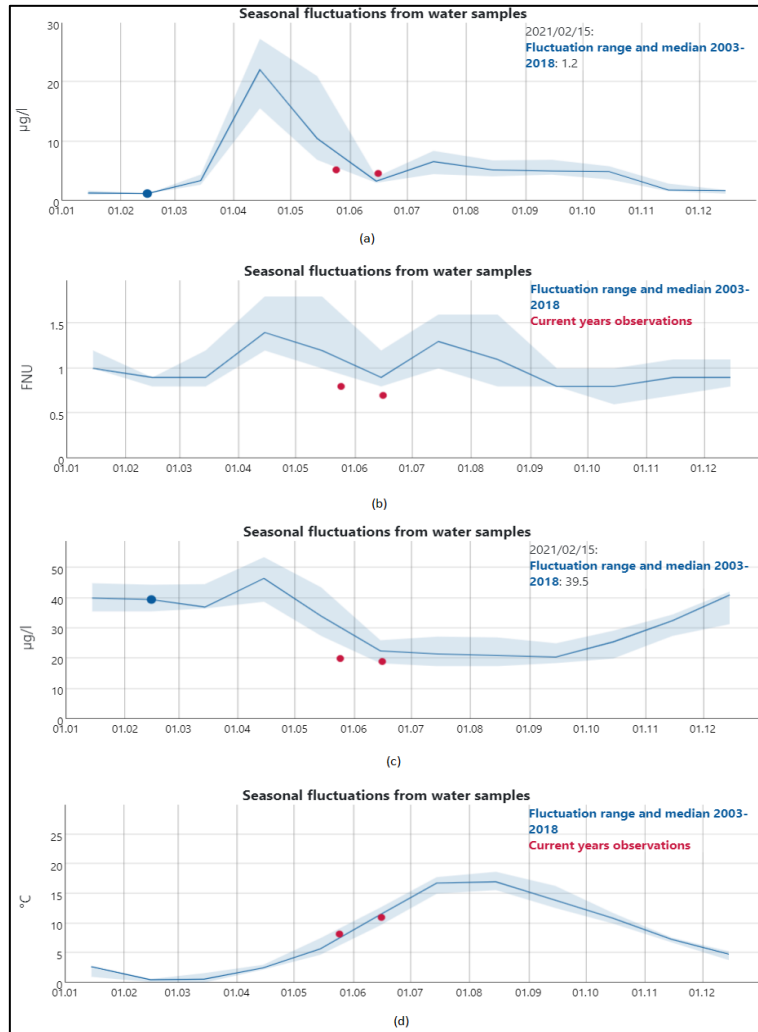


Figure 13: Seasonal variation of (a) amount of algae [63] (b) turbidity [64] (c) phosphorous content [62] (d) temperature levels of the seawater at Länsi-Tonttu station [65]

### 3. Methods of Ice Slurry Generation

Archaeological findings have suggested that mankind has been using ice to preserve food since over 5000 years ago. The first patent for producing ice slurry was done in 1935 to shave peak loads in dairies in Sweden [66]. The 70s and the 80s saw a plethora of patent applications being filed for ice slurry generators. Since then, ice slurry has developed from being a niche product into an applied science being used across the world in various disciplines. However, the pursuit for an efficient ISG, subsequent storage and crystal measurements has been never-ending for the scientists. There is no silver bullet when deciding what ice slurry generator to use for a certain application. Different ice slurry generators are used for different purposes. Some methods are developed at a laboratory scale, while others have been fully commercialised. This section reports the different types of ISGs, their merits and demerits and their suitability for our application.

#### 3.1 Scraped-Surface Ice Slurry Generator

Over the last three decades ice slurry generation has garnered the interest of thousands of scientists and no other technique in this field has been more widely acknowledged and scientifically developed than the scraped surface ice slurry generator. The generator comprises of a circular shell-and-tube heat exchanger, a rotating scraping device on the inner side, a refrigerant stream and a process fluid stream.

It is a double pipe element, with the process fluid flowing through the inner pipe while coolant flows in the annulus between inner and outer pipe. The coolant is a refrigerant that evaporates and is usually present on the shell side. Crystals are formed on the cold inner pipe wall. Inner pipe scraping assembly, usually consisting of spring-loaded rotating blades or orbital rods or brushes, prevents the deposit of crystals on the surface by scraping between the pipe walls (see Figure 14). The absence of scraping would result in a sheet of ice forming on the walls of the pipe, affecting the heat transfer rate and over a period of time this might result in blockages. Therefore, to reduce the probability of formation of ice layers on the wall, there is a requirement of a minimum amount of freezing point depressant (like NaCl) to be added to the water. [31]

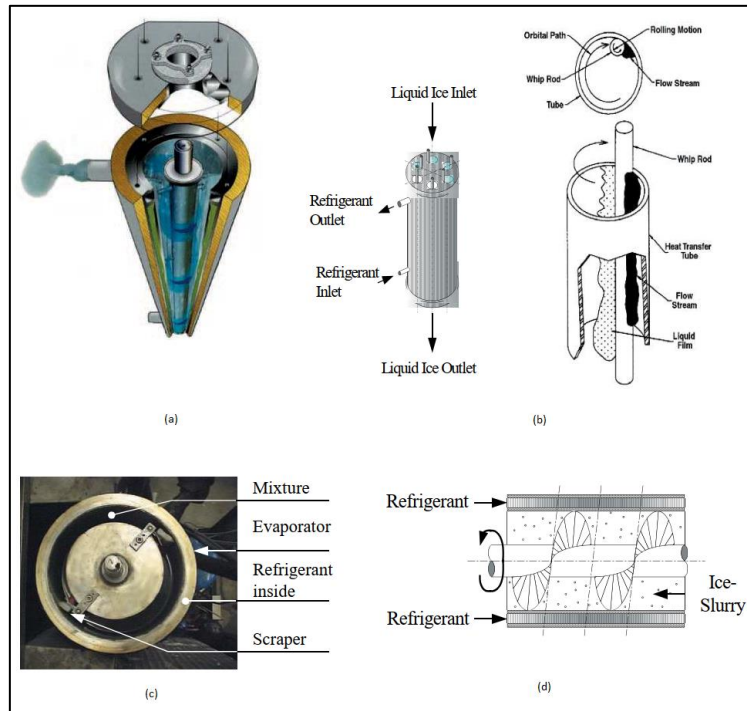


Figure 14: (a) Scraped-surface ice slurry generator (b) Orbital rod ice slurry generator (c) Scraped-surface ice slurry – top view (d) Scraped-surface ice slurry with a helical screw– cross section [31]

In addition to reducing the thermal resistance and increasing the heat transfer rate through agitation, the scraping action also enables the crystals to flow axially. These crystals, in turn act as a seed and acts as a nucleation spot and creates more crystals. Thus, the scraped surface ice slurry generator produces a mixture of small ice crystals and water (i.e., ice-water slurry) from a binary solution.

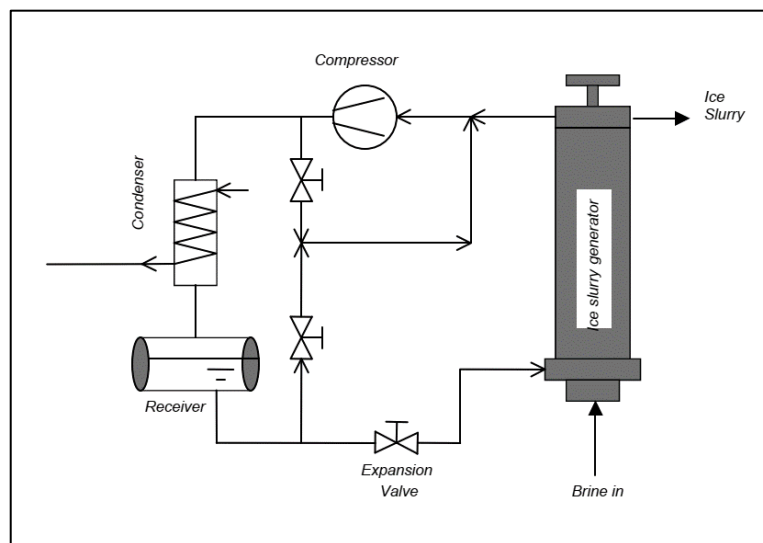


Figure 15: Schematic diagram of an ice slurry generation system [31]

As Figure 15 depicts, a refrigerating unit, typically consisting of a compressor, condenser, and an expansion valve, delivers the refrigerant to the shell-side of the ISG. The refrigerant evaporates at low pressure through the outer pipe of the ISG, withdrawing heat from its surroundings, and thus, cools the incoming solution that flows through the inner pipe. Here, cooling is done indirectly, and ice slurry is generated on the tube side. At the evaporator exit, the superheated refrigerant vapour is sent through a compressor and condenser at high pressure and the cycle continues.

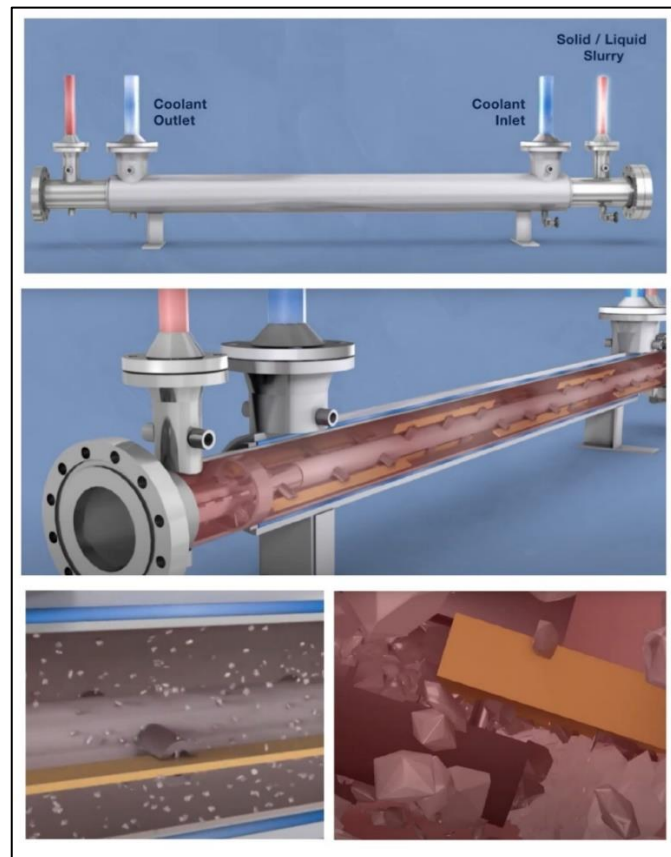


Figure 16: Working of a scraped-surface ice slurry generator with rotating blades [67]

As Russell et.al state in their work [68], the rate of nucleation chiefly depends on the degree of supercooling at the wall, which in turn is inherently dependent on the refrigerant temperature. Therefore, by operating the units at high temperature difference between the refrigerant and ice slurry flows, one can obtain improved heat transfer rates. However, as the refrigerant temperature is lowered below a certain limit, the heat duty is reduced owing to a low thermal length [69]. Although the addition of a freezing point depressant innately drives down the temperature driving force, it helps in reducing the probability of ice formation in the heat exchanger and hence a trade-off must be made to ensure efficient functioning of the scraped surface ISG [31].

Figure 17 summarises the typical specifications of the scraped surface ISGs and OREs. Depending on the application, one chooses either the scraped-surface ISG or the orbital rod evaporators (ORE). The former uses an electric motor to propel the scraper blades at speeds of ~450 rpm. A higher rotational speed results in a higher heat transfer rate, but this comes at the cost of increased power requirements. They have a wide range of refrigerant capacity (10-1400kW) and are available in both horizontal and vertical setups, with the tubes being around 2m long and the ice slurry generation side having a diameter of about 15cm. They provide the benefit of being modular, making the expansion of such a system straightforward, while this is not the case with the OREs.

	Scraped-surface	Orbital rod
<b>Ice slurry side</b>		
Tube material	304 grade stainless steel	304 grade stainless steel for NH <sub>3</sub> Copper 122 for HCFC
Freezing point depressant	NaCl, ethanol, glycol	NaCl, ethanol, glycol, urea
Crystal sizes	250 to 500 μm	50 to 100 μm
Heat transfer area	0.85 m <sup>2</sup> per tube	0.13 m <sup>2</sup> per tube
Tube length	1.8 – 2.4 m	1.20 m
Flow rate per tube	10-23 litres/min	6 litres/min
Ice fraction change per tube	15%	6-8%
Nominal cooling capacity	21-85 kW	10-1800 kW
Agitation mechanism	Plastic scraper blades	Metal orbital rods
Agitation speed	450 rpm	850 rpm
Power requirements per heat transfer area	1.2-1.8 kW/m <sup>2</sup>	0.22 kW/m <sup>2</sup>
<b>Refrigerant Side</b>		
Refrigerant type	R22, R404, R717	NH <sub>3</sub> , R22, R717, R134a
Evaporating temperature	-10 and -19°C	-10 to -8°C for stainless steel -10 to -4.4°C for copper tubes
Typical refrigerant flow rate	0.15 kg/s	matches instantaneous evaporator capacity
<b>Economics</b>		
Cost	US\$300 - \$600/kW	US\$160/kW

Figure 17: Specifications for ice slurry generator – scraped-surface and OREs [31]

On the other hand, OREs are falling-film type ISG and are essentially assembled in a vertical orientation to accommodate the vertical spinning rods [70]. The effect of this rod is to agitate by creating a turbulent flow of fluid around tube, thereby enhancing the tube side film coefficient. Thus, the agitated flow also prevents the ice crystals from sticking to the surface. The falling film liquid performs the role of a lubricant and thereby minimises wear and tear and along with the centrifugal force, this ensures that the rods do not come in contact with the walls [70]. They require lesser power per m<sup>2</sup> (~0.2 kW/m<sup>2</sup>) as compared to scraped surface ISG (~1.2-1.8 kW/m<sup>2</sup>) [31].

From an economic standpoint, the scraped-surface ISG are more expensive, costing between 300-600 USD/kW. As Gladis et al., stipulate in their work [70], OREs are one of the most economical methods of generating ice slurry, with a capital cost of about 160 USD/kW and a cost of ~USD 550 per ton of ice produced. Even though they have a high capital cost, the scraped-surface ISGs are available in all sizes, with smaller units requiring less power and this results

in shorter payback periods [71, 70]. One thing to consider while doing a cost-benefit analysis before investing in ISGs is the wear of rods and blades over time and their replacement cost and duration.

The ice fraction to be generated by the ISG is dependent on the application and the scraped surface ISG has an upper limit of 35%. On further recirculation of streams and cascading heat exchangers, one could achieve higher ice fractions as well. The size of the crystals generated is dependent on the agitating speed and the additive added. Studies have shown that the scraped-surface ISG produces homogeneous ice slurry with crystal size ranging from 25-250 $\mu\text{m}$ , while OREs could produce ice crystals of sizes between 50-100  $\mu\text{m}$  [71, 31].

Since our application entails using the Baltic seawater, which is less saline, from an additive concentration viewpoint, this is less likely to be feasible. A lower concentration of freezing point depressant results in increased freezing up of walls and thereby resulting in higher scraper power requirements. In addition, the high investment costs and the constant need for maintenance and replacement of the rotating blades and rods because of wear [31] makes this system not suitable for our purpose.

### 3.2 Direct Contact Ice Slurry Generators with Immiscible Primary Refrigerant

One method of ice slurry generation is by using direct contact generator with immiscible refrigerant. This has been in the works since the late 80s, with some works focussing on its application of desalination of sea water [31]. As the name suggests, the immiscible refrigerant is expanded and then infused into a tank where it vaporises. Thus, on evaporation, the water cools and is in a supersaturated state and ice crystals are formed which are then dispersed. An additional equipment in the form of injection devices is required in the tank where evaporation occurs to distribute the primary refrigerant to ensure a homogeneous slurry formation throughout and to induce turbulence that aids in slurry formation. A schematic diagram is shown in Figure 18.

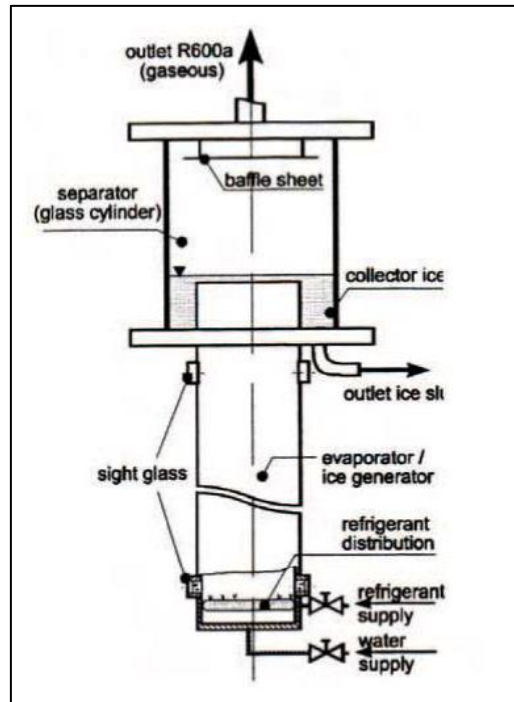


Figure 18: Schematic illustration of a direct contact ice slurry generator [72]

As depicted in Figure 19, in the COLDECO-process, the refrigerant is expanded and then injected into the evaporating tank and mixed with the water [73]. The refrigerant, being immiscible, evaporates, while the water cools down and transitions to a well-circulated ice slurry. Since there is no intervening heat transfer surface between water and the refrigerant, attrition of ice on a solid does not occur. As it was the case with the scraped-surface ISG, the components must ensure smooth slurry transport and blockages should be avoided.

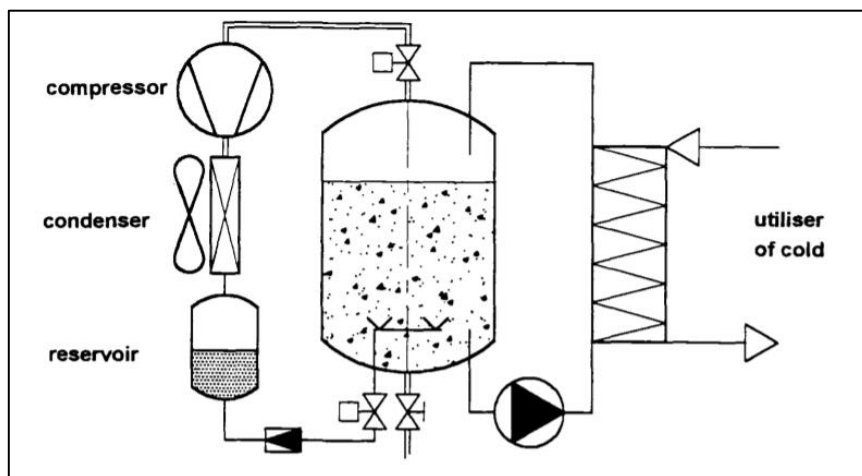


Figure 19: Schematic representation of the COLDECO process [73]

The absence of any physical boundary between the refrigerant and the ice slurry is the major advantage in this system and this results in reduced power requirements, reduced investments (no heat transfer surface) and increased heat transfer rates. The evaporator tank doubles up as a storage tank, and this is an added benefit as well [72]. Scaling up is not straightforward as several of these generators should be assembled in parallel and this reduces the economic benefits usually associated with scaling up of systems [31].

However, due to the pressure differential between the system and the atmosphere, possible withdrawal of the slurry formed in the tank might pose an issue [31]. It should be ensured that the injecting devices, which add to the investment cost and reduces the efficiency of the system, should be fabricated in such a manner that there is no threat of ice formation on themselves and should ensure uniform distribution.

The maximum ice fraction realised in a direct contact ISG, as reported by Fukusako et al. is 40% [74]. At 40%, the flow is hindered due to the high viscosity and thus, flow of it is challenging. Another issue that is encountered in this system is the refrigerant – even if it is immiscible with water, they are trapped in the ice slurry when they crystallise. Now, in our application, we do not utilise the slurry for any purpose and pump it back into the sea and consequently, these potentially unsafe refrigerant-trapped ice crystals pose a threat to the aquatic life and a serious impact on the environment. There are a few direct contact generators with immiscible primary refrigerant built on a laboratory scale [32, 72, 73], and with the usage of an environment friendly refrigerant, this method for our application might be a feasible choice, but they are yet to be commercialised and hence, are not pursued further for this study.

### 3.3 Direct Contact Generators with Immiscible Secondary Refrigerant

Another variant of the direct contact heat exchanger was reported by Fukusako et al. in their work [74]. The schematic of such a direct contact ice slurry generator is illustrated in Figure 20. Here the primary refrigerant cools down an immiscible liquid, which is then sprayed into the feed water, using injectors for direct evaporation. In contrast to the previous method, the advantage here is that the miscibility of the primary refrigerant with water is immaterial. However, the non-soluble liquid must have a higher density and a lower freezing point than water.



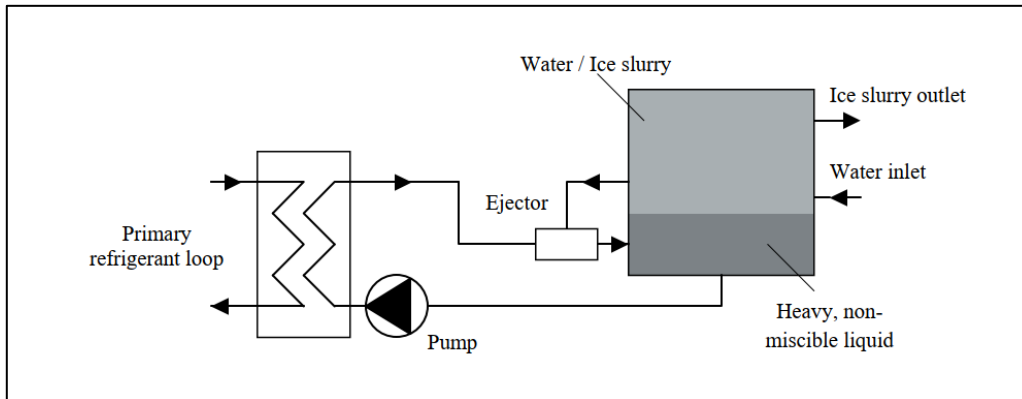


Figure 20: Schematic diagram of a direct contact liquid coolant type ISG [31]

Another difference is that, in this system, there is an additional cycle in which a heavy, non-soluble liquid transfers heat amid the ice slurry loop and the primary refrigeration cycle. This results in increased investment costs and energy consumption. This liquid is cooled by the evaporator of the primary cycle and is mixed with water/ice solution in the ejector. Ice crystals begin to form in the generator owing to the lower temperature of liquid, which is below the freezing point of the solution. And as a result, due to density difference, the crystals rise upward and the liquid settles to the bottom and the cycle continues. Some applications of this system could be found in the referenced literature [74, 75, 76].

In this system as well, some portion of the heavy, non-miscible liquid is trapped in the crystals and when it is pumped back to the sea, it becomes an environmental hazard. As stated in the previous chapter, utilising an eco-friendly refrigerant might make it viable from a safety viewpoint, but owing to high investment and energy costs [31] and lack of commercialisation, the suitability of this method for our application is not investigated any further.

### 3.4 Supercooled Method

Another approach in generating ice slurry is using the supercooled technique (Figure 21). In this mechanism, the water is supercooled to a temperature below the freezing point. The water is then 'released' from this state, undergoing phase change as it flows. This slurry is then fed to an ice slurry storage tank where due to density differential, water, and ice separates. It should be ensured that the water sent to the supercooler is free of ice crystals that could bring about secondary nucleation. There are different variants of this method, with the differing characteristic being the type of supercooler (Shell & Tube type/ Plate-type) and the type of releaser (Falling to pipe/ Falling to tank/ Ultrasonic waves/ Mechanical vibration). [31, 77].

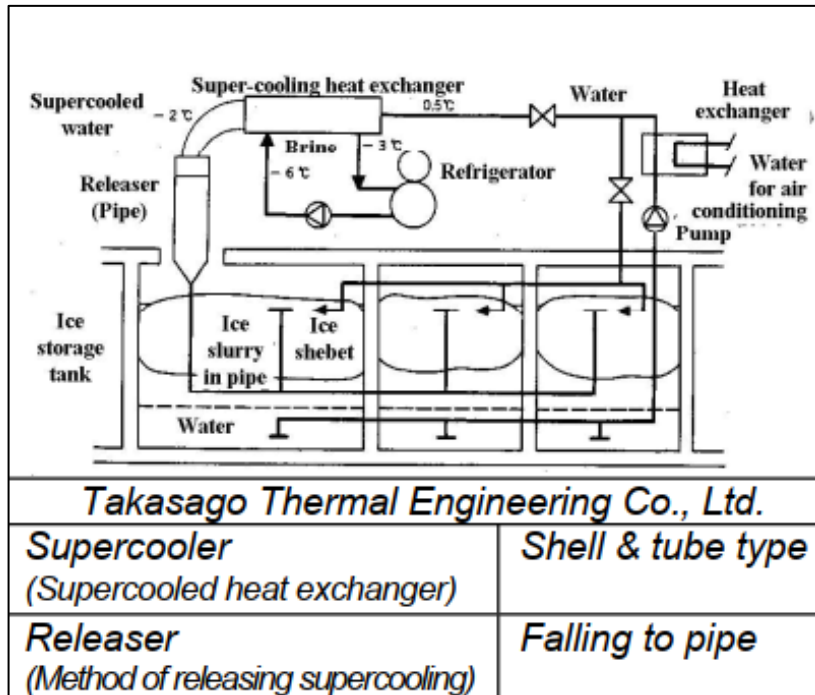


Figure 21: Supercooled large-scale on-site-type system by Takasago Thermal Engineering Co., Ltd [78]

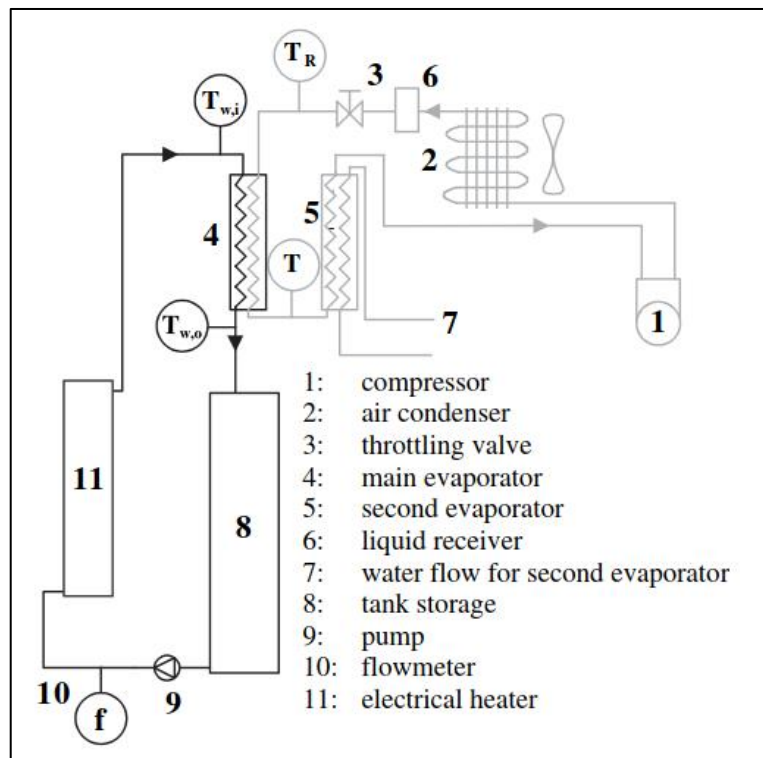


Figure 22: Schematic diagram of an experimental setup of a supercooled ice slurry generator [77]

One specific work [77] is studied further to understand the working in detail. In a supercooled ISG, the system usually consists of a refrigeration circuit and an ice slurry flow circuit. The former consists of components depicted in grey in Figure 22 and is used to cool down the water exiting the first evaporator. In their work, Bedecarrats et.al used R134a as the refrigerant [77]. This loop is in charge to cool down the water passing through the first evaporator and the second evaporator ensures complete phase change of refrigerant. The components in the ice slurry loop are illustrated in black colour in Figure 22. The tank receives the supercooled water from the evaporator, and as it exits the heat exchanger, ice slurry is formed. Water and ice crystals later separate due to difference in density.

This technique uses exclusively pure water for the generation of ice slurry. As a result, in our application, where we use seawater directly, this would not be suitable. Seawater from the Baltic sea without filtration, contains  $\alpha$ -chlorophyll, impurities and other inorganic salts that would result in crystallisation of the water at an undesired location, and this might lead to blockage of pipes. As a result, this approach is not investigated any further.

### 3.5 Hydro-Scraped Ice Slurry Generator

By controlling the flow rate of the ice slurry and the evaporating temperature of the primary refrigerant, ice slurry with high concentration of freezing point depressants can be generated in standard heat exchangers [31]. As the name suggests, in this approach, the ice crystals are scraped away by the fluid itself.

As shown in Figure 23, the hydro scraped ISG consists of a primary refrigeration loop and a secondary refrigerant or ice slurry flow loop. The components and working are described below.

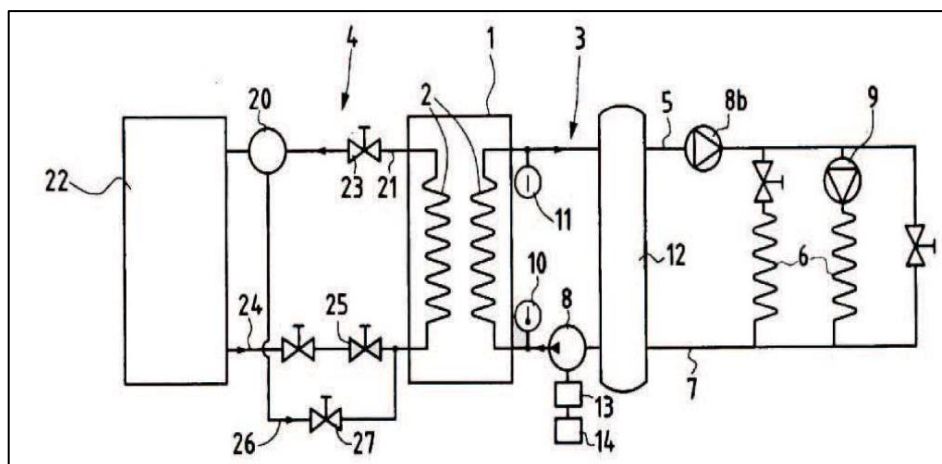


Figure 23: Schematic of the hydro-scraped ice slurry generator [31]

- Primary refrigeration cycle: Evaporator (1), Compressor (20), Condenser (22), Regulation valves (23, 27), Expansion valve (25)
- Ice slurry loop: Pump (8), Temperature gauge (10, 11), Storage tank (12), Variable speed motor (13), Control box (14)
- Distribution of ice slurry: Distribution line (5), Heat exchangers to melt ice slurry (6), Return line (7), Pump (8b)

The parameters determining the formation of crystals in the evaporator are temperature and pressure of the slurry loop. The increase in pressure difference between the input and output stream of the refrigerant and the decrease of the temperature difference is an indicator of formation of ice crystals. Then, the electronic controller increases the flow rate of the ice slurry because of which, turbulence is created, and the crystals start to disengage from the surface of the evaporator. The increase in velocity accompanying the increase in flow rate helps in removal of the forming ice crystals. Simultaneously, the refrigeration capacity is decreased and this aids in the removal as well. Ice slurry is then formed by the removed crystals in the secondary refrigerant flow. Now, the flow rate and the associated properties return to nominal conditions and the cycle resumes.

One could also apply special coating, like sol-gel, on the surface of the evaporator to avoid the adhesion of ice [31]. The absence of no moving parts like rods or blades, reduces the investment costs and the O&M costs. Nonetheless, salt-based solutions for ice slurry generation are inclined to present greater adhesiveness, and thus, are less suited for this type of ISG, unless a suitable coating material that solves this issue is developed.

### 3.6 Fluidised Bed Crystalliser

Klaren's work paved the way for ice slurry generation by the fluidised bed crystalliser method [31]. In this system, the primary refrigerant (for instance, ammonia) evaporates on the shell side, while ice crystals are formed on or near the inner periphery of the tubes. A fluidised bed, comprising of little steel or glass elements, with a radius of 0.5-2.5mm, is present within the tubes. As the ice slurry feed flow flows upwards in a liquid state, the particle beds are fluidised. This is followed by a constant impingement of the solid particles on the inner walls of the tubes, preventing a build-up of a layer of ice on the heat transfer surface and improved heat transfer rates. This mechanism is displayed in Figure 24.

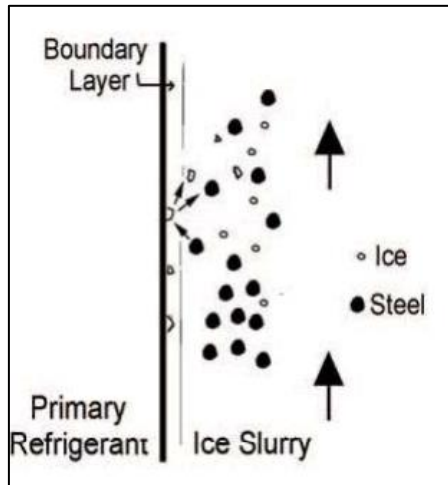


Figure 24: Ice Removal Mechanism in a Fluidised bed crystalliser [31]

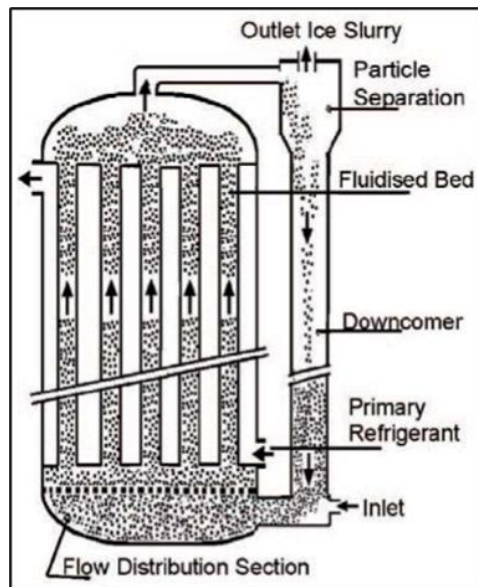


Figure 25: Schematic – Fluidised bed heat exchanger

A major advantage of this method is the low investment and O&M costs, because of no complex moving mechanical components, except for the pump [79]. Ice fractions up to 30% could be generated in a single pass, while multiple passes could be employed to generate a higher fraction of ice particles in the slurry.

Although this system has the above-mentioned benefits, certain limitations prevent it from being utilised for our application. Even though this has been working well in a laboratory scale, its commercial viability has not been tested. Since the current work calls for a district heat of  $\sim 300\text{MW}$ , scaling up without prior studies is not feasible. Since seawater is the fluid being used to generate ice slurry, the salt present in it might corrode the components. So,

components having materials like stainless steel, for example, should be coated with a non-corrosive layer. This increases the expenditure of the system. The vertical layout of the beds poses a space issue, requiring a lot of floor space and very high ceilings. With the proposed system planned to be built underground [46], this limitation makes it almost infeasible to consider this option. The trade-off between the allowable temperature difference between the refrigerant and the working fluid, and its relationship with the freezing up of the heat exchanging walls rounds up the reasons behind the non-pursual of this method for this work [79]. As a result, further attributes of the system, including the rate of residence, the velocity, circulation, presence of a cyclone etc., are not explored any further.

### 3.7 High-Pressure Ice Slurry Generator

As the term 'high-pressure ice slurry generator' implies, this technique employs the application of high-pressure to generate ice/ice-slurry. Otero et. al., in their work have described two high-pressure freezing processes that are described in brief below [80]:

#### *High-pressure assisted freezing (HPAF)*

In this process, ice or associated polymorphs are obtained by applying a constant high pressure and simultaneously reducing the temperature to the corresponding freezing point. Governed by thermal gradient, the cooling of the process fluid follows from the surface to the centre, with the nucleation of ice occurring in the outer periphery of the surface with the crystals growing in a dendritic manner towards the centre radially.

#### *High-pressure shift freezing (HPSF)*

Pascal's principle states that a pressure change at any point in an enclosed incompressible fluid is transferred throughout the fluid such that the change is reflected everywhere else. In accordance with this principle, a pressure release takes place almost spontaneously upon expansion throughout the entire sample and, consequently, a decrease in the temperature corresponding to the pressure drop is produced. This in turn results in a high degree of supercooling, and subsequently, higher nucleation rates [80].

There is another high-pressure freezing process known as high-pressure induced freezing wherein, phase transition is instigated by a rise in pressure and is sustained at the same pressure. This method has not been studied in detail and hence is not explored further [81].

In HPSF method, the transition of phase is induced due to a change in pressure that fosters metastable conditions and spontaneous ice generation. The change in pressure could be gradual, over several minutes, or rapid, within a couple of seconds. The kinetics of the freezing process depends on the level of supercooling attained, which in turn depends on the manner of release of pressure. Usually, water is compressed and then pre-cooled to a temperature close to its freezing point, where it remains in a liquid state. The pressure is then released, which causes uniform supercooling, which in turn causes uniform nucleation, which ensues the release of latent heat. This heat is absorbed, and the temperature rises to the freezing point and crystals are formed, the fraction being determined by the pressure and temperature before the expansion.

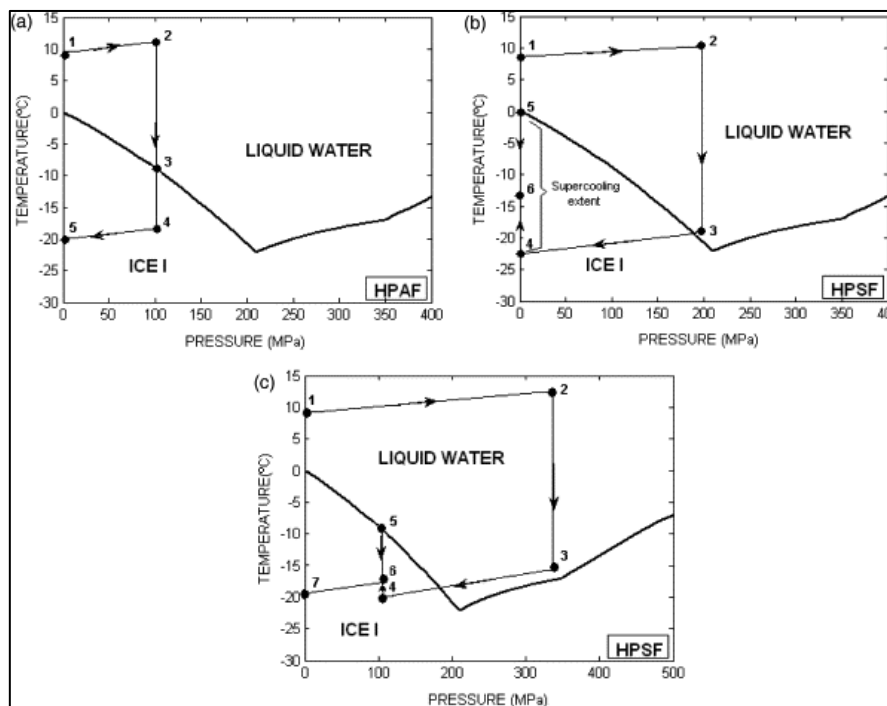


Figure 26: High-pressure freezing processes inserted on the phase diagram of water. (a) HPAF (b) HPSF with phase transition at atmospheric conditions (c) HPSF with phase transition under pressure [81]

One of the drawbacks of this process is the high economic cost of high-pressure equipment as compared to other ISGs. Also, it is common knowledge that the dendritic particles, characteristically elongated and rough in texture tend to form large, entangled clusters which results in plugging and hence, are considered far from optimal for ice slurry generation [82]. In addition, the current level of knowledge of high-pressure equipments for continuous processes also deters the author from exploring this technique any further.

### 3.8 Recuperative Ice Making

Contrary to other commercially available ISGs, wherein supercooling of a secondary fluid occurs in the evaporator with ice crystals forming on the surface and then later scraped off, in the recuperative ice slurry system, the ice formation on the cold surface i.e., ice buildup is reduced and it is removed at regular intervals through a recuperative heat exchanger.

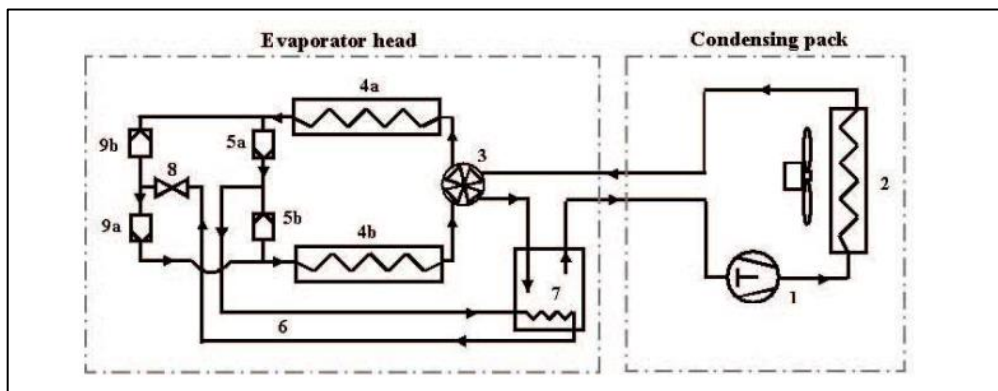


Figure 27: Refrigeration circuit for recuperative ice slurry generator [31]

As depicted in the Figure 27, the pair of heat exchangers (4a, 4b) act as the interface between the refrigeration loop and the ice-generating loop. Other numbered components include compressor (1), air-cooled condenser (2), reversible 4-way valve (3), heat exchangers (4a), (4b), check valves (5a), (5b), accumulator with heat exchange coil (7), expansion valve (8), check valves (9a), (9b).

The refrigerant flows from the condensing pack [consisting of a compressor and air-cooled condenser] and is fed to a reversible 4-way valve, which regulates the flow of refrigerant to either of the heat exchangers. Firstly, the hot exhaust gas from the compressor passes through the condenser and condenses in the heat exchanger (4a), releasing ice and raising the temperature. As the temperature increases, approaching that of ambient air, condensation starts happening in the condenser, with the warmer liquid flowing to (4a) at a controlled temperature. The sub-cooled liquid refrigerant then exits (4a) is then directed by check valves (5a, b) to an accumulator, and is then expanded at (8), resulting in wet vapour. This is then sent via the second set of check valves (9a, b) to the second heat exchanger (4b), which, takes up the role of an evaporator and acts as the site for generating ice crystals. The amount of flash gas formed is small because of the relatively low temperature change of



the refrigerant between the two heat exchangers, owing to the falling film. [31].

After a certain time, de-icing is done by reversing the refrigerant flow. Since, this process is done in a cyclical manner, this method is aptly termed recuperative. The corrugated/grooved surface of the turbo-chiller plate, creates a highly turbulent flow, leading to higher heat transfer rates.

One chief advantage of this system is its ability to generate ice slurry continuously without utilising moving components like scrapers or orbital rods. This reduces the investment costs and the O&M costs as well [31]. Further, since the evaporator operates at a higher temperature, this reduces the amount of freezing point depressant required. But the cost of the additional evaporator surface, difficulty in maintaining the cooling capacity of the refrigerant and lack of commercialisation at large scale dissuades us from actively investigating this method for our application.

### 3.9 Vacuum Ice Generation

The most efficient method of producing ice slurry using water utilises a direct contact heat transfer vacuum freeze process. Figure 28 shows the phase diagram for the three phases of water – vapour, liquid and solid. The idea behind this mechanism is that, at triple point, all three phases co-exist. As water molecules (maintained at triple point in vacuum) are evaporated, energy is removed from the neighbouring liquid particles, causing them to freeze and form ice particles [83]. Let us now delve deep into the system.

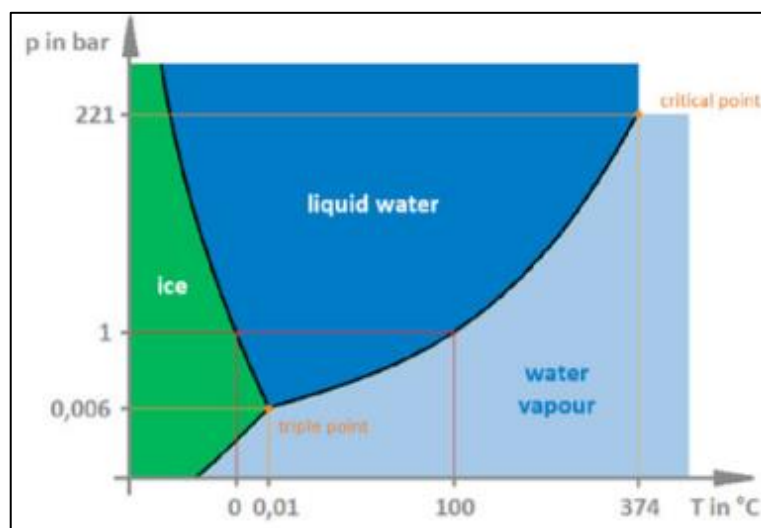


Figure 28: Phase diagram of water indicating the triple point [33]

Figure 29 depicts the schematic illustration of a vacuum ice generator. The numbered components relevant to the ice slurry generation are evaporator (1), compressor (2), heat exchanger (3), ice slurry pumped out (4,5)

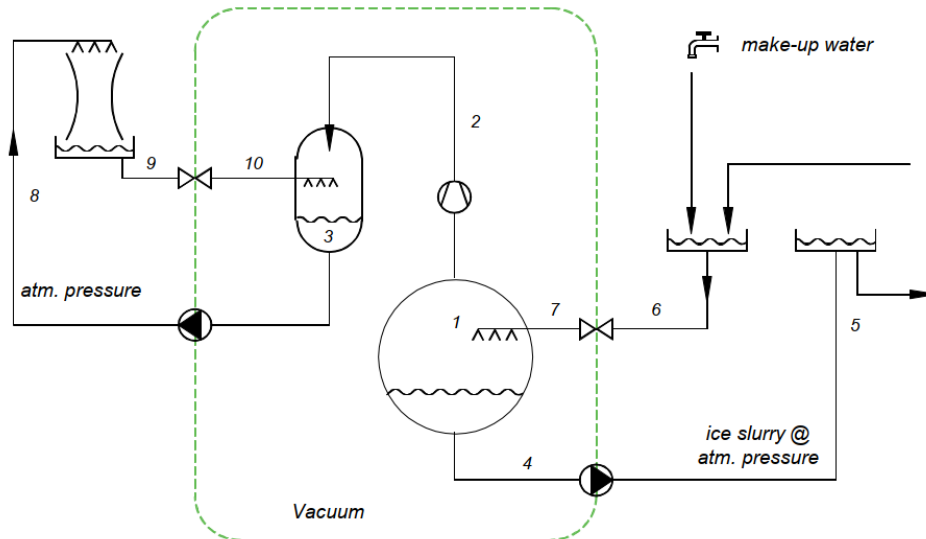


Figure 29: Vacuum ice generation with water as refrigerant [31]

The evaporator contains a pure water or saltwater solution and is maintained at near the triple point conditions. The water is evaporated in the evaporator (1) and compressed to condenser pressure at (2). Owing to the low pressure and correspondingly, low density of water vapour, compression of it is a cause of concern. However, some institutions have developed solutions in the form of centrifugal compressors and turbo compressors. Since seawater contains dissolved gases that are non-condensable, over a period of time, they start to build up, leading to increased pressure on the condenser side. To avoid it, and thereby, reduce the work done by the compressor, a vacuum pump is required on the condenser side. [32].

If pure water is used, freezing up of the walls of the evaporator might occur and defrosting cycles become necessary. When used in combination with seawater, the vacuum ice generator partly freezes the water, leading to larger enthalpies being removed (latent heat) as compared to sensible cooling of sea water in conventional heat pumps [31]. For our specific application, we need to utilise seawater in the winter, exhibiting temperatures just above freezing point, as a heat source.

A similar system was in operation from 1986 till it was decommissioned in 2005 in Denmark. In addition, ILK Dresden are attempting to establish a similar system as well. The two systems are studied in detail subsequently.

## Augustenborg DH system [83, 84]

This sub-section describes the vacuum ice generator pilot plant, used as a heat pump, with seawater as source for the Augustenborg District Heating Plant. For this process to be continuous and functioning over long periods of time, the water vapour needs to be extracted continuously. For pure water, at triple point, the pressure is 6.103 mbar abs, and the temperature is 0.01°C. But since, seawater is being utilised, the triple point pressure depends on the salinity of water ( $S$ ) as well in the following manner:

$$P_t = 6.103 - 0.246 S \text{ (mbar)} \quad (1)$$

Since the pressure is very low, at around 6mbar, the density of the water vapour is low as well. This poses a problem while compressing it owing to the large required swept volume, but some establishments such as IDE, Solid Energy etc., have developed solutions to combat this cause of concern. This vacuum ice maker (VIM) works well with all water temperatures and is therefore suited for being used in a DH plant.

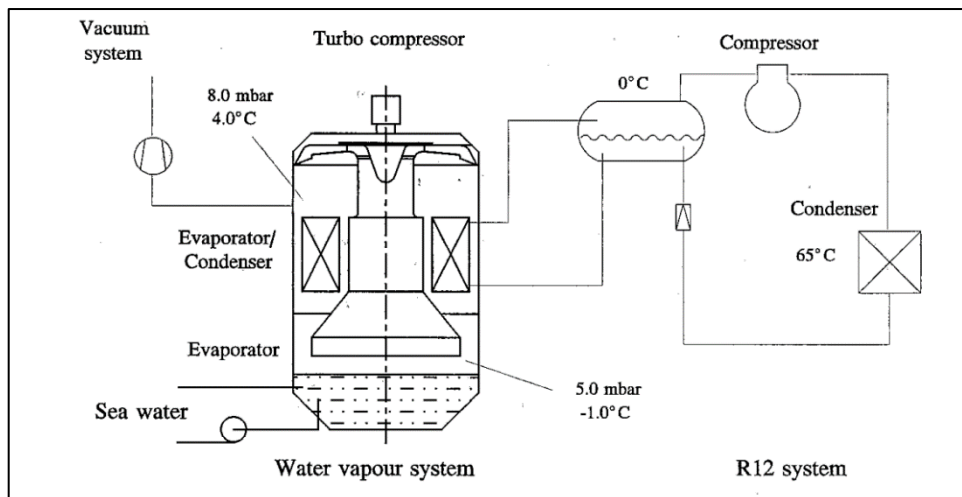


Figure 30: Schematic illustration of the vacuum ice generation system for Augustenborg DH plant [83]

Figure 30 displays the schematic diagram of the plant in Augustenborg. Sea water was initially fed to the evaporator, which was maintained at triple point condition of 5 mbar, -1°C for the corresponding salinity level of around 4.5‰. As the vapour evaporated, it passed through a turbo compressor (swept volume of  $\sim 75 \text{ m}^3/\text{s}$ ) and a pressure ratio of 1: 1.45, corresponding to a temperature increase of about 5°C. The refrigerant cycle employed R12 as the

refrigerant. The water vapour condensed at  $\sim 0^{\circ}\text{C}$ , while the refrigerant condensed at  $\sim 65^{\circ}\text{C}$ . Meanwhile, in the evaporator, partial freezing occurred, and an ice-water slurry was generated, which was then pumped back to the sea. A vacuum pump was placed on the condenser side of the heat exchanger to remove the non-condensable gases.

This system was built in conjunction with associated electric motors powered from a generator, driven by a direct coupled Liquefied natural gas (LNG) motor to enhance the transfer of energy, as depicted in Figure 31. To optimise the COP of the compressors, heat transfer from the condenser to the DH system was done in stages. The whole system and the associated LNG motors, its economic analysis, although interesting, is of less priority in this work, which focusses on the technical aspects. More details about the system could be read in the [Appendix section A1](#).

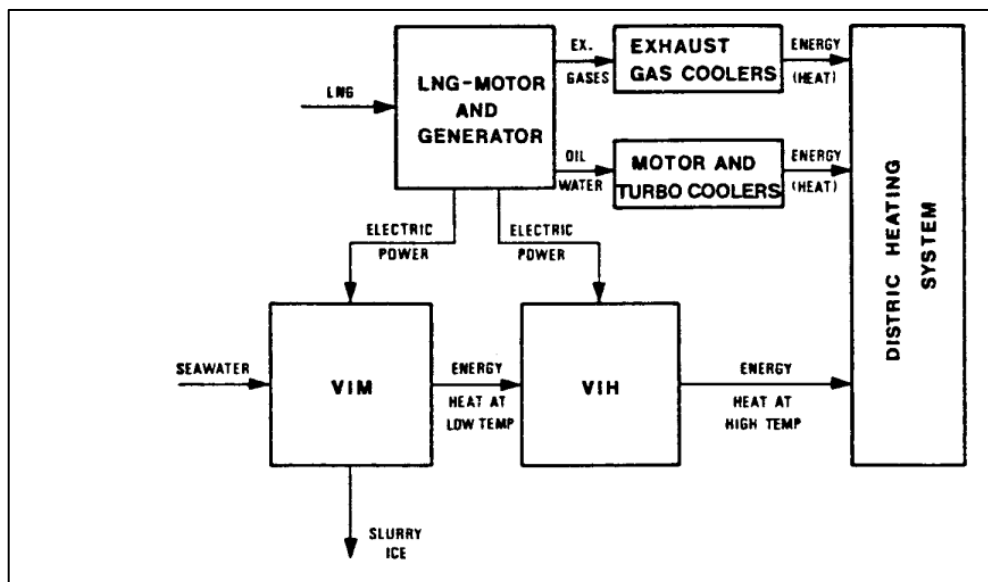


Figure 31: Vacuum Ice generation plant connected to the Augustenborg DH system [83]

### ILK DRESDEN [33, 85, 86]

ILK Dresden are developing a similar ice slurry storage system using vacuum ice slurry generation method. To tackle the vapour compression issues, they have developed their own turbo compressors. This system is diverse in application – it could be integrated in existing DC networks or chilled water network (Figure 32) or be cascaded with heat pumps to satisfy DH demand. The charging and discharging capacity can be varied according to the application by choosing an apposite heat exchanger.

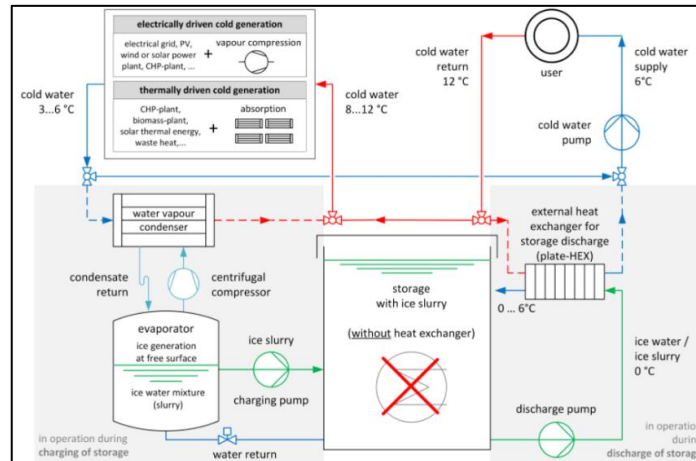


Figure 32: Integration of vacuum ice slurry generation with a chilled water network [33]

A pilot plant with 90m<sup>3</sup> slurry storage unit has been designed to operate in operation at the Westsächsische Hochschule Zwickau. A maximum of ~500kW of refrigerating capacity/ice slurry generation could be achieved by utilising a single compressor [87]. The storage unit allows for flexibility in operations and reduces the discrepancy between the supply and demand, along with a reduced fiscal strain, if charged during low tariff periods. In addition, the stored ice slurry, which is pumpable as well, can also be utilised for process cooling as a coolant.

This system uses R717 as a refrigerant. Refrigerant grade Ammonia is commonly used in industrial refrigeration plants and is of safety class B (toxic). However, since ammonia is hazardous and a leak could potentially cause severe injuries to those handling it in the plant, intensive safety regulations are to be met [88]. A 3D illustration of a water vapour compressor in the vacuum ice slurry generation system of the experimental plant is displayed in Figure 33.

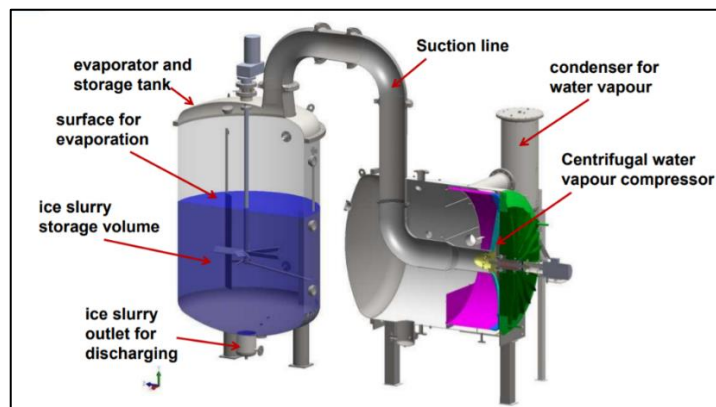


Figure 33: Design of the experimental plant in ILK Dresden presented at the ATMOSphere Europe 2013 conference [29]

It is now observed how this system could be used in heating applications. Integration of heat pumps in DH systems is a chief contributor towards increased cleaner energy shares. This system developed at ILK Dresden enables the use of water, even during winter, as source of heat without the risk of frosting. This makes this system and the one in Augustenborg ideal ‘prototypes’ for our application. The system could be used to generate heat in the following manner, as depicted in Figure 34.

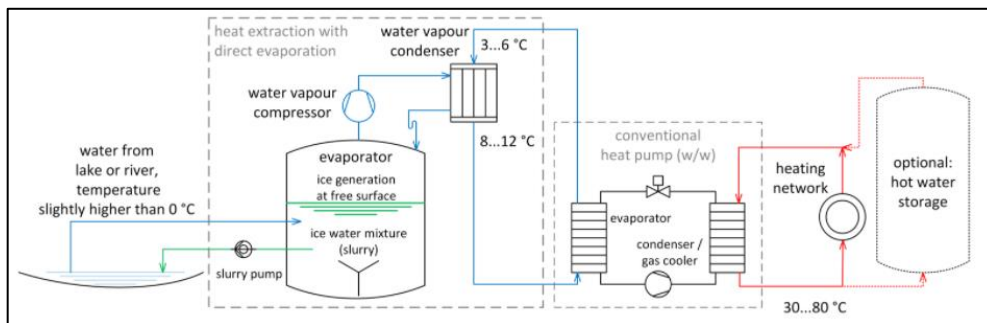


Figure 34: Cascading of heat pumps enabling the use of water at  $\sim 0^{\circ}\text{C}$  as a heat source [33]

Water is initially taken from a water source (at temperatures close to  $0^{\circ}\text{C}$ ) and fed to an evaporator. The evaporator is maintained at triple point and the vapour is compressed by a specially designed turbo-compressor that raises its temperature by a small value. This in turn, causes the partial freezing of water and ice-slurry is formed that could be either stored or pumped away. The vapour is then passed through a heat exchanger (condenser), with heat being transferred to a refrigerant. The heated refrigerant, then transfers the heat to the water to be heated through a conventional heat pump cycle. Thus, the temperature of the hot water is raised to the desired levels. This is how this vacuum ice generation system designed by ILK Dresden could be integrated with heat pumps for heating purposes.

The above two large-scale applications of using ice slurry in DH played a pivotal role in the selection of vacuum ice generation method for our work. We then proceed to model the vacuum ice generator, in combination with a heat pump to produce the necessary District heating in Aspen Plus.

## 4. Modelling in Aspen Plus

This section includes all the aspects regarding the modelling of the vacuum ice generation + District Heating system. Moreover, upstream and downstream system characteristics, choice of refrigerant, heat exchangers, ice slurry pumping are also described to get a better understanding of the system level design.

### 4.1 Introduction to Aspen Plus

Aspen Plus is a product of Aspen Technologies, which was founded in 1981. It is a process simulation software package, i.e., it is a modelling tool that enables the user to design a process and select suitable thermodynamic models and it simulates it using appropriate mathematical models and envisages the performance of the process. It is further used to optimise a process from a technical and economic standpoint, perform sensitivity analysis, maximise, and minimise functions. Despite being a sequential modular simulator, Aspen Plus has multiple functionalities and could be used to simulate complex processes involving reactors, compressors, pumps, distillation columns, flash system, electrolytes, crystallisers, heat exchangers etc., and it finds its application in chemical process, oil, and gas, pharmaceutical, food and beverage industries, to name a few. Owing to the above-mentioned reasons, it was chosen to model the vacuum ice system in Aspen Plus and analyse the technical viability of it. [89, 90, 91].

### 4.2 Choice of Refrigerant - R1234ze

HFCs (Hydrofluorocarbons) like R134a, R404a are one of the most used refrigerants across the globe. But, due to rising environmental concerns, HFCs are being phased out and being replaced by alternatives having lower GWP and ODP levels. With the advent of HFOs (Hydrofluoro-olefins), a class of environment-friendly refrigerants having low GWP values and abiding by Kigali amendment of the Montreal Protocol, this certainly seems to be beginning of the end for HFCs. With desirable GWP, ODP values and good thermodynamic properties, HFOs have already been adopted in several parts of Western Europe, while other countries are following suit [92].

One among the HFO refrigerants - 1,3,3,3-tetrafluoropropene, commonly known as R1234ze, was developed to adhere to the F-gas regulation laid down by the European Union [93] to control emissions from fluorinated greenhouse gases. R1234ze, being more energy efficient than conventional refrigerant like R404A, is utilised in several medium temperature

applications such as heat pumps, chillers and in industrial cooling [94]. It has a boiling point at 0 bar (g) of  $-18.95^{\circ}\text{C}$  and thus, it is similar to R134A in this sense [95]. The physical properties of R1234ze are displayed in in Table A. 2 in the appendix. Further, an EIA report in 2021 [96] recommends the use of R1234ze as the refrigerant for the seawater heat recovery project (“Lämpöpumppujen kylmäaineista todennäköisin on HFO-yhdiste R1234ze (GWP<sub>100a</sub>=0”). Owing to the aforementioned reasons, the refrigerant R1234ze is considered to be the refrigerant for our work.

## 4.3 The Aspen Plus Model

### 4.3.1 Overview

Let us look at the overview of the system that has been modelled in Aspen Plus to produce 300MW of district heat (Figure 35). The components and the parameters are explained in detail later. As we can see, seawater initially enters the evaporator (EVAP) and as mentioned in the preceding section, it is maintained at triple point. The triple point pressure is calculated according to equation 1. Now, on the application of very small amount of heat, a molecule of water turns into vapour and travels to the water vapour compressor (H<sub>2</sub>O-COMP), while due to removal of heat, ice is generated at the slurry generator. In this work, the vacuum ice slurry generator is modelled in two stages and the heat duties are set to be the same. The two components include the evaporator from which the supercooled liquid exits and the cooler (ISG) which produces ice slurry at desired fraction.

The compressed water vapour (S4) exchanges heat with the cold refrigerant (R1234ze) flowing through a heat exchanger (HEATX-1). Once heat has been exchanged, the water vapour stream, in a liquid state (indicated in green colour), is recirculated back to mixer (B8) where it is mixed at atmospheric pressure along with incoming seawater and enters the evaporator.

The refrigerant which is now in a vapour state (S7) is raised to a higher pressure by means of a compressor (REF-COMP). Now, this refrigerant is fed into a heat exchanger (HEATX-DH) where it condenses, releasing heat and raising the temperature of the DH water from  $45^{\circ}\text{C}$  to  $90^{\circ}\text{C}$ . This heat exchange is an integral component of the system and serves to recompense the  $\sim 300\text{MW}$  lost due to the retiring of the Salmisaari CHP plant. The refrigerant now, after the exchange of heat is now in a cooled state (COOL-REF) and is now reduced to the initial pressure by means of an expansion valve. The refrigerant is then re-circulated back to HEATX-1 and the cycle continues.



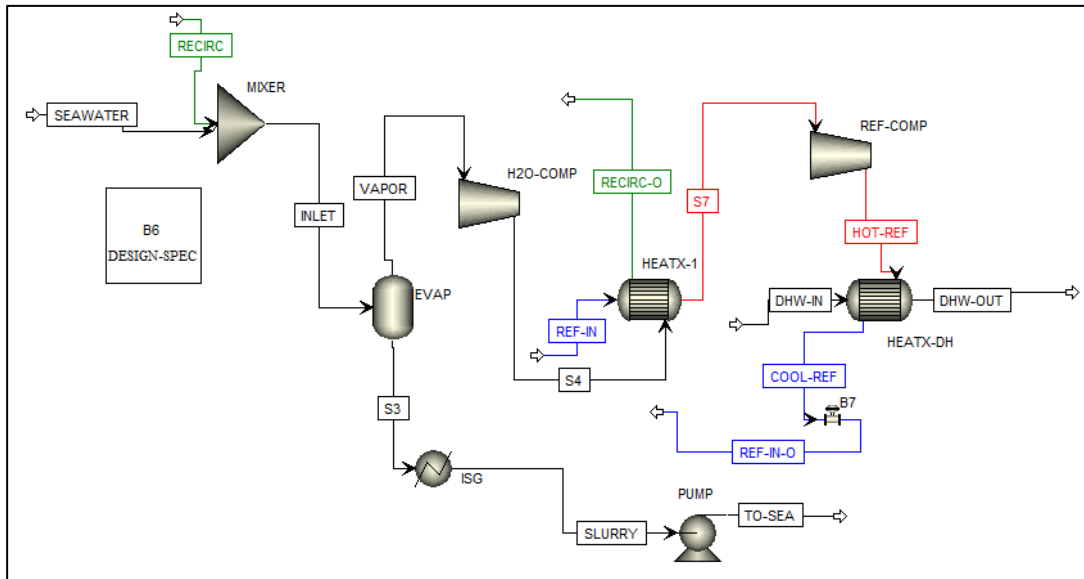


Figure 35: Process Flowsheet of the simulated model in Aspen Plus

On the other hand, the ice slurry generated by the generator is now discharged back into the sea. But since there will be a pressure loss accompanying the transport of ice slurry through long distances (in this case, about 500m [45]), this necessitates the involvement of a pump. The pump then increases the pressure by an amount equal to the drop incurred by the transport of ice slurry, and thus, the ice slurry is pumped back into the sea.

#### 4.3.2 Components and Setup parameters

The challenging part here is the determination of mass flow of input (mass flow of seawater). It should be fixed such that the ice slurry generated is of desired ice fraction and the district heat produced is what is required. For this purpose, a Design-spec is used (B6 in Figure 35). It is similar to a feedback controller, wherein the desired value for a variable is specified and another variable is manipulated to obtain it. In this case, the mass flow rate was varied such that the ice slurry generated has a liquid fraction of 80% (LFRAC = 0.8) and thereby, ice fraction of 20%. This is illustrated in Figure 36. The reasoning behind utilising slurry having 20% ice fraction is explained in the next section.

Design specification expressions	
Spec	LFRAC
Target	0,8
Tolerance	0,01

Figure 36: Design specification to set the liquid fraction of the generated slurry as 0.8.

For the Mixer, it is set such that the incoming seawater and the recirculated water are combined into a single stream at atmospheric pressure.

The inlet seawater properties are as illustrated in the Figure 37. The temperature and pressure were set to  $\sim 0^{\circ}\text{C}$  and 1 bar respectively to model conditions during winter [45]. Further, the 0.6% saline seawater [51] was modelled as water + sodium chloride proportionately. The mass flow calculations are initialised at 3000kg/s and based on the design-spec are iterated till the desired value is reached.

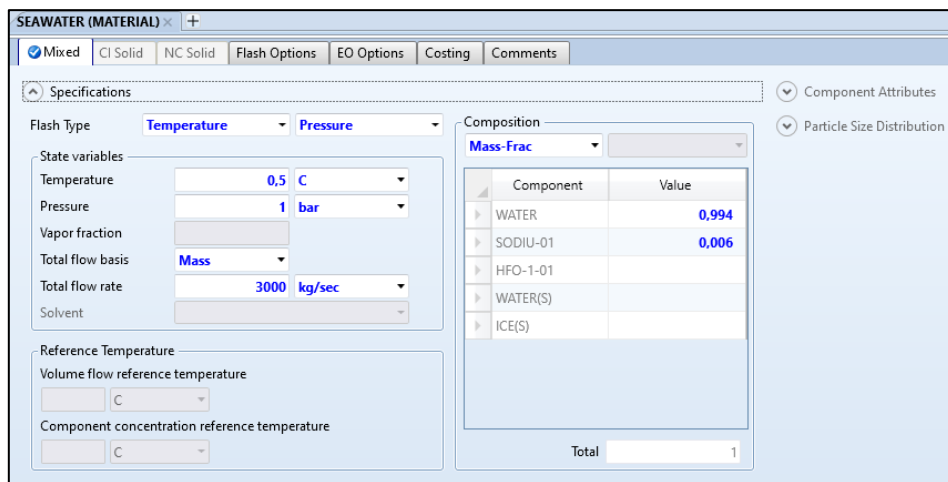


Figure 37: Inlet seawater properties in Aspen Plus

As mentioned earlier, the evaporator is set to triple point conditions as depicted in the Figure 38. Here, in Aspen Plus, the evaporator is modelled using separator Flash2, which determines the thermal and phase conditions of the inlet stream on specifying the outlet conditions. In this case, we specify the triple point pressure (equation 13) and the heat duty [97]. The valid phases are set to be vapour-liquid.

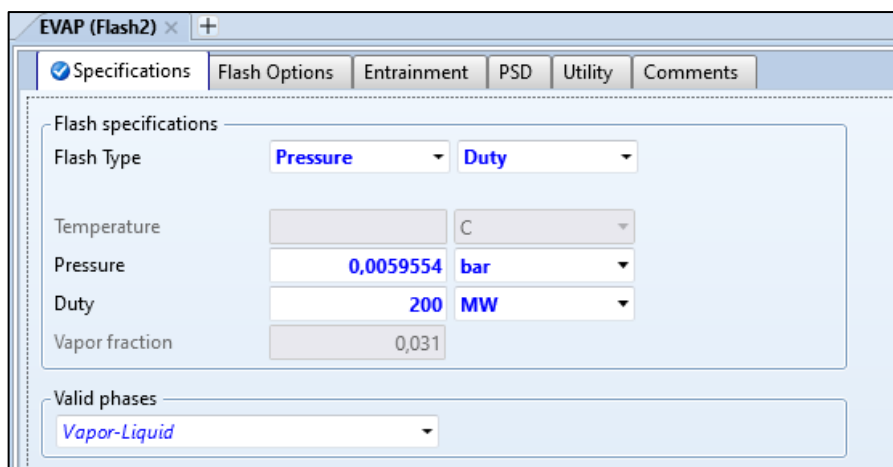


Figure 38: Evaporator specifications in Aspen Plus

The Flash2, in conjunction with the cooler (model Heater in Aspen Plus, denoted by ISG in Figure 35), constitutes the ice slurry generator. The heat duty and the pressure of the ISG was set to be the same as the evaporator. The slurry coming out of the ISG is to be pumped to a distance of about 1000m. The hydraulic and driver efficiency of the pump as set to be 75% and 90% respectively [98]. The pump outlet specification is set to ‘Pressure increase’ and the value is set based on calculations in the Section 6 and can be varied as per the requirement.

The water vapour compressor was set to type ‘isentropic’ and the pressure ratio was adjusted according to the condenser pressure. The efficiencies were set to be the default values [97].

The refrigerant used, R1234ze, acquires its properties from REFPROP in the Aspen physical property system. It provides thermodynamic and transport properties of fluids predominantly utilised in the industries, with particular focus on refrigerants and hydrocarbons [99]. It is ensured that the streams REF-IN and REF-IN-O have the same stream properties. The mass flow here is obtained on adjustment to ensure ~300MW of DH is produced. The input data of the refrigerant is displayed in Figure 39.

Component	Value
WATER	
SODIU-01	
HFO-1-01	1
WATER(S)	
ICE(S)	
<b>Total</b>	<b>1</b>


Figure 39: Input specifications for the refrigerant R1234ze

For the input parameters of the heat exchanger (HEATX-1), the model fidelity is set to ‘Shortcut’, which performs simple material and energy balance calculations. The flow direction is set to ‘countercurrent’ for optimal output and the exchanger specification for the cold stream output vapour fraction is set to be 1, meaning the refrigerant on passing through the heat exchanger should completely change into vapour phase.

The pressure ratio of REF-COMP is varied to a value slightly less than the critical pressure of the fluid [95] to have a high COP. The efficiencies are set to the default values [97].

The other heat exchanger, HEATX-DH, is designed in a similar way as HEATX-1, with only the exchanger specification being different. In this case, the cold stream output temperature is set to 90°C, which is the intended target [45]. The inlet temperature of the DH water (DHW-IN) is set at 45°C, based on Helen Oy's usual practice [45]. The expansion valve (B7) is set to release the fluid at its initial pressure of 1.5 bar.

One shortcoming of Aspen Plus is its inability to model closed loops. To work around it, the recirculating water stream (RECIRC-O & RECIRC) and the refrigerant stream (REF-IN-O & REF-IN) are split and the inlet values are set the same as the output values.

Prior to all this modelling in the simulation part, we need to define the properties and the materials in the Properties part. Since saltwater transforming into ice involves electrolytes, the base method was set as 'ELECNRTL' and the method filter 'COMMON'. Similar to REFPROP for the refrigerant, we use 'STEAM-TA' for District water properties. The model is then simulated by pressing the  symbol or the functional key F5.

A parametric study was done to determine the mass flows that would aid in the designing of a flexible system. And for this reason, the model was simulated for three cases by fixing the ice slurry generator capacity to 3 MW, 200MW, 300MW. The reasoning behind these numbers was 3 MW was the biggest ISG currently in commercial use [31, 100], while 200MW and 300MW were chosen with the idea that the ensuing DH produced would be comparable to what the city of Helsinki would require. Lastly, the pressure ratio of the water vapour compressor is varied to study how it affects the COP of the system. The results of this are then utilised in the next section to calculate the pressure drop for the resulting ice slurry generated.

### **4.3.3 Model Validation**

The pressure drop values obtained in the model developed in this work has been validated with the results obtained by IDE's ice slurry generator. The ice slurry generated at IDE's plant had a flow rate of 240 m<sup>3</sup>/h (1057 gpm). The pressure drop values in the system and the model developed were in agreement [45] and hence the work proceeded in this direction.

## 5. Pressure drop analysis of ice slurry during transport

Prior experiments have led to researchers concluding that ice slurry behaves as a Newtonian fluid at lower ice fraction (~20%) and as a non-Newtonian fluid at higher concentrations [101]. A Newtonian fluid is a fluid whose ratio of shear stress to that of shear strain (i.e., viscosity) is independent of the rate of shear [102]. In our case, the flow is assumed to be isothermal. For isothermal ice-slurry flow, the pressure drop could be calculated by means of Darcy-Weisbach equation:

$$\frac{\Delta P}{L} = \frac{f * \rho * v^2}{2 * D} \quad (2)$$

where the notations are as described in section Symbols and abbreviations

### 5.1 Pressure loss evaluation based on laboratory-scale experimental data

In this method, the pressure drop is expressed in terms of the diameter and mass flow. Subsequently, it would then be able to evaluate the pressure drop for our application by utilising pressure drop data from previous experiments for a certain mass flow and diameter.

We know the formula for pressure loss per length (equation 2). Here, one of the friction factor models is substituted for  $f$  and the velocity is written in terms of mass flow.

Mass flow rate,  $m$ :

$$\dot{m} = \rho A v \quad (3)$$

$$v = \frac{4 \dot{m}}{\rho \pi D^2} \quad (4)$$

Blasius friction factor model for turbulent flow [103],

$$f = 0.316 . Re^{-0.25} \quad (5)$$

$$f = 0.316 * \rho^{-0.25} * v^{-0.25} * D^{-0.25} * \mu^{0.25} \quad (6)$$

Substituting the above two into equation 2,

$$\frac{\Delta P}{L} = \frac{0.316 * \rho^{-0.25} * v^{-0.25} * D^{-0.25} * \mu^{0.25} * \rho * \left( \frac{4 * \dot{m}}{\rho * \pi * D^2} \right)^2}{2 * D}$$

$$\frac{\Delta P}{L} = 0.158 * \left( \frac{4}{\pi} \right)^{1.75} * \rho^{-1} * D^{-4.75} * \mu^{0.25} * \dot{m}^{1.75} \quad (7)$$

Now, on dividing the pressure loss per length for our case and the values obtained from an experimental work, we obtain the below mentioned ratio.

$$\frac{\frac{\Delta P}{L}}{\left( \frac{\Delta P}{L} \right)_{exp}} = \frac{0.158 * \left( \frac{4}{\pi} \right)^{1.75} * \rho^{-1} * D^{-4.75} * \mu^{0.25} * \dot{m}^{1.75}}{\left( 0.158 * \left( \frac{4}{\pi} \right)^{1.75} * \rho^{-1} * D^{-4.75} * \mu^{0.25} * \dot{m}^{1.75} \right)_{exp}}$$

The subscript exp stands for the experimental value of the parameter. Now, the constants get cancelled out and there will be a minimal difference in the density (~2.8%) and viscosity (~3%) between our case and the experimental case, owing to the difference in salinity in the experiments performed that we would be using as a reference. When the ratio of the product of  $\mu$ ,  $\rho$  were calculated and raised to respective powers, it was found out that they were found to be close to 1 (~1.04 for 20% ice fraction) and therefore, the product of ratio of density and viscosity raised to the respective powers were approximated to 1.

Subsequently, the above equation is now reduced to:

$$\frac{\frac{\Delta P}{L}}{\left( \frac{\Delta P}{L} \right)_{exp}} = \frac{D^{-4.75} * \dot{m}^{1.75}}{\left( D^{-4.75} * \dot{m}^{1.75} \right)_{exp}} \quad (8)$$

In addition to Blasius friction factor, the friction factor proposed by Knodel et. al, was also considered [34].

$$f = 0.174064 * Re^{-0.2} \quad (9)$$

Doing a reduction for Knodel's friction factor as done previously results in the pressure loss per metre length in the following manner:

$$\frac{\frac{\Delta P}{L}}{\left( \frac{\Delta P}{L} \right)_{exp}} = \frac{D^{-4.8} * \dot{m}^{1.8}}{\left( D^{-4.8} * \dot{m}^{1.8} \right)_{exp}} \quad (10)$$

So, now we get an equation where pressure drop per length is dependent on mass flow rate and diameter. We fix mass flow rate and vary the diameter (in steps of 0.025m) and observe the pressure losses.

The experimental values obtained in Meewisse et. al [104], Lee et. al [105] and Grozdek et. al [106] (presented in Appendix A3) were utilised and were substituted in the above equations and the pressure drops were comparatively studied.

## 5.2 Viscosity based pressure drop calculation

Although the above method provides us with a rough approximation of the pressure drops, these values cannot be used in critical applications. The difference between the actual values and the ones calculated from the method mentioned above arises from a combination of factors - the density and viscosity differences that are inherent of the fluid used (varying degrees of freezing point depressant used, as compared to 0.6% salinity we use for this work), experimental inaccuracies, instrumentation errors and since the friction factor model is highly sensitive (raised to power of 4.75-4.80), this has a magnifying effect on the error as well. As a result, we estimate the pressure drop using equation 2, that couples the measured ice slurry viscosity values and the various friction factor models found in the literature.

The friction factor models utilised are the earlier discussed Blasius [103], Knodel [34] and Petukhov [31].

$$f = (0.79 \ln Re - 1.64)^{-2} \quad (11)$$

$$3000 \leq Re \leq 5 \times 10^6$$

The viscosity measurements used in the calculation were UASCS (Rot visc in 1996, hereafter referred to as Rot96), UASCS (Rot visc in small storage, hereafter referred to as UASCS), Cemagref (Online visc) [107], as depicted in Figure 40. The experiments done at the University of Applied Sciences of Central Switzerland (UASCS) were done with a Haake Type-RV 20 rheometer with 10% mass fraction of talin and a small storage tank (Rot96) and a relatively larger tank (UASCS), while those done by CEMAGREF were performed with 11% mass fraction of ethanol in an Ostwald rheometer and no storage.

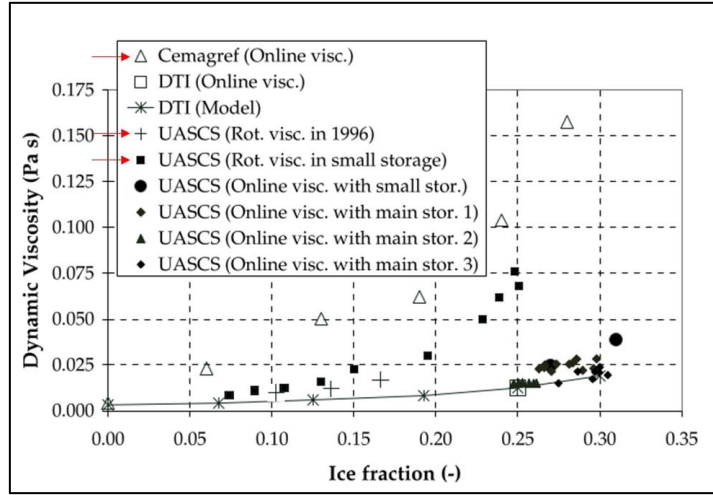


Figure 40: Measured dynamic viscosities of ice slurries by DTI, UASCS and Cemagref [107]. The ones indicated by red arrows are utilised in this study.

The mass flows of the ice slurry generated when the Aspen simulation is run for the ISG capacity of 3 MW, 200 MW and 300 MW (discussed in section 6.2) are 50 kg/s, 3236.75 kg/s, 4799.47 kg/s. For these mass flows, we calculate the pressure drop using equation 2. Since we know the mass flow, we increase the diameter in steps of 0.025m and the velocity is automatically adjusted (equation 4). The pressure loss per length values obtained are compared with the experimental papers mentioned earlier.

In addition, a ratio of pump power to latent heat released by ice was calculated to get an idea of how much power would be required as compared to the heat released by the phase change. The length of the pipe has been assumed to be 1000m for pumping purposes. The formulas used are:

### Pumping Power,

$$P \text{ (in W)} = \frac{Q * \Delta p}{\eta_{\text{pump}}} \quad (12)$$

- Q = Flow rate of slurry (m<sup>3</sup>/s)
- Δp = pressure drop (Pa)
- η<sub>pump</sub> = efficiency of pump

### Latent heat released,

$$Q_{\text{water} \rightarrow \text{ice}} \text{ (in W)} = \dot{m} * L_{\text{water} \rightarrow \text{ice}} * x \quad (13)$$

- $\dot{m}$  = mass flow rate (in kg/s)
- $L_{\text{water} \rightarrow \text{ice}}$  = latent heat of fusion of water (334 kJ/kg)
- x = ice fraction



## 6. Results and Discussions

### 6.1 Selection of Ice Slurry Generation method

The ice slurry generation methods and their suitability for our application are analysed and summarised in Table 2.

*Table 2: Ice slurry generation methods and its suitability for current work*

<b>Method</b>	<b>Suitability</b>
<b>Scraped-surface ice slurry generator</b>	<p><b>Not likely</b></p> <ul style="list-style-type: none"> <li>- Continual freezing up of heat exchanging surfaces on utilisation of low salinity water</li> <li>- High power requirements</li> <li>- Need for frequent maintenance</li> <li>- Large space requirement (for vertical configuration)</li> </ul>
<b>Direct contact ice slurry generator with immiscible refrigerant</b>	<p><b>Not likely</b></p> <ul style="list-style-type: none"> <li>- Possibility of refrigerant being trapped in the slurry, thus posing an environmental threat when pumped back to the sea.</li> <li>- Threat of ice formation on the injectors</li> </ul>
<b>Direct contact ice slurry generator with an immiscible secondary refrigerant</b>	<p><b>Not likely</b></p> <ul style="list-style-type: none"> <li>- The additional cycle results in increased investment cost and energy consumption</li> <li>- Possibility of an environment hazard when the immiscible liquid-trapped crystals are pumped back into the sea</li> </ul>

<p><b>Supercooled method</b></p>	<p><b>Not likely</b></p> <ul style="list-style-type: none"> <li>- Seawater from the Baltic Sea contains solid impurities that would result in crystallisation at an undesired location and leads to freeze-up of pipes.</li> </ul>
<p><b>Hydro-scraped ice slurry generator</b></p>	<p><b>Not likely</b></p> <ul style="list-style-type: none"> <li>- Adhesiveness of salt-based solutions on the ISG causing impairment of effective performance</li> <li>- Lack of commercialisation</li> </ul>
<p><b>Fluidised bed crystalliser</b></p>	<p><b>Not likely</b></p> <ul style="list-style-type: none"> <li>- Commercial viability has not been tested</li> <li>- No prior studies on scaling up from laboratory scale</li> <li>- Vertical layout of the beds poses a space constraint</li> </ul>
<p><b>High pressure methods</b></p>	<p><b>Not likely</b></p> <ul style="list-style-type: none"> <li>- High economic cost of high-pressure equipment</li> <li>- Formed crystals are dendritic in shape and might result in plugging</li> </ul>
<p><b>Recuperative ice making</b></p>	<p><b>Not likely</b></p> <ul style="list-style-type: none"> <li>- Costly additional evaporator surface</li> <li>- Difficulty in maintaining cooling capacity of the refrigerant</li> <li>- Lack of commercialisation at large scale</li> </ul>

<b>Vacuum Ice Method</b>	<p style="text-align: center;"><b>Seemingly feasible</b></p> <ul style="list-style-type: none"> <li>- Previous similar application at Augustenborg DH plant, Denmark</li> <li>- A scaled-up system from laboratory scale has been fabricated and operated, so seems technically viable.</li> </ul>
--------------------------	--

Thus, vacuum ice method is chosen to generate ice slurry as the proposed solution in this work and this is followed by further studies of the system. The following sections deal with the pressure drop evaluations and the performance of the system.

## 6.2 Pressure Drop Analysis

As discussed earlier, the Aspen Plus model was simulated for three cases by fixing the ice slurry generator capacity to 3 MW, 200 MW, 300 MW. The corresponding DH produced, and the mass flow of the generated ice slurry are tabulated in Table 3.

*Table 3: District Heating produced and Ice slurry flow rate for fixed duty of the ice slurry generator*

Case	Ice Slurry Generator Duty (MW)	District Heating produced (MW)	Ice slurry flow rate (kg/s)
1	3	5.18	50
2	200	320.46	3240
3	300	518.39	4800

The mass flow of 3240 kg/s, i.e.,  $\sim 3.24 \text{ m}^3/\text{s}$  for a DH capacity of 320MW is in agreement with the preliminary estimates of Helen Oy [28]. Further, for each diameter for each mass flow, the corresponding minimum velocity required to ensure no phase separation occurs was calculated using the following formula [31, 101] and if flow velocity is less than minimum velocity, the diameters were not subsequently studied:

$$v_{min} = 1.4 * \sqrt{g * D * \left(1 - \frac{\rho_i}{\rho_{cf}}\right)} \quad (14)$$

It was later proposed by Guilpart et. al. [108], for safety purposes, the minimum velocity be twice of  $v_{min}$  and this is what is used in our work. For instance, as we can deduce from Figure 41, for a mass flow of 3240kg/s, the

upper limit on diameter, in accordance with Guilpart's minimum velocity formula, is 1.725 m.

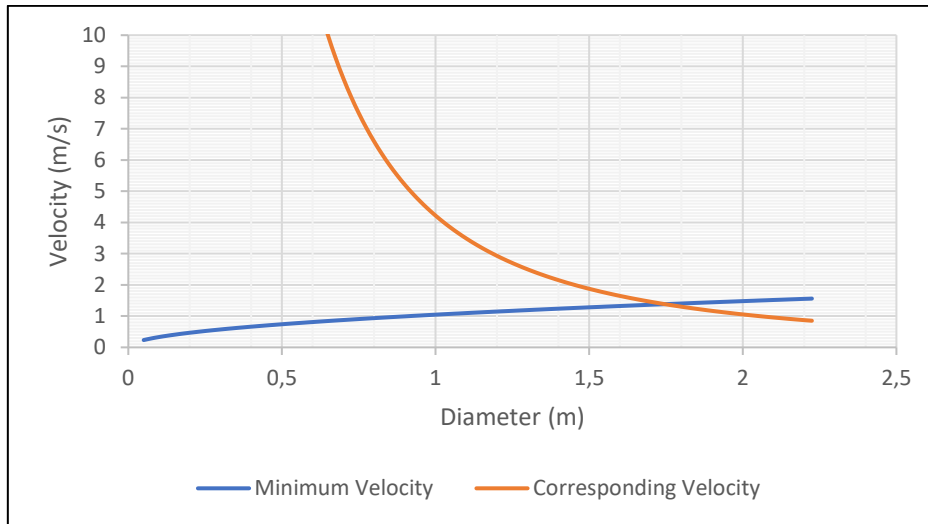


Figure 41: Velocity vs Diameter plot for mass flow of 3240kg/s. The blue line denotes the minimum velocity, based on Guilpart's formula, while the orange line indicates the flow velocity.

A comparative plot between the pressured drop per length of the three mass flow rates against the viable diameters for 20% ice fraction is illustrated in Figure 42 below. The pressure drop in the graph was deduced from the pressure ratio analysis (Chapter 5.1), using Blasius friction factor and experimental work [104]. Since the decommissioning of the Salmisaari CHP plant creates a paucity of ~300MW of DH, case 2 (ice slurry flow rate of 3240 kg/s) alone is presented in detail in this report. The data for the other two cases can be found in the appendix section A4.

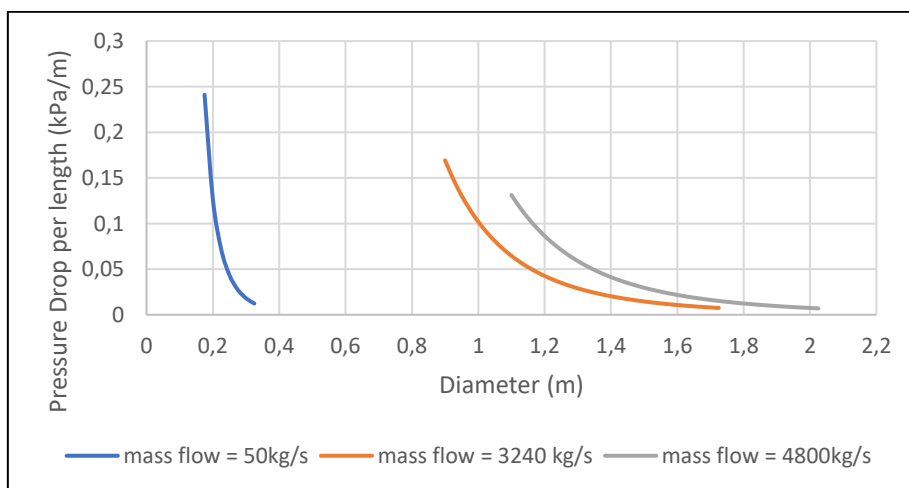


Figure 42: Comparison of Pressure Drops per length of the three mass flows for an ice fraction of 20%

Further, it was found out that the ratio of pump work to latent heat was the least in case of ice fraction of 20%, irrespective of mass flow of the ice slurry. A lower ratio implies that the work done by the pump is less as compared to the energy released during the phase transition. This is validated by evaluating the ratio using both pressure ratio analysis and viscosity-based pressure drop calculations. Due to discrepancies in experimental measurements of viscosity and pressure drop in the literature, we have selected the values in a way so as to evaluate the best- and worst-case pressure drop for our application. As it can be observed from the figure, a system having 20% ice fraction offers the best benefit from an energy expenditure point of view.

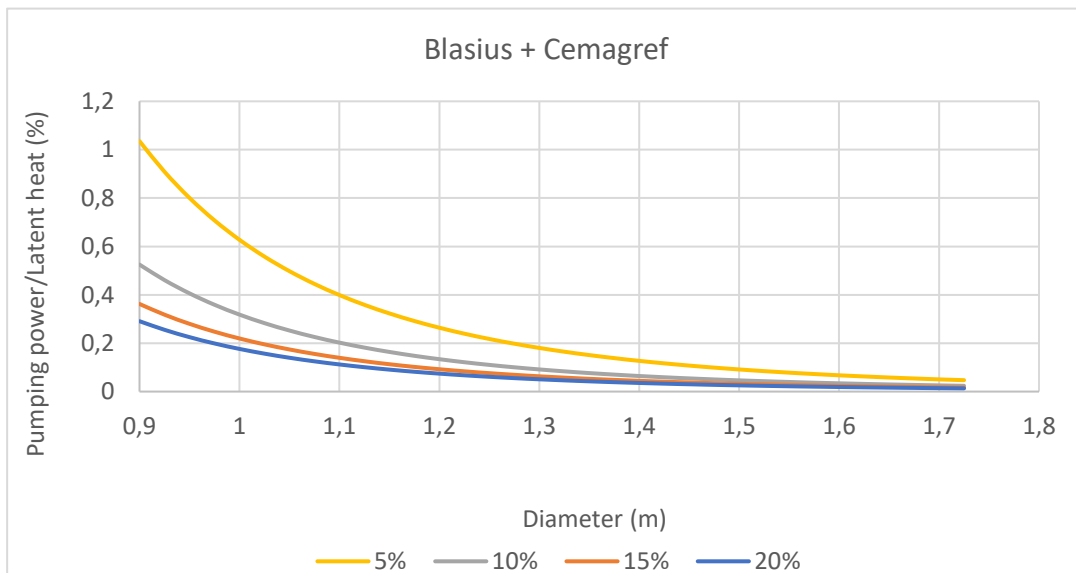


Figure 43: Pumping power/Latent heat vs Diameter for varying ice fractions for worst-case pressure drop scenario.

In addition, although all diameters up to 1.725 m are technically possible without phase separation, from a practical point of view, it need not be the case. For instance, for a mass flow of 3240 kg/s, a diameter of 0.5 m corresponds to a velocity of 16.88 m/s. In real-world situations, ice slurries are pumped at much lower rates, with Snoek et.al, in their work, specifying a value of 0.5-2.5 m/s in District cooling networks [109]. As a result, we consider diameters having reasonable velocities ( $> 0.9$  m,  $< 1.725$  m). Now, let us look at the results obtained using pressure ratio analysis.

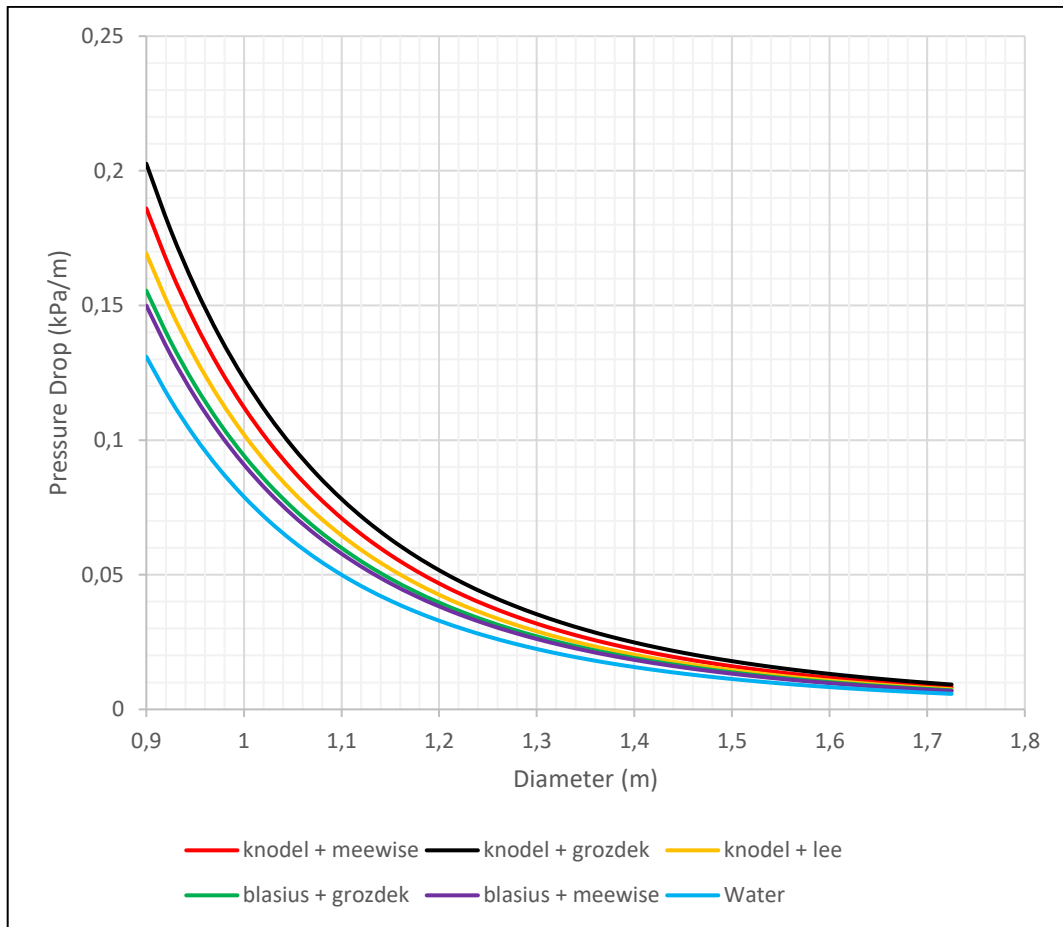


Figure 44: Pressure drop vs diameter using pressure ratio analysis for a mass flow rate of 3240 kg/s. The first word in the legend (e.g., knodel) is the friction factor model, while the other one (e.g., lee) is the experimental paper used as reference

Figure 44 depicts the results of the pressure ratio analysis for 20% ice slurry and a mass flow rate of 3240 kg/s. As we can see, the pressure drop experienced in ice slurries is greater than that of water (blue), albeit not so much. The pressure drop of water was calculated using Colebrook's friction factor [110] and using the pressure ratio analysis method (Knodel's friction factor) and the results were found to be in agreement. The small difference could be attributed to the difference in additive concentration as stated earlier. Hence, we also try to compare this with the results obtained using viscosity-based pressure drop calculation.

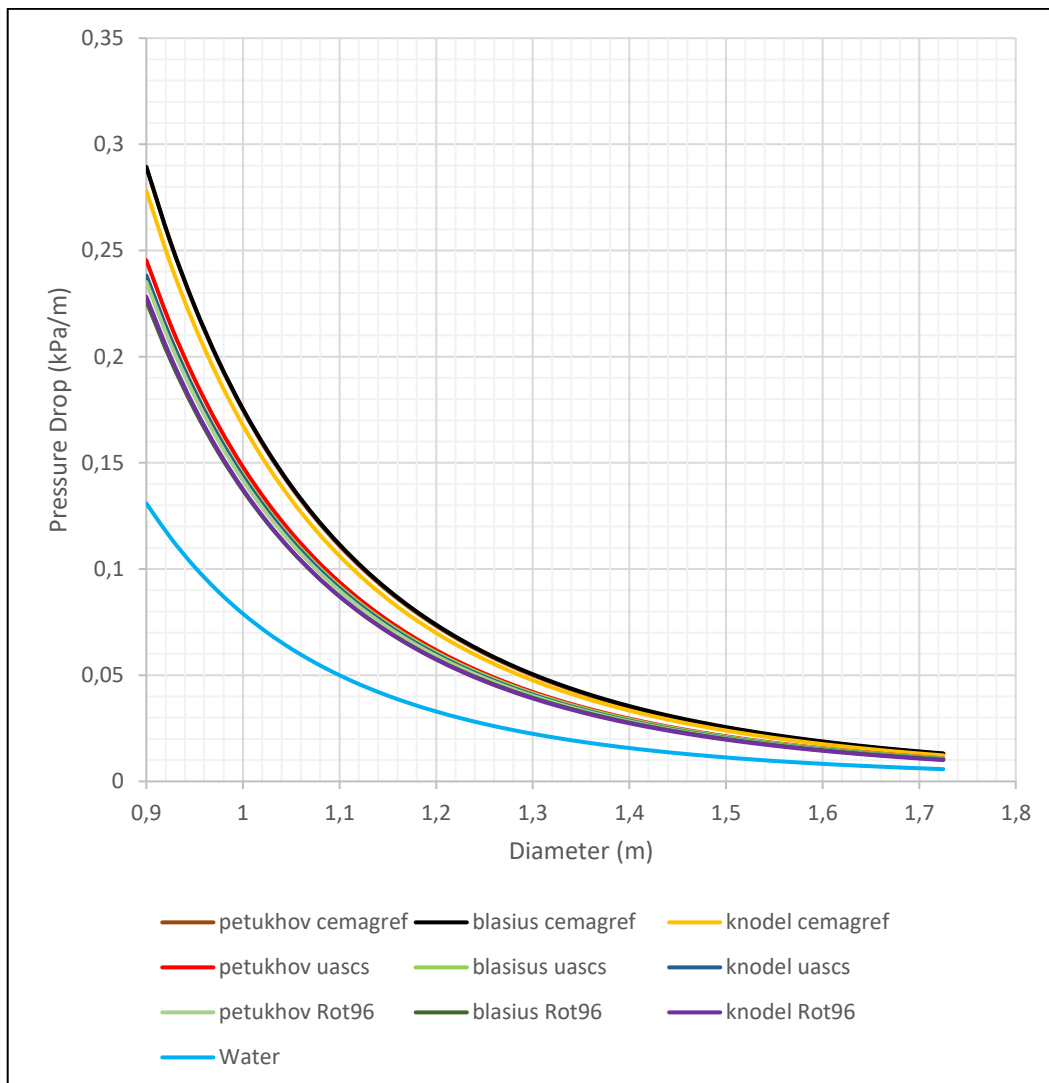


Figure 45: Pressure drop vs diameter using viscosity-based pressure drop calculation for a mass flow rate of 3240 kg/s. The first word in the legend (e.g., knodel) is the friction factor model, while the other one (e.g., Rot96) is the viscosity used as reference

As we can see from Figure 45, the relative increase in pressure drop between water and ice slurry is much more pronounced. When determining the pressure drop for critical applications, it is advisable to align with the worst-case scenario. Even though this might seem like a bit of overdesign, a safer design is better than one that fails. We observe that when Blasius' friction factor is used in combination with the viscosity values obtained at Cemagref, the pressure drop values are the highest. As a result, when deciding the pump specifications, one should base it on these values.

For this mass flow, and an arbitrary diameter of 1.5m (based on realistic velocity estimates), plotted friction factor vs ice fraction to get an idea of how the ice fraction and the various viscosity values used influences the friction

factor (Figure 46). We realise that the viscosity values used (based on the experiment) has a bigger role than the friction factor model, with the values presented by Cemagref resulting in the highest pressure drop values.

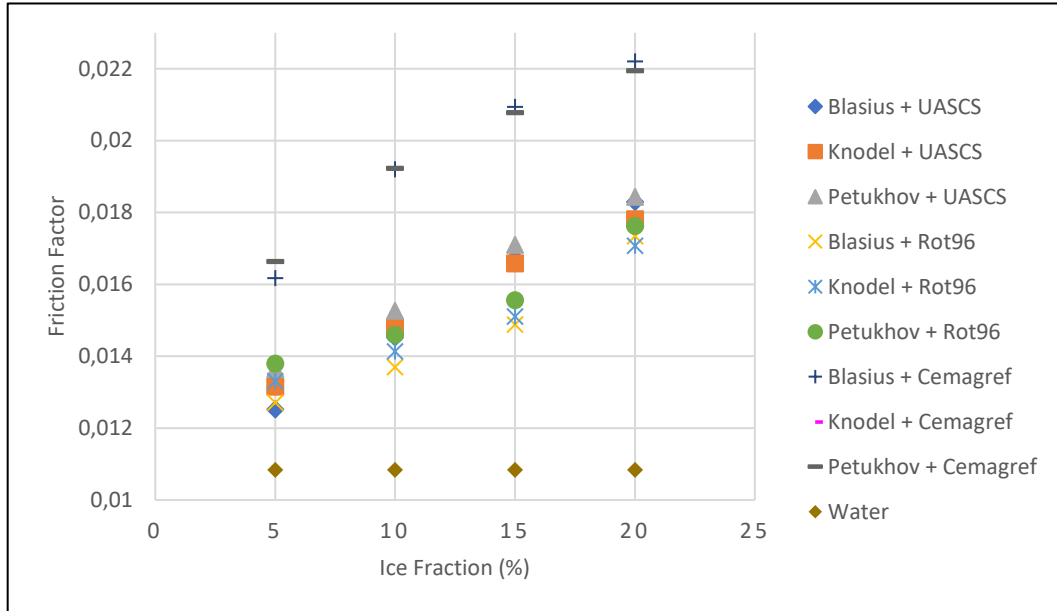


Figure 46: Calculated friction factor plotted against ice fraction (in %) for a mass flow of 3240kg/s and a diameter of 1.5m. The first word in the legend (e.g., Knodel) is the friction factor model, while the other one (e.g., Rot96) is the viscosity used as reference

Since we have determined that the desired ice fraction for pumping for our application is 20%, a graph is plotted between the pumping power required in three different cases depending on the viscosity values used. The pump power was calculated using equation 12 and the efficiency of the pump was set to 0.8, which is subject to change, depending on the supplier. The length of the pipe was assumed to be 1000m, based on discussions with the concerned people [45]. The power required to pump the same volume of pure water is also calculated and is provided as a baseline. The highest pressure drop, which is observed when using Blasius friction factor model in conjunction with the viscosity values we termed as ‘Rot96’, is almost twice of what is required to pump water.



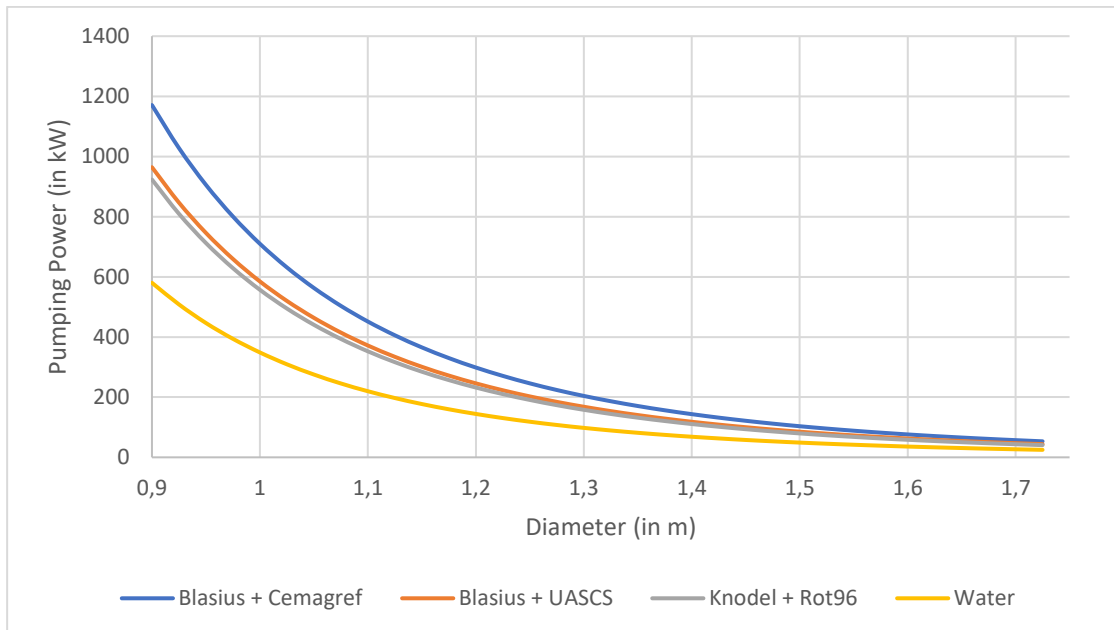


Figure 47: Pumping power vs diameter - a comparison between water and ice slurry (20% ice fraction) based on the viscosity models. Pump efficiency = 0.8.

### 6.3 Performance of the system

Once the pressure drop was calculated, for a mass flow of 3240 kg/s, ice fraction of 20% and a pipe diameter of 1.5 m, a pump was appended to the Aspen model, and it was made to raise the pressure equivalent to what is lost while pumping it for a distance of 1000 m. This corresponded to a pump work of about 106 kW, as it can be observed from Figure 48.

Fluid power	85,0993	kW
Brake power	106,374	kW
Electricity	106,374	kW
Volumetric flow rate	199686	l/min
Pressure change	0,255699	bar
NPSH available	0,000975092	m-kgf/kg
NPSH required		
Head developed	2,6793	meter
Pump efficiency used	0,8	
Net work required	106,374	kW
Outlet pressure	0,261655	bar
Outlet temperature	-0,621573	C

Figure 48: Summary of the results of working of the pump.

The pressure ratio of the water vapour compressor was varied and the influence of it on the COP was studied. This is presented in the graph below. We can see that as the pressure ratio is increased, there is a drop in the overall performance of the system. The COP is calculated as the ratio of the useful energy produced (District Heating) to the energy required (sum of pump and compressor work). It was discovered that the pump work is relatively small compared to the work done by the compressor on the fluid and its effect on the COP of the system is minimal.

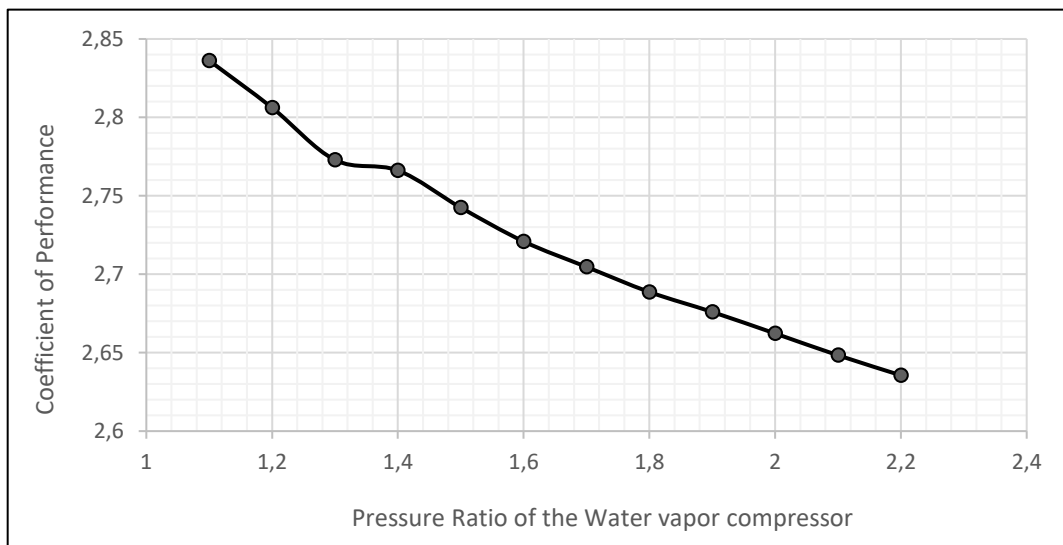


Figure 49: Plot of COP vs Pressure ratio of the water vapour compressor.

However, it should be noted that the actual COP values of the system in operation might be lower than the theoretical COP values obtained above. Since the water compressors must operate at very low-pressure levels (around 6 mbar), they are subject to high mechanical losses [97]. However, since no definite data was available on the efficiency of the water vapour compressors, the efficiencies of standard compressors are instead used in this work and this incongruity gives raise to potential difference in the COP of the system.

## 6.4 Contribution to SDG

The 2030 Agenda for Sustainable Development, adopted by the member states of the United Nations in 2015, introduces 17 Sustainable Development Goals (SDGs) with 169 targets [111, 112]. The present thesis contributes chiefly to 5 of the SDGs and has an impact on the others as well. The main synergies are presented in Figure 50.



Figure 50: United Nations Sustainable Development Goals that are in synergy with the current work

By means of this work, we attempt to suggest a cleaner alternative to the existing coal CHP plant in Salmisaari. This decarbonised alternative would lead to lesser pollution and thus, would have a positive interaction with SDG 3 (Ensure healthy lives and promote well-being for all at all ages), SDG 7 (Ensure access to affordable, reliable, sustainable, and modern energy for all) and SDG 13 (Take urgent action to combat climate change and its impacts). Further, the construction of such a seawater-based DH system, is a step further in achieving SDG 9 (Build resilient infrastructure, promote inclusive and sustainable industrialization and foster innovation). In addition, extracting the refrigerant from naturally available seawater, and disposing the generated slurry back into the sea ensures that we are on track to achieve SDG 12 (Ensure sustainable consumption and production patterns).

## 6.5 Future Work

The present work is set to serve as one of the baseline support material for Helen Oy in their continued work and materialisation of this project. In addition to what has been done in the timeframe for this thesis, the following will help in getting a better understanding of the subject and would impact the work in a positive manner.

Before the construction of a 300 MW DH plant is constructed, a pilot plant based on the current model and the corresponding pressure drop studies

could be built and its functioning studied, and shortcomings rectified. The model could be improved in later works to enable the selection of multiple pipelines for flow of slurry based on the amount of DH produced. The size of the pipes should factor in the effect of elbows at the conjunction, and minimum slurry velocities to avoid phase separation. In addition, the performance of the water vapour compressor could be modelled more accurately. In the current work, the particle size of ice slurry is assumed to be constant and is considered to be the same as the experimental papers that were referenced. The referenced papers did not employ the same method of ISG as our application and hence, this variation should be factored in and analysed further. A back-up plan (green and clean) must be worked out in case of the plant fails before a major share of Helsinki's citizens starts to rely solely on this plant.

When the seawater from the Baltic Sea is used, it should initially be filtered using a rough filter to keep away substances like fish, rocks that might damage the system. From a manufacturing point of view, Solid Energy has the design for a 2.6 MW compressor, but since the company has been liquidated, they no longer manufacture compressors [97]. But the design is ready and hence, with the help of suitable manufacturers, it could be built. A team at DTI are trying to develop a 100 kW unit that is tentatively set to start operating by next autumn. If the results are successful, a possible collaboration could be considered. A vacuum pump must be used to continuously remove the dissolved gases in water, as it was the case with the Augustenborg DH plant [97].

Further, it would also be interesting to study if the ice slurry generated could be utilised for some purpose, as it was done in Denmark, where they stored it and used for district cooling in Copenhagen during the summer months [97]. But since Helsinki's district cooling requirements are not so high, the slurry could be used in other applications, like for example, a ski hill in Helsinki. Another important thing would be the selection of the location in the sea to dump the ice slurry. An extensive EIA should be performed to study how the ice slurry dissolves, and it should be ensured that there is a constant current to prevent disastrous environmental consequences. Lastly, this work is a part of a collaboration between Helen Oy, AFRY, Aalto University, VTT and Luode Consulting and thus, the results of the individual works should be compared and discussed in detail before proceeding further.

## 7. Conclusion

In this work, an attempt was made to identify the best-suited ice slurry generation method that, on integration with heat pumps, would enable the extraction of heat from surface seawater. All viable ice slurry generation methods were analysed, and the chosen method of vacuum ice generation was found likely to work for our application and has the potential to provide ~300 MW of District Heating capacity for the city of Helsinki. Prior applications similar to ours (Augustenborg DH, ILK Dresden) point to vacuum ice generation system being a promising alternative for Helen Oy's future.

A model of the proposed system was developed, with the incorporation of a refrigerant/heat pump cycle, in Aspen Plus. The system was modelled to cater to three different district heating demands, with one of the cases (~300MW) explored in detail in the main report and the rest in the appendix. The later part of the study, involving pressure drop analysis, attempts to answer the second research question. Two methods of pressure drop studies are carried out, utilising previously performed experiments on ice slurry, and the scenario having the largest pressure drop is studied further. It is concluded that the pressure drop, characteristic of transport of ice slurry, is quite minimal in the overall scheme of things, being less than 0.5% of the total power consumed.

This is further complemented by a study of performance of the system and a sensitivity analysis of the pressure ratio of the water vapour compressor on the COP of the system. It is advisable to keep the pressure ratio of the water vapour compressor slightly greater than 1 to prevent any loss in performance of the system.

To sum up, this solution seems promising for the city of Helsinki and Helen Oy to adopt such an alternative for district heating to realise its carbon-neutrality goals before the proposed timeline. Although this model should not be taken at its face value and the assumptions and limitations are to be addressed, it however acts as a blueprint and a supporting document in bringing such a clean source of district heating to fruition.

## 8. Bibliography

- [1] IPCC, “Global Warming of 1.5°C: An IPCC Special Report on the impacts of global warming of 1.5°C above pre-industrial levels and related global greenhouse gas emission pathways,” 2018.
- [2] United Nations, “Paris Agreement,” United Nations Framework Convention on Climate Change, Paris, 2015.
- [3] European Commission, “Paris Agreement,” European Union, [Online]. Available: [https://ec.europa.eu/clima/policies/international/negotiations/paris\\_en](https://ec.europa.eu/clima/policies/international/negotiations/paris_en). [Accessed 20 September 2021].
- [4] European Council, “Climate change: what the EU is doing,” European Union, [Online]. Available: <https://www.consilium.europa.eu/en/policies/climate-change/>. [Accessed 06 July 2021].
- [5] General Secretariat of the Council, “Proposal for a Regulation of the European Parliament and of the Council establishing the framework for achieving climate neutrality and amending Regulation (EU) 2018/1999 (European Climate Law),” Council of the European Union, Brussels, 2020.
- [6] Ympäristöministeriö, “Finland's national climate change policy,” Ministry of the Environment, [Online]. Available: <https://ym.fi/en/finland-national-climate-change-policy>. [Accessed 15 July 2021].
- [7] City of Helsinki, “Making Helsinki carbon-neutral,” My Helsinki, [Online]. Available: <https://www.myhelsinki.fi/en/think-sustainably/making-helsinki-carbon-neutral>. [Accessed 15 July 2021].
- [8] City of Helsinki, “The Carbon-neutral Helsinki 2035 Action Plan,” City of Helsinki, Helsinki, 2018.
- [9] Carbon Neutral Cities Alliance, “Helsinki, Finland,” CNCA, [Online]. Available: <https://carbonneutralcities.org/cities/helsinki/>. [Accessed 17 July 2021].
- [10] City of Helsinki, “Environmental Sustainability Issues and Challenges in Helsinki 2010,” Kopio Niini Oy, Helsinki, 2010.
- [11] Helen Oy, “Carbon-Neutral Energy,” Helen Oy, [Online]. Available: <https://www.helen.fi/en/company/responsibility/responsibility->

- report/environmental-responsibility/carbon-neutral-energy. [Accessed 18 July 2021].
- [12] City of Helsinki, "Carbon-neutral Helsinki 2035: Summary," City of Helsinki, Helsinki, 2019.
- [13] Helen Oy, "Helsinki closes Hanasaari power plant almost two years ahead - carbon storage disappears from street view," Helen Oy, 22 June 2021. [Online]. Available: <https://www.helen.fi/uutiset/2021/helsinki-sulkee-hanasaaren-voimalaitoksen-lahes-kaksi-vuotta-etuajassa>. [Accessed 12 November 2021].
- [14] Rockplan, "Salmisaaren hiilivarastot," Rockplan, [Online]. Available: <https://www.rockplan.fi/referenssit/salmisaaren-hiilivarastot/>. [Haettu 20 July 2021].
- [15] Helen Oy, "Salmisaaren Voimalaitosten Turvallisuustiedote," Helen Oy, Helsinki, 2016.
- [16] "Salmisaaren voimalaitos," Wikipedia, [Online]. Available: [https://fi.wikipedia.org/wiki/Salmisaaren\\_voimalaitos](https://fi.wikipedia.org/wiki/Salmisaaren_voimalaitos). [Haettu 23 July 2021].
- [17] Helen Oy, "Salmisaari power plant," Helen Oy, [Online]. Available: <https://www.helen.fi/en/company/energy/energy-production/power-plants/salmisaari-power-plant>. [Accessed 18 July 2021].
- [18] Helen Oy, "Kellosaari reserve power plant," Helen Oy, [Online]. Available: <https://www.helen.fi/en/company/energy/energy-production/power-plants/kellosaari-stand-by-power-plant>. [Accessed 19 July 2021].
- [19] Helen Oy, "Kierrätyspesulla Tehoa Merivesi-lämmönvaihtimiin," Motiva, Helsinki, 2016.
- [20] A. Fin, "Salmisaari B powerplant in Helsinki, Finland. Built 1984, Architects: Timo Penttilä, Heikki Saarela and Kai Lind.," Wikimedia Commons, 2007.
- [21] BMH Technology, "Bioflame solution in Salmisaari Power Plant, Helsinki, Finland," BMH, [Online]. Available: <https://www.bmh.fi/references/bioflame-solution-in-salmisaari-power-plant-helsinki-finland/>. [Accessed 20 July 2021].
- [22] A. Sherrard, "Helen inaugurate Finland's largest pellet-fired boiler," Bioenergy International, 21 February 2018. [Online]. Available: <https://bioenergyinternational.com/heat-power/helen-inaugurate-finlands-largest-pellet-fired-boiler>.
- [23] Helen, "First bioenergy heating plant in Helsinki inaugurated," Euroheat & Power, 14 February 2018. [Online]. Available:

<https://www.euroheat.org/news/first-bioenergy-heating-plant-helsinki-inaugurated/>.

- [24] S. Morgan, “Finland confirms coal exit ahead of schedule in 2029,” Euractiv, 12 April 2018. [Online]. Available: <https://www.euractiv.com/section/energy/news/finland-confirms-coal-exit-ahead-of-schedule-in-2029/>.
- [25] Ministry of Economic Affairs and Employment, “Investment incentives to promote rapid phase-out of coal in energy production,” Suomen valtioneuvosto, 27 March 2020. [Online]. Available: <https://valtioneuvosto.fi/en/-/1410877/investment-incentives-to-promote-rapid-phase-out-of-coal-in-energy-production>.
- [26] Finlex, ”Laki hiilen energiakäytön kieltämisestä,” Suomen oikeusministeriö, 16 April 2019. [Online]. Available: <https://www.finlex.fi/fi/laki/alkup/2019/20190416>.
- [27] Eduskunta, “Hallituksen Esitys eduskunnalle laeiksi hiilen energiakäytön kieltämisestä ja oikeudenkäynnistä markkinaoikeudessa annetun lain 1 luvun 2 §:n muuttamisesta,” Eduskunta, Helsinki, 2018.
- [28] Helen Oy, *Sea water heat recovery*, Helsinki: Personal communication, 2021.
- [29] ILK Dresden, “Energy efficient vacuum freezing ice slurry generation using a R718 compressor,” ATMOSphere, Brussels, 2013.
- [30] D. R. Legates, “Latent Heat,” in *Encyclopedia of World Climatology, Encyclopedia of Earth Sciences Series*, Dordrecht, Springer, 2005.
- [31] Michael Kauffeld, Masahiro Kawaji, Peter W. Egolf, *Handbook on Ice Slurries: Fundamentals and Engineering*, Paris: International Institute of Refrigeration, 2005.
- [32] T. M. Hansen, E. Noergaard and B. Frei, “Transport,” in *Handbook on Ice Slurries*, Paris, International Institute of Refrigeration, 2005, pp. 167-201.
- [33] ILK Dresden, “Ice Slurry: For Refrigeration and Heat supply,” Institute for Air Handling and Refrigeration, Dresden, 2016.
- [34] B. Knodel, D. France, U. Choi and M. Wambsganss, “Heat transfer and pressure drop in ice-water slurries,” *Applied Thermal Engineering*, vol. 20, no. 7, pp. 671-685, 2000.
- [35] E. Stamatiou, J. Meewisse and M. Kawajia, “Ice slurry generation involving moving parts,” *International Journal of Refrigeration*, vol. 28, no. 1, pp. 60-72, 2005.



- [36] J. W. Mullin, *Crystallization*, Butterworth-Heinemann, 2001, p. 600.
- [37] C. Okolieocha, D. Raps, K. Subramaniam and V. Altstädt, “Microcellular to nanocellular polymer foams: Progress (2004–2015) and future directions – A review,” *European Polymer Journal*, vol. 73, pp. 500-519, 2015.
- [38] Hydrology and Atmospheric Sciences - University of Arizona, “Formation and Growth of Ice Crystals,” 2011. [Online]. Available: [http://www.atmo.arizona.edu/students/courselinks/fall11/atmo551a/ATMO\\_451a\\_551a\\_files/ColdClouds.pdf](http://www.atmo.arizona.edu/students/courselinks/fall11/atmo551a/ATMO_451a_551a_files/ColdClouds.pdf). [Accessed 15 May 2021].
- [39] P. Pronk, J. Meewisse and C. Infante Ferreira, “Fluidized bed for ice slurry production,” Delft University of Technology WbMT, Delft, 2002.
- [40] Ishita Gupta, “Why sphere minimizes surface area for a given volume?,” Physics Stack Exchange, 29 November 2015. [Online]. Available: <https://physics.stackexchange.com/questions/221210/why-sphere-minimizes-surface-area-for-a-given-volume>.
- [41] X. Liu, K. Zhuang, S. Lin, Z. Zhang and X. Li, “Determination of Supercooling Degree, Nucleation and Growth Rates, and Particle Size for Ice Slurry Crystallization in Vacuum,” *Crystals*, vol. 7, no. 5, 2017.
- [42] A. M. Helmenstine, “Melting Definition in Chemistry,” Thought Co., 05 June 2019. [Online]. Available: <https://www.thoughtco.com/definition-of-melting-604568>.
- [43] C. Huber, “What Makes an Ice Cube Melt?,” sciencing.com, [Online]. Available: <https://sciencing.com/ice-cube-melt-7485740.html>. [Accessed 15 November 2021].
- [44] L. Makkonen, “Surface melting of ice,” *The Journal of Physical Chemistry B*, vol. 101, no. 32, pp. 6196 - 6200, 1997.
- [45] J. Nummelin and L. Korhonen, Interviewees, *Personal Communication*. [Interview]. 2021.
- [46] “Helen Oy, Salmisaaren voimalaitos,” Google, [Online]. Available: <https://www.google.com/maps/place/Helen+Ab,+Sundholmens+kraftverk/@60.1652638,24.9034219,17z/data=!3m1!4b1!4m5!3m4!1sox46920a4892065ccd:ox7895f728616ecoa1!8m2!3d60.1652638!4d24.9056106>. [Accessed 05 April 2021].
- [47] Marine Finland, “Water Quality,” 04 June 2021. [Online]. Available: [https://marinefinland.fi/en-US/The\\_Baltic\\_Sea\\_now/Water\\_quality](https://marinefinland.fi/en-US/The_Baltic_Sea_now/Water_quality).
- [48] “Distance from West Tukan to Helen Ab, Sundholmens kraftverk,” Google, [Online]. Available: [https://www.google.com/search?rlz=1C1GCEU\\_enFI961FI962&sxsrf=AOaemvKWa5p-](https://www.google.com/search?rlz=1C1GCEU_enFI961FI962&sxsrf=AOaemvKWa5p-)

mgOZLPAIzIoaHEOBgwN4A:1632386427736&q=lansitoukki+to+helen+salmisaari+distance&spell=1&sa=X&ved=2ahUKEwiFoKSp2ZTzAhUCyosKHQpDBN4QBSgAegQIARAx&biw=1536&bih=722&dpr=1.25#. [Accessed 10 June 2021].

- [49] Pekka Alenius, Kai Myrberg, Alexei Nekrasov, "The physical oceanography of the Gulf of Finland: A review," *Boreal Environment Research*, vol. 3, no. 2, pp. 97-125, 1998.
- [50] D. Ghosh, "Gulf Of Finland," World Atlas, 01 April 2021. [Online]. Available: <https://www.worldatlas.com/gulfs/gulf-of-finland.html>.
- [51] "Salinity," Marine Finland, [Online]. Available: [https://www.marinefinland.fi/en-US/The\\_Baltic\\_Sea\\_now/Water\\_quality/Salinity](https://www.marinefinland.fi/en-US/The_Baltic_Sea_now/Water_quality/Salinity). [Accessed 05 May 2021].
- [52] CK-12 Foundation, "Freezing Point Depression and Boiling Point Elevation," LibreTexts, 20 February 2021. [Online]. Available: <https://chem.libretexts.org/@go/page/47559>.
- [53] Marine Finland, "Salinity," [Online]. Available: [https://www.marinefinland.fi/en-US/The\\_Baltic\\_Sea\\_now/Water\\_quality/Salinity](https://www.marinefinland.fi/en-US/The_Baltic_Sea_now/Water_quality/Salinity). [Accessed 11 June 2021].
- [54] Xiangyu Hou, Lili Gao, Zhendong Cui, Jianhua Yin, "Corrosion and Protection of Metal in the Seawater Desalination," in *IOP Conference Series: Earth and Environmental Science*, 2017.
- [55] City of Helsinki, "Baltic Sea," City of Helsinki, 06 December 2019. [Online]. Available: <https://www.hel.fi/helsinki/en/housing/nature/waters/baltic/>.
- [56] Marine Finland, "Water quality: Oxygen," [Online]. Available: [https://www.marinefinland.fi/en-US/The\\_Baltic\\_Sea\\_now/Water\\_quality/Oxygen\\_conditions](https://www.marinefinland.fi/en-US/The_Baltic_Sea_now/Water_quality/Oxygen_conditions). [Accessed 12 June 2021].
- [57] HELCOM, "Eutrophication in the Baltic Sea – An integrated thematic assessment of the effects of nutrient enrichment in the Baltic Sea region," Baltic Sea Environment Proceedings No. 115B, Helsinki, 2009.
- [58] P. R. Roberge, "Corrosion Basics—Water Constituents," Materials Performance, 05 April 2020. [Online]. Available: <https://www.materialsperformance.com/articles/corrosion-basics/2018/07/corrosion-basicswater-constituents>.

- [59] Hayden Allwright, Hossein Enshaei, "Investigation of the Impact of Marine Algae on the Corrosion of Mild Steel," *Journal of Basic and Applied Scientific Research*, vol. 6, no. 3, pp. 28-37, 2016.
- [60] City of Helsinki, "Sea water temperature and amount of algae," City of Helsinki, 06 December 2019. [Online]. Available: <https://www.hel.fi/helsinki/en/housing/nature/waters/baltic/algae>.
- [61] Jeffrey Poon, David C. Madden, Rebecca J.L. Welbourn, Finian J. Allen, Fahmida Khan, Hans Sonke, Stuart M. Clarke, "Corrosion inhibition of steel in seawater through surface phosphate formed from oil," *Surface and Coatings Technology*, vol. 410, 2021.
- [62] Marine Finland, "Nutrients: Phosphorous," Marine Finland, [Online]. Available: [https://www.marinefinland.fi/en-US/The\\_Baltic\\_Sea\\_now/Water\\_quality/Phosphorus](https://www.marinefinland.fi/en-US/The_Baltic_Sea_now/Water_quality/Phosphorus). [Accessed 10 May 2021].
- [63] Marine Finland, "Water quality: Amount of algae," [Online]. Available: [https://www.marinefinland.fi/en-US/The\\_Baltic\\_Sea\\_now/Water\\_quality/Amount\\_of\\_algae](https://www.marinefinland.fi/en-US/The_Baltic_Sea_now/Water_quality/Amount_of_algae). [Accessed 13 June 2021].
- [64] Marine Finland, "Water quality: Turbidity," [Online]. Available: [https://www.marinefinland.fi/en-US/The\\_Baltic\\_Sea\\_now/Water\\_quality/Turbidity](https://www.marinefinland.fi/en-US/The_Baltic_Sea_now/Water_quality/Turbidity). [Accessed 13 June 2021].
- [65] Marine Finland, "Water temperature," [Online]. Available: [https://www.marinefinland.fi/en-US/The\\_Baltic\\_Sea\\_now/Water\\_quality/Water\\_temperature](https://www.marinefinland.fi/en-US/The_Baltic_Sea_now/Water_quality/Water_temperature). [Accessed 13 June 2021].
- [66] Michael Kauffeld, Sebastian Gund , "Ice slurry – History, current technologies and future developments," *International Journal of Refrigeration* , vol. 99, pp. 264-271, 2019.
- [67] Armstrong Chemtec Group, "Scraped Surface Heat Exchangers," 23 May 2017. [Online]. Available: <https://www.armstrong-chemtec.com/products/scraped-surface-heat-exchangers.html>.
- [68] A. Russell, P. Cheney and S. Wantling, "Influence of freezing conditions on ice crystallisation in ice cream," *Journal of Food Engineering*, vol. 39, no. 2, pp. 179-191, 1999.
- [69] Alfa Laval, "The theory behind heat transfer," 2004. [Online]. Available: <https://www.alfalaval.com/globalassets/documents/microsites/heating-and-cooling->

hub/alfa\_laval\_heating\_and\_cooling\_hub\_the\_theory\_behind\_heat\_transfer.pdf. [Accessed 18 October 2021].

- [70] S. P. Gladis, M. J. Marciniak, P. Joseph B. O'Hanlon and P. and Brad Yundt, "Ice Crystal Slurry Tes System Using The Orbital Rod Evaporator," 2006. [Online]. Available: <http://www.icesynergy.com/L3-8-PDFlibrary/Ice%20Crystal%20Slurry%20Tes%20System%20Using%20The%20Orbital%20Rod%20Evaporator.pdf>.
- [71] M. Wang and N. Kusumoto, "Ice slurry based thermal storage in multifunctional buildings," *Heat and Mass Transfer*, vol. 37, pp. 597-604, 2001.
- [72] Wobst Eberhard, Vollmer Dietrich, "Ice Slurry Generation by Direct Evaporating of Refrigerant," in *First IIR Workshop on Ice Slurries*, Yverdon-les-Bains Switzerland, 1999.
- [73] M. Chuard and J. P. Fortuin, "COLDECO - A New Technology System for Production and Storage of Ice," in *First Workshop on Ice Slurries of the International Institute of Refrigeration*, Yverdon-les-Bains, Switzerland, 1999.
- [74] S. Fukusako, Y. Kozawa, M. Yamada and M. Tanino, "Research and Development Activities on Ice Slurries in Japan," in *First IIR Workshop on Ice Slurries*, Yverdon-les-Bains, Switzerland, 1999.
- [75] H. Inaba, "Fundamental Research and Development of Ice slurry for Its Cooling System Design in Japan," in *Fourth IIR Workshop on Ice Slurries*, Osaka, Japan, 2001.
- [76] U. Z, "Slurry ice based cooling systems.," in *CIBSE National Conference 1997. Proceedings*, London, United Kingdom, 1997.
- [77] Jean-Pierre Bédécarrats, Thomas David, Jean Castaing-Lasvignottes, "Ice slurry production using supercooling phenomenon," *International Journal of Refrigeration*, vol. 33, pp. 196-204, 2010.
- [78] Masayuki Tanino, Yoshiyuki Kozawa, "Ice-water two-phase flow behavior in ice heat storage systems," *International Journal of Refrigeration*, vol. 24, no. 7, pp. 639-651, 2001.
- [79] J. Meewisse and C. Infante Ferreira, "Ice Slurry Production with a Fluidised Bed Heat Exchanger," in *Second IIR Workshop on Ice Slurries*, Paris, France, 2000.
- [80] Laura Otero, Pedro D. Sanz, "High-Pressure Shift Freezing. Part 1. Amount of Ice Instantaneously Formed in the Process," *Biotechnology Progress*, vol. 16, pp. 1030-1036, 2000.

- [81] P. Fernández, L. Otero, B. Guignon and P. Sanz, “High-pressure shift freezing versus high-pressure assisted freezing: Effects on the microstructure of a food model,” *Food Hydrocolloids*, vol. 20, no. 4, pp. 510-522, 2006.
- [82] S. Zhu, H. Ramaswamy and A. Le Bail, “Ice-crystal formation in gelatin gel during pressure shift versus conventional freezing,” *Journal of Food Engineering*, vol. 66, pp. 69-76, 2005.
- [83] Knud Andersen, Flemming V. Boldvig, “Large Capacity Heat Pump Using Vacuum Ice Production as Heat Source,” in *Proceedings of the XVIIth international Congress of Refrigeration*, Vienna, Austria, 1987.
- [84] Hans Madsbøll, Gunnar Minds, Jesper Nyvad, Frank Elefsen, “The State of Art for Water Vapour Compressors and Cooling Plants Using Water as Refrigerant,” in *Proceedings of the third International Symposium on the Large Scale Applications of Heat Pumps*, Oxford, England, 1987.
- [85] M. Honke, “Ice Slurry Generation,” ILK Dresden, [Online]. Available: <https://www.ilkdresden.de/en/project/ice-slurry-generation/>. [Accessed 20 March 2021].
- [86] F. Hüchelheim, “Heizen mit Eis,” Handelsblatt Media Group, 27 November 2014. [Online]. Available: <https://www.handelsblatt.com/technik/das-technologie-update/nachgeforscht/v-wie-vakuum-fluessigeis-technologie-heizen-mit-eis-seite-2/10951156-2.html?ticket=ST-639511-HItWgWuyBqQRTZQEBhew-ap2>.
- [87] WindNODE, SINTEG, “Showcasing Smart Energy Systems from Northeastern Germany,” WindNODE, Berlin, 2020.
- [88] United National Environmental Protection Agency, “Hazards of Ammonia Releases at Ammonia Refrigeration Facilities,” US EPA, Washington D.C, 2001.
- [89] E. Ortega, “What is Aspen Plus?,” ChemEngGuy, [Online]. Available: <https://www.chemicalengineeringguy.com/the-blog/process-simulation/what-is-aspen-plus/>. [Accessed 15 April 2021].
- [90] C. T. Lira, “ASPEN Tutorial,” Michigan State University, [Online]. Available: <https://www.chems.msu.edu/resources/tutorials/ASPEN>. [Accessed 07 April 2021].
- [91] R. Schefflan, “Introduction to Aspen Plus,” in *Teach Yourself the Basics of Aspen Plus*, John Wiley and Sons, 2016.

- [92] V. Nair, "HFO refrigerants: A review of present status and future prospects," *International Journal of Refrigeration*, vol. 122, pp. 156-170, 2021.
- [93] European Commission, "EU legislation to control F-gases," European Union, [Online]. Available: [https://ec.europa.eu/clima/policies/f-gas/legislation\\_en](https://ec.europa.eu/clima/policies/f-gas/legislation_en). [Accessed 25 April 2021].
- [94] "The advantages of R1234ZE refrigerant," Daikin Applied Europe S.p.A., 15 April 2020. [Online]. Available: <https://www.daikinapplied.eu/news-center/the-advantages-of-r1234ze-refrigerant/>.
- [95] Darment Oy, "R1234ze ecological option for many medium temperature applications," Darment Oy, [Online]. Available: <https://darment.eu/refrigerant/r1234ze/>. [Accessed 27 April 2021].
- [96] Helen Oy and AFRY Finland Oy, "Meriveden lämmöntalteenottohanke, Helsinki: Ympäristövaikutusten arviointiohjelma," AFRY Finland Oy, Helsinki, 2021.
- [97] H. Madsbøll, Interviewee, *Personal Communication*. [Interview]. 21 May 2021.
- [98] Page Bloomer Associates, "Pump Efficiency Guidelines," [Online]. Available: [http://www.landwise.org.nz/wp-content/uploads/EEC1427-Pump-Efficiency-Guidelines-2\\_0.pdf](http://www.landwise.org.nz/wp-content/uploads/EEC1427-Pump-Efficiency-Guidelines-2_0.pdf). [Accessed 28 July 2021].
- [99] Aspen Technology Inc., "Aspen Physical Property System," Aspen Technology Inc., Massachusetts, 2013.
- [100] I. Bellas and S. Tassou, "Present and future applications of ice slurries," *International Journal of Refrigeration*, vol. 28, pp. 115-121, 2005.
- [101] Andrej Kitanovski, Christian Doetsch, Torben Hansen, Patrick Reghem, Beat Frei, Didier, "Fluid Dynamics: Pressure Drop," in *Handbook on Ice Slurries: Fundamentals and Engineering*, Paris, International Institute of Refrigeration, 2005.
- [102] A. Yahia, S. Mantellato and R. Flatt, "7 - Concrete rheology: A basis for understanding chemical admixtures," in *Science and Technology of Concrete Admixtures*, P. Aïtcin and R. J. Flatt, Eds., Woodhead Publishing, 2016, pp. 97-127.
- [103] M. Awad, "Two-Phase Flow," in *An Overview of Heat Transfer Phenomena*, IntechOpen, 2012.
- [104] J. W. Meewisse and F. Infante, "Freezing point depression of various ice slurries," in *Thermophysical properties and transfer processes of new*

- refrigerants*, Paris, International Institute of Refrigeration, 2001, pp. 166-174.
- [105] D. Lee, C. Yoon, E. Yoon and M. Joo, “Experimental study on flow and pressure drop of ice slurry for various pipes,” in *Proceedings of 5th Workshop on Ice Slurries*, Stockholm, 2003.
- [106] M. Grozdek, R. Khodabandeh and P. Lundqvist, “Experimental investigation of ice slurry flow pressure drop in horizontal tubes,” *Experimental Thermal and Fluid Science*, vol. 33, no. 2, pp. 357-370, 2009.
- [107] P. Frei and P. Egolf, “Viscometry applied to the Bingham substance ice slurry,” in *Proceedings of the second Workshop on Ice Slurries of the IIR*, Paris, 2000.
- [108] J. Guilpart, E. Stamatiou and L. Fournaison, “The control of ice slurry systems: an overview,” *International Journal of Refrigeration*, vol. 28, no. 1, pp. 98-107, 2005.
- [109] C. W. Snoek, S. Walosik, R. P. Gupta and B. G. Ltd., “Ice slurry transport for district cooling networks,” in *Slurry handling and pipeline transport*, Brugge, 1993.
- [110] Engineering-abc, “Pipe Flow pressure drop,” [Online]. Available: [https://www.tribology-abc.com/calculators/pipeflow\\_fluid.htm](https://www.tribology-abc.com/calculators/pipeflow_fluid.htm). [Accessed 01 September 2021].
- [111] Francesco Fusco Nerini, Julia Tomei, Long Seng To, Iwona Bisaga, Priti Parikh, Mairi Black, Aiduan Borrion, Catalina Spataru, Vanesa Castán Broto, Gabriel Anandarajah, Ben Milligan, Yacob Mulugetta, “Mapping synergies and trade-offs between energy and the Sustainable Development Goals,” *Nature Energy*, vol. 3, pp. 10-15, 2018.
- [112] Division for Sustainable Development Goals, “The 17 Goals,” United Nations Department of Economic and Social Affairs (UNDESA), [Online]. Available: <https://sdgs.un.org/goals>. [Accessed 28 April 2021].
- [113] H. Madsbøll, *Development of Water Vapor Compressors and future market implementation*, IEA Heat Pump Workshop: Danish Technological Institute, 2015.
- [114] The Engineering Mindset, “R1234ze (E) Pressure Enthalpy Chart,” Danfoss, [Online]. Available: <https://theengineeringmindset.com/r1234ze-e-pressure-enthalpy-chart/>. [Accessed 03 July 2021].
- [115] Gas Servei, “R1234-ze Technical Data sheet,” Gas Servei, Barcelona.

- [116] Honeywell Belgium N.V., "Low GWP Hydrofluoroolefins (HFO): The Environmental Alternative to Traditional Refrigerants," Honeywell, Heverlee, Belgium, 2015.
- [117] Helen Oy, "Salmisaaren voimalaitokset: Ympäristölupahakemus lupamääräysten tarkistamiseksi suurten polttolaitosten BAT- päätelmien julkaisun takia," Helen Oy, Helsinki, 2018.
- [118] D. Patience, J. B. Rawlings and H. A. Mohameed, "Crystallization of paraxylene in scraped-surface crystallizers," *American Institute of Chemical Engineers*, vol. 47, no. 11, pp. 2441-2451, 2001.
- [119] Yle, "Surprise rise in Helsinki carbon emissions, coal main culprit," Yle, 28 December 2017. [Online]. Available: [https://yle.fi/uutiset/osasto/news/surprise\\_rise\\_in\\_helsinki\\_carbon\\_emissions\\_coal\\_main\\_culprit/9996445](https://yle.fi/uutiset/osasto/news/surprise_rise_in_helsinki_carbon_emissions_coal_main_culprit/9996445).
- [120] M. Kauffeld, K. G. Christensen, S. Lund and T. M. Hansen, "Experience with ice slurry," in *Proceedings of the First Workshop on Ice Slurries*, Yverdon-les-Bains, Switzerland, 1999.
- [121] A. A. Sonin, "The physical basis of Dimensional Analysis," Massachusetts Institute of Technology, Cambridge, 2001.



## Appendix

### A1 – Augustenborg District Heating Plant

#### A 1.1. Water Vapour compressor

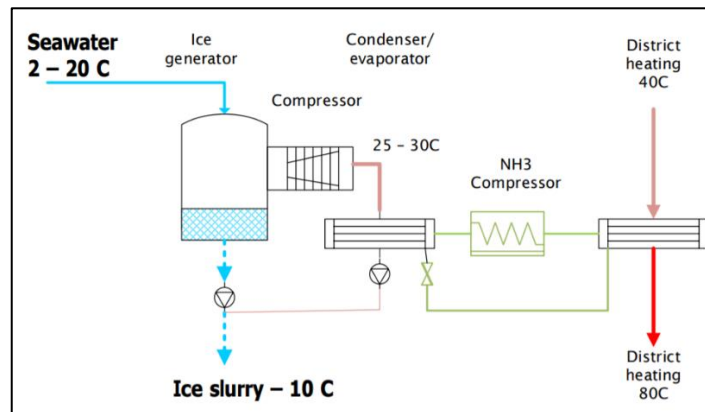


Figure A. 1: DTT's Water vapour compressor for Augustenborg District Heating plant [113]

#### A 1.2. Operation Data of Heat Pump System

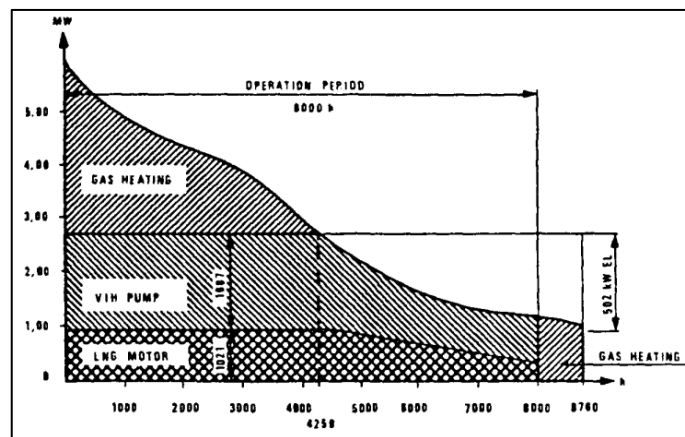


Figure A. 2: Supply diagram of share of Thermal energy sale over an average of 3 years [83]

Figure A. 2 indicates that VIH condensers expel 1687 kW of thermal energy, while the LNG motor cooling (incl. exhaust gas cooling) expel 1021 kW. Regarding the operating time, it was noted that the VIH ran at 100% load for 4250 h/a, and at a partial load for 3750 h/a. The relationship between the load and the consumption could be studied more in detail in this paper [83].

Table A. 1: Process data for heat pump of Augustenborg DH plant [84]

<b>Time period</b>	<b>Heat Production (MWh)</b>	<b>Power consumed (MWh)</b>	<b>COP</b>	<b>Operating time (h)</b>	<b>Operating time (%)</b>
3 <sup>rd</sup> quarter 1991	1151.2	332.03	3.47	1704	78.9
4 <sup>th</sup> quarter 1991	2665.5	791.15	3.37	2116	98.0
1 <sup>st</sup> quarter 1992	2657.4	758.75	3.50	2114	97.9
2 <sup>nd</sup> quarter 1992	2008.5	575.11	3.49	1974	91.4
3 <sup>rd</sup> quarter 1992	1258.0	349.76	3.60	1831	84.8
4 <sup>th</sup> quarter 1992	2819.5	781.11	3.61	2193	99.3
1 <sup>st</sup> quarter 1993	2357.4	627.2	3.76	2052	95.0

The numbers in Table A. 1 show the average values for an operating interval of around 21 months. It is serviced in the summer when the demand is low, and it is praiseworthy that the plant had been operating with a high COP value.

## A2 – Refrigerant R-1234ze

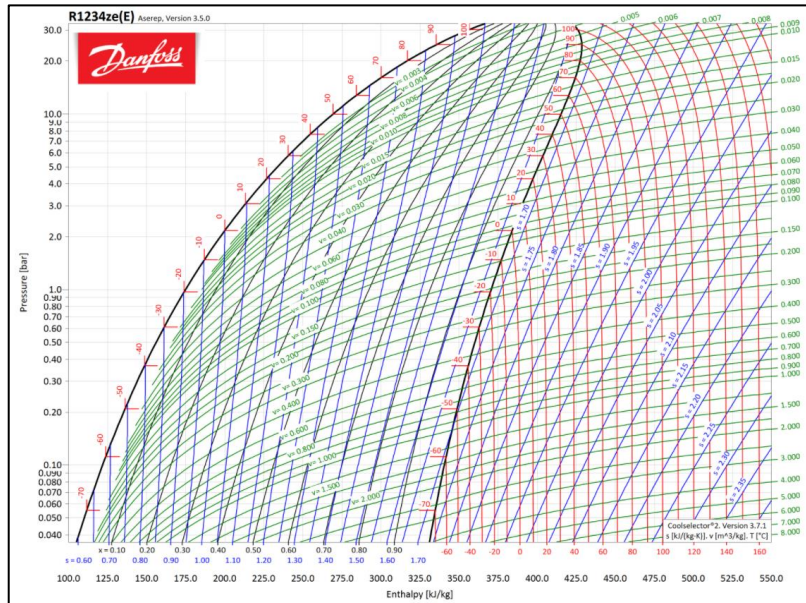


Figure A.3: Mollier diagram of the refrigerant R1234ze [114]

Table A. 2: Physical properties of the refrigerant R1234ze [115, 116]

Properties	Value	Units
Molecular weight	114	g/mol
Boiling Point (at 101.3 kPa)	-18.95	°C
Freezing Point (at 101.3 kPa)	156	°C
Critical Pressure	36.36	bar
Critical Temperature	109.4	°C
Critical Density	489	kg/m <sup>3</sup>
Vapour pressure (at 20°C)	4.27	bar
Solubility in water	0.037	wt%
Heat of vaporisation at boiling point	195.4	kJ/kg
Liquid heat capacity at 25°C	1.383	kJ/kg °C

Vapour heat capacity at 25°C	0.9822	kJ/kg °C
Safety classification	A2L	-
GWP		
(according to IPCC AR4/CIE)	7	-
(according to revised 5 <sup>th</sup> IPCC)	< 1	-
ODP	0	-

### A3 – Experimental values used in Pressure drop studies

Meewise et. al., in their experiments used a tube having a diameter of 20 mm and a mass flow of 0.96454 kg/s [104]. The pressure drop values corresponding to the ice fraction are extracted from the paper and tabulated in the table below.

*Table A. 3: Measured pressure drop and corresponding ice fraction based on experiments by Meewise et. al.*

Ice Fraction	Pressure Drop Pa per length (Pa/m)
5%	6336.6
10%	6579.2
15%	6905.1
20%	7220.0

Lee et. al., in their experiments used a tube having a diameter of 24 mm and a velocity of 2 m/s [105]. The pressure drop values corresponding to the ice fraction are extracted from the paper and tabulated in the table below.

*Table A. 4: Measured pressure drop and corresponding ice fraction based on experiments by Lee et. al.*

Ice Fraction	Pressure Drop Pa per length (Pa/m)
5%	2059.3
10%	2157.4
15%	2255.5
20%	2402.6

Grozdek et. al., in their experiments used a tube having a diameter of 9 mm and a velocity of 1.8 m/s [106]. The pressure drop values corresponding to the ice fraction are extracted from the paper and tabulated in the table below.

Table A. 5: Measured pressure drop and corresponding ice fraction based on experiments by Grozdek et. al.

Ice Fraction	Pressure Drop Pa per length (Pa/m)
5%	6925.5
10%	7024.1
15%	7268.5
20%	7786.2

#### A4 – Extension of Pressure Drop studies

The main body of the report discusses in detail the pressure drop studies for mass flow rate of 3240 kg/s. This corresponds to a DH capacity of ~300MW. But, in real life, the demand will not be fixed and there will be variations on either side. As a result, two other cases were also studied – for mass flow rates of 50kg/s and 4800 kg/s, that corresponded to DH capacity of ~5 MW and ~500 MW respectively.

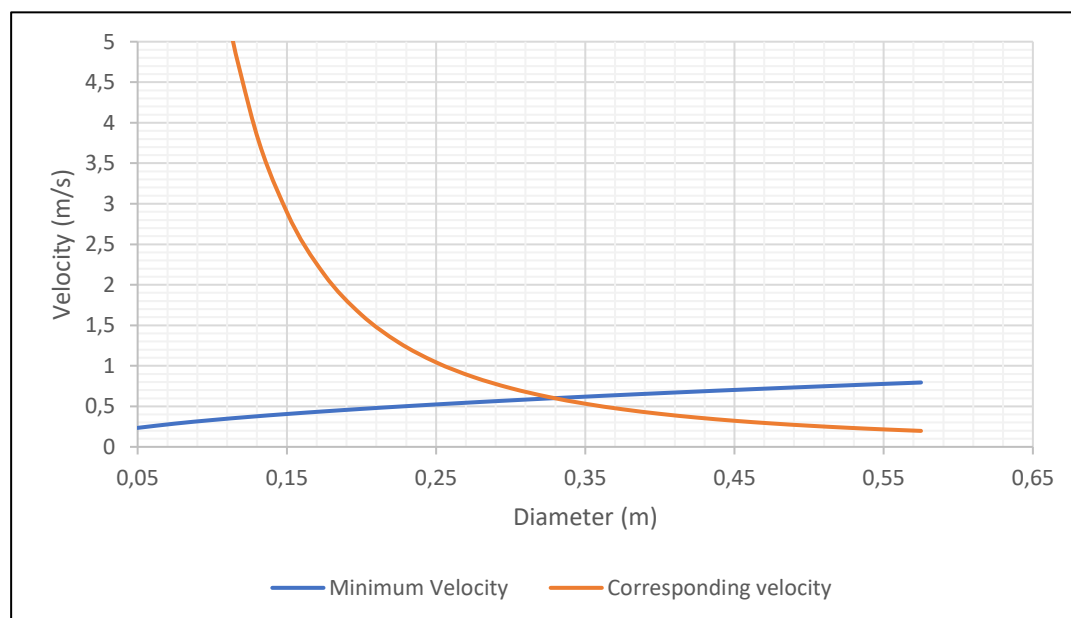


Figure A. 4: Plot of Velocity vs Diameter for mass flow of 50kg/s. The blue line denotes the minimum velocity required according to Guilpart's work, while the orange line indicates the corresponding velocity for the diameter.

As it can be observed from the plot above, for mass flow of 50kg/s, the diameters that do not allow for phase separation are up to 0.325m. Although, diameters of 0.05m, 0.1m are viable, the corresponding velocities are not practically possible. Hence, this study covers the diameter range from 0.15 m to 0.325m. For 20% ice fraction, for this mass flow, the pressure drop vs diameter characteristics is plotted in Figure A. 5.

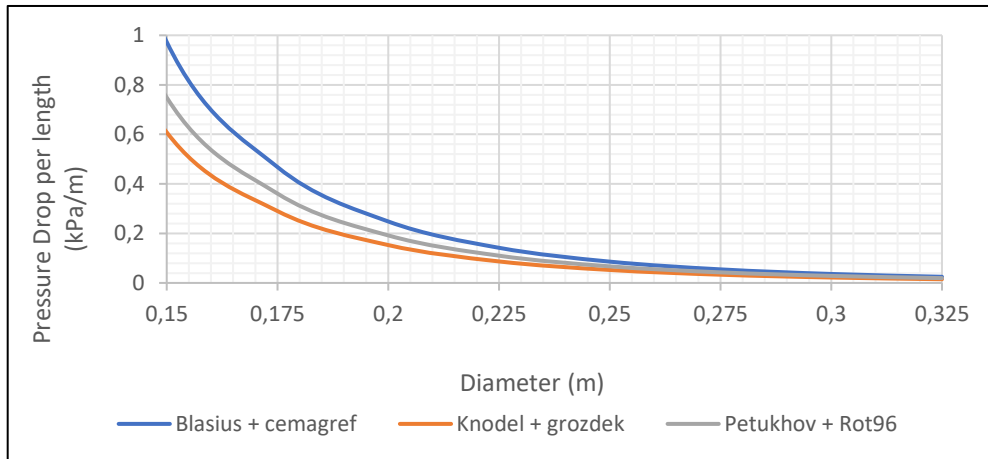


Figure A. 5: Pressure drop vs diameter for a mass flow rate of 50 kg/s, for 20% ice fraction

When selecting the pump and the pipe, care should be taken care to ensure that the worst-case scenario (Blasius + Cemagref) is used to base the design on to avoid any disastrous consequences. For this case, the ratio of pumping power to latent heat released is plotted in Figure A. 6. It can be observed that irrespective of the mass flow, a 20% ice fraction is the most desirable in terms of energy consumed.

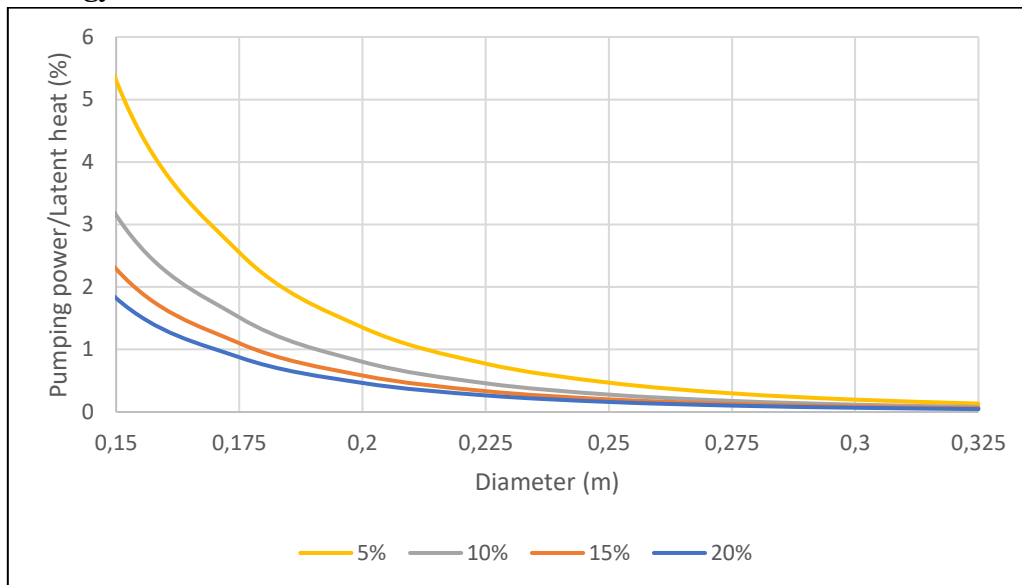


Figure A. 6: Ratio of Pumping power to latent heat released (in %) vs diameter for various ice fractions for a mass flow rate of 50 kg/s.

Similarly, we repeat the same for ice slurry mass flow rate of 4800 kg/s. For this flow rate, up to a diameter of 2.025 m, the flow velocity is greater than the minimum velocity required, according to Guilpart, and hence, no phase separation occurs. But, owing to practical reasons, viable diameters less than 1.5 m are not studied (the velocities are too high) and hence, the graph plotted here is for diameters ranging from 1.5 m to 2.025 m (Figure A. 7).

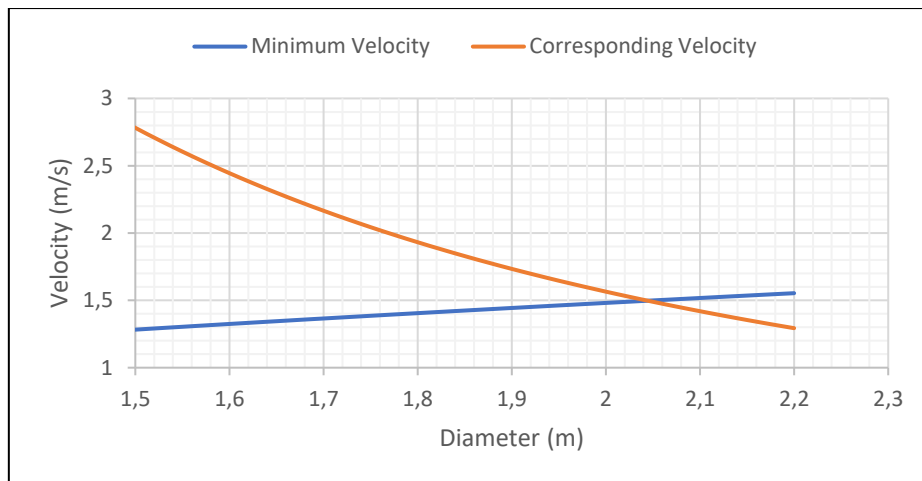


Figure A. 7: Plot of Velocity vs Diameter for mass flow of 4800 kg/s. The blue line denotes the minimum velocity required according to Guilpart's work, while the orange line indicates the corresponding velocity for the diameter.

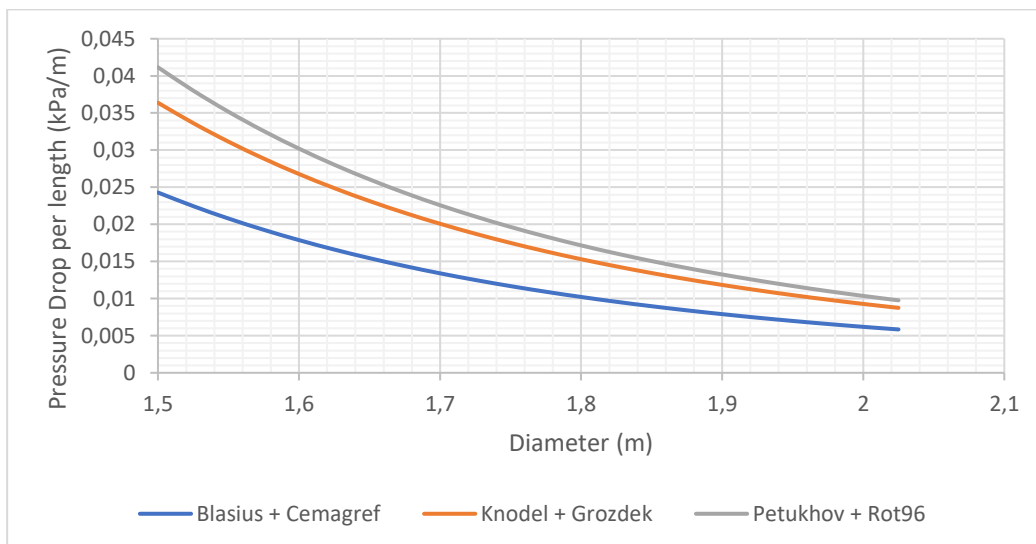


Figure A.8: Pressure drop vs diameter using pressure ratio analysis for mass flow of 4800 kg/s.

For 20% ice fraction, for this mass flow, the pressure drop vs diameter characteristics is plotted in Figure A.8. Also, since we have already established that a 20% ice fraction is the most ideal for our application, regardless of the mass flow rate, a graph is plotted between the pumping power and the diameter in the Figure

A.9. This done using the values calculated for the worst-case scenario (Blasius friction factor model, used alongside Cemagref viscosity values).

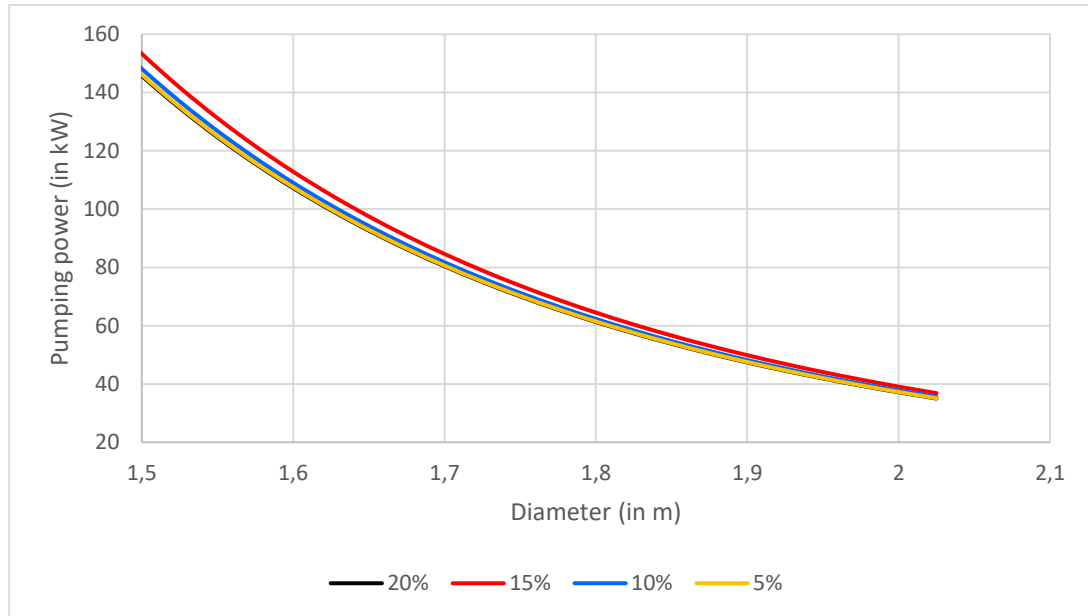


Figure A.9: Pumping power vs diameter - a comparison between different ice slurry fractions based on the viscosity models. Pump efficiency = 0.8.

One interesting thing that could be observed is that the pumping power required is almost similar for both 5% and 20%. What leads us to opt for the latter is the latent heat released when 20% of water turns to ice is four times that of 5% ice fraction. This leads to significant reduction in extra energy spent, thereby being energy efficient and hence is best suited for our application.



